

DTIC FILE COPY

(13)

AD-A955 309

DTIC
ELECTE
S OCT 19 1987 D

D
∞

U. S. NAVY
WIRE-ROPE HANDBOOK

VOLUME II

ON

WIRE-ROPE ANALYSIS AND
DESIGN DATA

DISTRIBUTION STATEMENT A
Approved for public release;
Distribution Unlimited

87 10 6 083

U. S. NAVY
WIRE-ROPE HANDBOOK

VOLUME II

ON

WIRE-ROPE ANALYSIS AND
DESIGN DATA



Accession For	
NTIS CRA&I	<input checked="" type="checkbox"/>
DTIC TAB	<input type="checkbox"/>
Unannounced	<input type="checkbox"/>
Justification	
By <i>per form 50</i>	
Distribution/	
Availability Codes	
Dist	Avail and/or Special
A-1	

UNANNOUNCED

Published by Direction of Commander, Naval Sea Systems Command
Washington, D. C.

1976

34 26

TABLE OF CONTENTS

<u>Section Number and Title</u>	<u>Page</u>
1. INTRODUCTION	1-1
2. FAILURE MODES IN ROPE WIRE	2-1
2.1 Mode 1 Fatigue Failures	2-1
2.2 Mode 2 Fatigue Failures	2-1
2.3 Tensile Failures	2-3
3. WIRE-ROPE SYSTEM DESIGN DATA AND TECHNIQUES	3-1
3.1. Wire-Rope Bending Fatigue Data	3-1
3.1.1. Types of Wire-Rope Bending	3-3
3.1.2. Stresses Induced by Bending Around a Sheave	3-3
3.1.3. Effects of Sheave-to-Rope Diameter Ratio, D/d	3-3
3.1.4. Effects of Rope Load	3-5
3.1.5. Correlation of Load and D/d Ratio With Rope Life	3-8
3.1.6. Effect of Wrap Angle	3-10
3.1.7. Effect of Fleet Angle	3-13
3.1.8. Effect of Rope Material	3-13
3.1.8.1. Wire Type	3-13
3.1.8.2. Wire Strength	3-13
3.1.9. Effects of Swivels	3-15
3.1.10. Effects of Rope Construction	3-15
3.1.10.1. Lay	3-15
3.1.10.2. Number of Strands	3-15
3.1.10.3. Arrangement and Size of Wires	3-18
3.1.10.4. Preforming	3-18
3.1.10.5. Core	3-18
3.1.10.6. Special Constructions	3-18
3.1.11. Effect of Sheave Hardness	3-18
3.1.12. Effects of Sheave Throat Shape	3-24
3.1.13. Effects of Corrosion, Lubrication, and Coatings	3-26
3.1.13.1. Corrosion	3-26
3.1.13.2. Lubrication	3-28
3.1.13.3. Coatings	3-28
3.1.14. Effect of Reversed Bends	3-30
3.2. Axial Fatigue of Wire Rope	3-33
3.2.1. Effect of Cyclic Axial Loads on Wire Rope Fatigue	3-33
3.2.2. Effect of Cyclic Axial Loads on Steel Strand Fatigue	3-33
3.2.3. Effects of End Fittings	3-36
3.2.4. Effects of Core	3-36
3.2.5. Effects of Lay	3-36
3.2.6. Effects of Rope Construction and Material	3-37
3.2.7. Effect of Frequency	3-37
3.2.8. Effect of Corrosion	3-39
3.2.9. Effect of Diameter	3-39
3.2.10. Effects of Lubrication and Coating	3-40
3.3. Rotation and Torque	3-40
3.3.1. Kink Formation	3-40
3.3.2. Breaking Strength	3-42

Table of Contents

Section Number and Title (Continued)	Page
3.3.3. Torque Calculation	3-43
3.3.3.1. General Theory for Analysis of Wire-Rope Torque	3-45
3.3.3.2. Simplified Equations for Wire Ropes With Single-Operation Strands	3-49
3.3.3.3. Simplified Equations Applied to Six-Strand Wire Ropes	3-51
3.3.3.4. Sample Calculations for Simple Wire Rope	3-53
3.3.3.5. Measurement of Rope Lay and Strand Lay	3-54
3.4. Relative Strand Motion in a Wire Rope on a Sheave	3-55
3.4.1. Graphical Results of Strand-Motion Solution	3-56
3.4.2. Discussion and Further Implications of the Strand-Motion Solution	3-56
3.4.3. Relative Motion of the Wires in the Strands	3-61
4. WIRE ROPE STRESS ANALYSIS	4-1
4.1. Tensile Stress	4-1
4.2. Bending Stress	4-2
4.2.1. Analysis of a Straight-Wire Rope	4-2
4.2.1.1. Wire-Rope Geometry	4-2
4.2.1.2. Derivation of Equations	4-6
4.2.1.2.1. Constant Angle Assumption	4-7
4.2.1.2.2. Uniform-Motion Assumption	4-8
4.2.1.3. Results	4-9
4.2.2. Analysis of a Wire Rope Wrapped on a Sheave	4-16
4.2.2.1. Wire-Rope Geometry	4-16
4.2.2.2. Derivation of Equations	4-20
4.2.2.3. Results	4-22
4.2.3. Analysis of Bending Stress	4-24
4.2.3.1. Derivation of Equations	4-24
4.2.3.2. Results	4-28
4.3. Contact Stresses	4-29
4.3.1. Wire-Sheave Interface	4-29
4.3.2. Wire Interfaces in a Strand	4-30
4.3.3. Interstrand Wire Contact	4-31
4.3.4. Interstrand Contact Forces	4-32
4.3.5. Interstrand Contact Stresses	4-33
4.3.6. Core-Strand Interface Stresses	4-34
4.3.7. Elastic-Plastic Analysis	4-34
4.4. Torsional and Shear Stresses	4-34
4.5. Wire Rope Dynamics	4-34
4.5.1. Longitudinal Forces	4-35
4.5.2. Transverse Forces	4-36
4.5.2.1. Strumming	4-36
4.5.2.1.1. Increased Drag Due to Strumming	4-38
4.5.2.1.2. Strumming Suppression	4-38
4.5.2.3. Aircraft Arresting-Gear Cable	4-38
5. APPENDIX	5-1
5.1. Rotation and Translation of Coordinates With Matrices	5-1
5.2. Derivation of Reference Angle Relationship in Straight Rope	5-2
5.3. Radius of Curvature Equations--Straight Rope Analysis	5-3

700.00 1026

Table of Contents

<u>Section Number and Title (Continued)</u>	<u>Page</u>
5.4. Computer Programs	5-4
5.5. Derivation of Geometrical Derivatives for the Rope Bent on a Sheave	5-7
5.6. Bending-Stress Analysis Computer Program	5-9
6. REFERENCES	6-1
7. ALPHABETICAL INDEX	7-1

77081 4026

LIST OF FIGURES

<u>Figure Number and Title</u>	<u>Page</u>
2-1. Initiation Site and Orientation of Mode 1 Fatigue Failures in Strand Outer Wires	2-2
2-2. Typical Mode 1 Fatigue Failure	2-2
2-3. Initiation Site and Orientation of Mode 1 Fatigue Failures in Strand Inner Wires	2-2
2-4. Initiation Site and Orientation of Mode 2 Fatigue Failures in Strand Outer Wires	2-4
2-5. Initiation Site and Orientation of Mode 2 Fatigue Failures in Strand Inner Wires	2-4
2-6. Typical Mode 2 Fatigue Failure (Final Failure in Tension)	2-5
2-7. Typical Mode 2 Fatigue Failure (Final Failure in Shear)	2-5
2-8. Typical Longitudinal Split in Fatigue-Cracked Wire	2-6
2-9. Initiation Site and Orientation of Mode 2 Fatigue Failures in Strand Outer Wires	2-6
2-10. Typical Mode 2 Fatigue Cracks at the Points of Interstrand Notching	2-7
2-11. Typical Mode 2 Fatigue Failure	2-7
2-12. Initiation Site and Orientation of Mode 2 Fatigue Failures in Strand Outer Wires	2-8
2-13. Typical Mode 2 Fatigue Failure	2-8
2-14. Typical Mode 1 Tensile Failure	2-9
2-15. Typical Mode 2 Tensile Failure	2-9
3-1. Results of Bending-Fatigue Experiments Completed in Various Laboratories	3-2
3-2. Comparison of Bending-Fatigue Data Generated in Different Laboratories on Similar Machines	3-2
3-3. Types of Wire Rope Bending	3-4
3-4. Effect of D/d Ratio on the Bending-Fatigue Life of IWRC Wire Rope at Three Load Levels	3-4
3-5. Effect of D/d Ratio on the Bending-Fatigue Life of Fiber-Core Wire Rope at Two Load Levels	3-6
3-6. Wire Rope Bending-Fatigue Results Expressed in Terms of Rope Tension and D/d Ratio	3-6
3-7. Results of Bending-Fatigue Tests on 3/4-Inch Wire Rope	3-7
3-8. Bending-Fatigue Data for a Wide Range of Loads and D/d Ratios	3-7
3-9. Comparison of Bending-Fatigue Data on the Basis of Bearing Pressure Ratio	3-9
3-10. Eighty Percent Confidence Bands for Selected Bending Fatigue Data	3-9
3-11. Bending Cycles to Failure Versus Life Factor, γ	3-11
3-12. Effect of Wrap Angle on Wire Rope Bending-Fatigue Life	3-11
3-13. Relative Wire Breakage as a Function of Wrap Angle	3-12
3-14. Tensile Strengths of Carbon-Steel Rope Wire as a Function of Diameter and Wire Grade	3-12

Figure Number and Title (Continued)	Page
3-15. Effect of Wire Strength on Bending Cycles to Failure--All Tests Completed at Equal Rope Tensions	3-14
3-16. Effect of Wire Strength on Bending Cycles to Failure--All Tests Completed at Equal Design Factors	3-14
3-17. Effect of Rope Lay on Bending-Fatigue Life for Different Groove Shapes	3-16
3-18. Effect of Rope Construction and Rope Load on Fatigue Life.	3-17
3-19. Comparative Reverse-Bend Fatigue Resistance of 6 x 19 and 6 x 37 Wire Rope	3-19
3-20. Effect of Design Factor on Bending-Fatigue Life	3-19
3-21. Effect of D/d Ratio on Bending-Fatigue Life	3-20
3-22. Bending-Fatigue-Life Data for Preformed and Nonpreformed Wire Rope Under Various Tensile Loads	3-20
3-23. Comparison of Bending-Fatigue Data for 3/4-Inch Wire Rope With Several Core Types, D/d = 25, df = 3	3-21
3-24. Comparison of Bending-Fatigue Data for 3/4-Inch Wire Rope With Several Core Types, D/d = 15, df = 8	3-21
3-25. Comparison of Bending-Fatigue Data for 3/4-Inch Wire Rope With Two Rope Core Types, D/d = 25, df = 8	3-22
3-26. Results of Bending-Fatigue Tests on Aluminum and Hardened Steel Sheaves	3-23
3-27. Effects of Sheave Material on Bending-Fatigue Life	3-24
3-28. Comparison of Bending-Fatigue Resistance of Several Rope Constructions on Nylon-Lined and Cast-Iron Sheaves	3-25
3-29. Comparison of Bending-Fatigue Resistance of Corroded and Uncorroded Wire Rope	3-26
3-30. Effect of Lubrication on the Bending-Fatigue Life of a Rope for Various Design Factors	3-29
3-31. Comparison of Bending Endurance of Wire Ropes Made From Bright (Uncoated) and Drawn Galvanized Wire	3-29
3-32. Comparison of Bending Endurance of Various Galvanized Wire Ropes	3-31
3-33. Bending-Fatigue Data for Uncoated and Nylon-Jacketed Cable	3-31
3-34. Effect of Plain and Reverse Bending on the Fatigue Life of Regular-Lay Wire Rope	3-32
3-35. Effect of Plain and Reverse Bending on the Fatigue Life of Lang-Lay Wire Rope	3-32
3-36. Characteristics of Load Cycle Pattern Used in Axial Fatigue Tests	3-33
3-37. Axial Fatigue Test Data for 1/2-Inch Diameter 6 x 25 Polypropylene Core and IWRC, Bright Improved Plow Steel, Wire Rope	3-34
3-38. Effect of Mean Load on the Axial Fatigue of IWRC and Polypropylene Core Wire Rope	3-34
3-39. Effect of Maximum, Mean and Range of Load on the Axial Fatigue Life of 1-Inch, 1 x 19 Galvanized Strand	3-35
3-40. Effect of Construction and Socketing Technique on the Axial Fatigue Life of Steel Strand	3-36
3-41. Effect of Diameter, Core Material, Construction and Socketing Technique on the Axial Fatigue Life of Steel Wire Rope	3-37

Figure Number and Title (Continued)	Page
3-42. Effect of Wire Strength on the Axial Fatigue Behavior of a Steel Wire Rope (Unknown Construction)	3-39
3-43. Effect of Wire Coating and Lubrication on the Axial Fatigue Life of 3/4-Inch, 1 x 37 Steel Wire Strand	3-40
3-44. Typical Torque Characteristics of 18 x 7 Nonrotating Wire Rope	3-43
3-45. Typical Rotational Characteristics of 18 x 7 Nonrotating Wire Rope	3-43
3-46. Geometry of a 6-Strand Wire Rope	3-45
3-47. Wire Rope Force Triangle	3-45
3-48. Force Contributing to Wire Rope Torque	3-45
3-49. Strand Force Triangle	3-47
3-50. One Layer of Wires in a Strand	3-48
3-51. Torque Developed by Helically-Wrapped Strands in a 6-Strand Wire Rope	3-51
3-52. Total Torque Developed by Helically Wrapped Wires in a Single-Operation Strand of a 6-Strand Wire Rope	3-51
3-53. Cross Section of a 6 x 31 Fiber-Core Wire Rope	3-52
3-54. Relative Strand Motion Between Nodal Planes in a Wire Rope Wrapped on a Sheave	3-56
3-55. Influence of Rope and Sheave Geometry on the Relative Strand Motion of a 6-Strand Wire Rope	3-57
3-56. Schematic Illustration of Nodal Angle on a Sheave	3-58
4-1. Typical Lang-Lay Wire Rope Construction	4-4
4-2. Straight-Rope Geometry	4-5
4-3. Reference-Angle Relationship Assuming Constant Wire Lay Angle, α	4-8
4-4. Variation in Wire Lay Angle, α , in a Straight Wire Rope Assuming Uniform Wire Motion	4-9
4-5. Variation in Wire Radius of Curvature Within a Wire Rope	4-10
4-6. Plane Section of a 6 x 25 Filler-Wire Strand	4-11
4-7. Illustration of Wire Position in the Standard Rope Relative to the $Z_1 - Z_2$ Coordinate System	4-12
4-8. Illustration of the Interrelationship Between Strand Lay Angle and Strand Length as Compared to Rope Length	4-14
4-9. Relationship Between Wire Lay Angle and the Constant of Motion	4-15
4-10. Sensitivity of Radius of Curvature to Wire Lay Angle - Constant Angle Assumption	4-17
4-11. Sensitivity of Radius of Curvature to Constant of Motion - Uniform-Motion Assumption	4-18
4-12. Geometry of a Wire Rope Wrapped on a Sheave	4-19
4-13. Radius of Curvature of Wires in a Rope Wrapped on a Sheave	4-23
4-14. Plane Section of a Rope Wrapped on a Sheave	4-23
4-15. Illustration of Wire Segments in Complex Bending	4-25
4-16. Coordinate Alignment Used for Comparing Radii-of-Curvature Results	4-27
4-17. Bending Stress in Rope Wires Resulting From Bending of the Standard Rope Around a 24-Inch Diameter Sheave	4-28
4-18. Strumming Drag Characteristics	4-39
5-1. Cartesian Coordinates--Common Origin; Arbitrary Orientation	5-1

LIST OF TABLES

<u>Table Number and Title</u>	<u>Page</u>
3-1. Results of Endurance Life Tests on 3/4-Inch Diameter Aluminum Coated and Galvanized Improved Plow Steel Wire Ropes 6 x 19--Fiber Core	3-27 3-30
3-2. Fatigue Life Reduction Due to Reverse Bends	3-38
3-3. Results of Cyclic Tension Tests	3-41
3-4. Torsional Characteristics of Various Constructions	
3-5. Influence of Rotation on Ultimate Strength of 1-1/2-Inch, 18 x 7 Nonrotating Wire Rope	3-42
3-6. Measurements and Calculations for Example Wire-Rope Construction	3-53
4-1. Comparison of Bending Stress Formulas	4-3
4-2. Cyclic Impact Test Data	4-36

LIST OF SYMBOLS

A	cross-sectional area, in ² , also constant in bending stress and contact stress analyses
A _c	area of core wire, in ²
A _i	area of individual wires in layer i, in ²
A _m	metallic rope area, in ²
A _n	area of wire n, in ²
a	constant in bending stress analysis
B	bearing pressure ratio, also constant in contact stress analysis
b	semiminor axis of ellipse formed by cross-wire contact, in, also constant in bending stress analysis
C	constant based on strand lay length, $\cos \beta' / \cos \beta$
C _b	constant in contact stress analysis
C _D	drag coefficient for stationary cable
C _{DS}	drag coefficient for strumming cable
C _G	constant in contact stress analysis
C _{ZS}	constant in contact stress analysis
C _σ	constant in contact stress analysis
C _τ	constant in contact stress analysis
c	subscript denoting core of strand or rope, also constant in bending stress analysis
D	pitch diameter of sheave, in
d	rope diameter, in
df	design factor, ratio of new rope breaking strength to design load
d _o	diameter of outside wire in a strand
d _s	strand diameter, in
d _w	wire diameter, in

List of Symbols

n_f	mode number
n_o	number of outer wires in a strand
n_t	number of wire images per tape, used in determination of strand lay length
P	point in bending stress analysis
P_o	loss in strength per wire due to rope manufacture, lb
P	average contact pressure, lb/in ²
R	pitch radius of strand, measured from rope centerline to strand centerline, in
R_b	rope bending radius, in
R_p	pitch radius of sheave or drum, in
R_r	Reynold's number
r	pitch radius of wire, measured from strand centerline to wire centerline, in.
r_o	pitch radius of outer wire in strand, in
r_w	wire radius, in
S	strand length, in
S'	length of tape used in determining the strand lay length, in
S_s	Strouhal number
s	true length of a strand on a sheave as measured from the point of rope tangency to a specific angle, ψ , on a sheave, in
Δs_{max}	maximum relative strand motion, in
T	rope tensile load, lb
T_s	strand tensile load, lb
T_w	wire tensile load, lb
U	wire strength, lb/in ²
V_o	free stream velocity, in/sec
X_1, X_2, X_3	coordinates used in bending stress analysis
x	coordinate axial to wire
Y_1, Y_2, Y_3	coordinates used in bending stress analysis

List of Symbols

n_f	mode number
n_o	number of outer wires in a strand
n_t	number of wire images per tape, used in determination of strand lay length
P	point in bending stress analysis
P_o	loss in strength per wire due to rope manufacture, lb
P	average contact pressure, lb/in ²
R	pitch radius of strand, measured from rope centerline to strand centerline, in
R_b	rope bending radius, in
R_p	pitch radius of sheave or drum, in
R_r	Reynold's number
r	pitch radius of wire, measured from strand centerline to wire centerline, in.
r_o	pitch radius of outer wire in strand, in
r_w	wire radius, in
S	strand length, in
S'	length of tape used in determining the strand lay length, in
S_s	Strouhal number
s	true length of a strand on a sheave as measured from the point of rope tangency to a specific angle, ψ , on a sheave, in
Δs_{max}	maximum relative strand motion, in
T	rope tensile load, lb
T_s	strand tensile load, lb
T_w	wire tensile load, lb
U	wire strength, lb/in ²
V_o	free stream velocity, in/sec
X_1, X_2, X_3	coordinates used in bending stress analysis
x	coordinate axial to wire
Y_1, Y_2, Y_3	coordinates used in bending stress analysis

y	coordinate tangential to wire
Z_1, Z_2, Z_3	coordinates used in bending stress analysis
Z_s	distance between wire surface and location of τ_{\max} and $\tau_{G\max}$, in
z	coordinate radial to wire
α	wire lay angle, degrees (positive for right-hand lay)
α_n	lay angle of wire n , degrees
α_o	lay angle of outer wires in a strand, degrees
β	strand lay angle, degrees (positive for right-hand lay)
β'	lay angle of a strand in a rope, measured between rope centerline and outer diameter, degrees
γ	life factor
γ_o	complement of angle between individual wire and centerline of rope, degrees
Δ	constant in contact stress analysis
ϵ	angle in bending stress analysis, degrees
e	strain, in/in
θ	angle defining the position of a strand in a wire rope, degrees
θ_c	wire crossing angle, degrees
θ_o	initial angular position of a strand, degrees
λ	general lay angle, degrees
μ	Poisson's ratio
r	difference between two wire radii of curvature, in
ρ	radius of curvature of wire, in
σ	tensile stress in a wire, lb/in ²
σ_b	bending stress in a wire, lb/in ²
σ_c	tensile stress in a core wire, lb/in ²
σ_{\max}	maximum tensile stress, lb/in ²
σ_n	tensile stress in wire n , lb/in ²

τ	shear stress, lb/in ²
τ_{Gmax}	maximum octahedral shear stress, lb/in ²
τ_{max}	maximum shear stress, lb/in ²
θ	angle defining position of a wire in a strand, degrees
θ'	first derivative of θ with respect to θ
θ''	second derivative of θ with respect to θ
ψ	sheave reference angle, degrees
ψ_n	nodal angle, degrees
Ω	angle between flow direction and cable axis, degrees
	single-bend wire rope fatigue data (European notation)
	reverse-bend wire rope fatigue data (European notation)

1.INTRODUCTION

Volume II of the Wire-Rope Handbook is intended for technically trained persons concerned with specific quantitative analyses of wire rope and wire-rope systems. This volume complements Volume I with a large amount of state-of-the-art technical data together with the most recent developments in analysis methods.

Over the years, a considerable quantity of field data has been collected by those who make and use wire rope, and a large volume of experimental and analytical information has been developed in various research laboratories. It would be of considerable significance if these compiled data could be used in some direct fashion to predict the service performance of wire ropes in actual operating systems. The problem is an extremely difficult one, however, because wire rope is a complex mechanical assembly and its performance is affected by a large number of factors which are difficult to simulate or quantify.

The experimental data and analyses presented in this volume represent most of the currently available information on the technology of wire rope. It is possible to gain considerable insight into the behavior of wire rope from the material presented here. It is important to remember, however, that almost all the experimental data were generated under somewhat idealized laboratory conditions, and practically all the analytical analyses were developed on the basis of simplifications or idealization of real wire-rope structures. Therefore, in most, if not all cases, the design data presented here must be used qualitatively, not quantitatively.

For the most part, a direct correlation between the laboratory data shown and field behavior cannot be made--but, the data do show trends with reasonable accuracy, and they identify the relative importance of certain rope and system design factors. In other words, if a change in a laboratory setup simulating a field condition improves the life of a rope being tested, that same change will probably improve the life of that rope in the field and in about the same proportion. This is of course, true only if the parameter that is changed is limiting field life. For example, if a rope is being discarded because of abrasion (say from rubbing against a stationary structural member in the system) changes that improve the bending fatigue life, such as larger sheaves, cannot help rope life.

Throughout this handbook the term "design factor" is used in place of "safety factor". It is defined as the ratio of NEW rope strength to design load. The design factor is not actually a measure of operational safety since, as a rope is used, its breaking strength decreases and so does its safety factor. The only time when a rope's design factor and safety factor are synonymous is when the rope is new and completely undamaged.

In the field, wire rope fails in many ways, depending on the type of service that it encounters. In this volume, the emphasis is on failure due to repeated bending and loading below the ultimate strength of the rope. The influence of other factors (such as corrosion) is also covered, but primarily as they affect the fatigue behavior and life.

2. FAILURE MODES IN ROPE WIRE

The following is a summary of rope wire failure modes that have been identified during examinations of wire ropes tested to failure on laboratory bending-fatigue machines. They are characteristic of many field failures, but do not illustrate the effects of either abrasion or corrosion. This discussion is derived from that in Reference 2-1, as are the figures.

2.1. MODE 1 FATIGUE FAILURES

Mode 1 wire fatigue failures, with the fracture surface oriented about 45 degrees to the longitudinal axis of the wire, have failure initiation sites located at a point of contact with adjacent wires. Some Mode 1 failures are found to initiate at points of interstrand contact. Typical failures of this type are shown in Figures 2-1 and 2-2. Mode 1 failures are also found with the initiation sites at parallel-wire marks, as shown in Figure 2-3.

Examination of the Mode 1 fatigue failures reveals a 45 degree shear failure with no obvious evidence of fatigue. The shear failure results from overload, and the orientation of the plane of failure is a result of the multiaxial stress state at the point of interwire contact (combined contact, tension and bending loads). Mode 1 failures have been produced in the laboratory under simulated loading conditions with a single application of load. This failure mode also occurs under slightly lower cyclic wire loads as a result of reduction in wire area because of the deepening notch-wear scar, or because of small surface fatigue cracks perpendicular to the wire axis. Some possible minute fatigue crack initiation sites at the point of interwire contact are observed under high magnification in many of the failures.

Mode 1 failures are predominant in high-load tests on laboratory bend-over-sheave wire-rope fatigue machines.

2.2. MODE 2 FATIGUE FAILURES

Mode 2 fatigue failure exhibits the more usual characteristics of a fatigue failure. Each fatigue crack propagates on a plane perpendicular to the longitudinal axis of the wire, and the characteristic "clam shell" or "beach" marks are present. No evidence of plastic flow or reduction of area is found at the failure sites. The cracks initiate at the points on the wires that experience the maximum combined tensile, bending, and contact stresses.

Mode 2 failures are the most common type found in ropes operating on hard sheaves under moderate conditions (within recommended practice). In these cases, the fatigue crack initiates at a point opposite the wire-sheave contact and propagates toward it. These breaks obviously occur in the outside, or crown wires, that contact the sheave.

Failures of this type are found to initiate on the as-drawn surface of the wires in areas not associated with points of interwire contact. On aluminum sheaves, these fatigue cracks appear on the outer surface of the wire rope well away from points of interstrand contact. This type of failure is illustrated in Figure 2-4. The inner wires of the strands often display a similar type of failure, with the fatigue crack initiating between two parallel-wire marks as illustrated in Figure 2-5. Both of these Mode 2 fatigue failures are found after low-load tests on laboratory fatigue machines.

For many Mode 2 failures, each fatigue crack propagates into the wire until the reduction in metallic area and the stress concentration at the crack root result in complete fracture. The lower the tensile load on the specimen, the further the cracks propagate. Final failure may then be either a tensile-type failure displaying a rather rough fracture surface approximately perpendicular to the wire axis, or a shear-type failure displaying a rather smooth fracture surface about 45 degrees to the wire axis. Examples of each of these failures are shown in Figures 2-6 and 2-7. Sometimes a Mode 2 failure is accompanied by a longitudinal splitting of the wire as shown in Figure 2-8. This wire splitting occurs more frequently at the lower test loads.

Another type of Mode 2 fatigue failure has been identified in wire-rope specimens where there is severe interwire notching. For these failures the fatigue cracks are found to initiate at the edge of a wire notch formed by interstrand contact as shown in Figure 2-9. Photographs of typical wires displaying this failure mode are shown in Figures 2-10 and 2-11.

Mode 2 fatigue cracks can also initiate on the side of the wire opposite the notch at or near the parallel-wire marks and propagate toward the notch. Examples of these failures are shown in Figures 2-12 and 2-13.

2.3. TENSILE FAILURES

During any type of wire-rope fatigue test, the wires begin to fail by one of the above-mentioned fatigue modes. The strength of the rope is gradually reduced until complete failure of a strand or strands results from tensile overload of the remaining wires. Some of these tensile failures display a standard cup-cone type of failure.

The fracture surface of the cup-cone tensile failure is symmetrical and exhibits large shear lips around the outer edge of the wire and creates the typical "cup" and "cone" as shown in Figure 2-14. The nominal orientation of the fracture surface is perpendicular to the longitudinal axis of the wire, and a large reduction of cross-sectional area is found at the fracture location. Failures of this type are typical of low-strain-rate round-bar tensile failures of a ductile material.

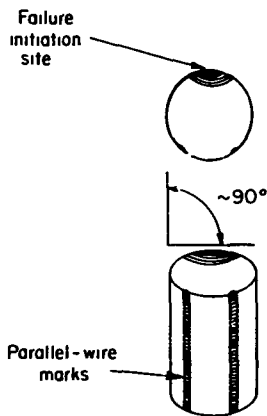


Figure 2-4. Initiation Site and Orientation of Mode 2 Fatigue Failures in Strand Outer Wires

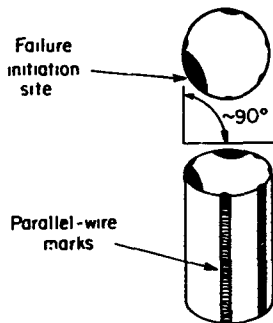


Figure 2-5. Initiation Site and Orientation of Mode 2 Fatigue Failures in Strand Inner Wires



10X

Figure 2-6. Typical Mode 2 Fatigue Failure
(Final Failure in Tension)



10X

Figure 2-7. Typical Mode 2 Fatigue Failure
(Final Failure in Shear)



Figure 2-8. Typical Longitudinal Split in Fatigue-Cracked Wire

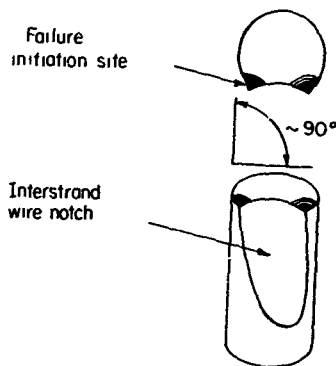


Figure 2-9. Initiation Site and Orientation of Mode 2 Fatigue Failures in Strand Outer Wires



Figure 2-10. Typical Mode 2 Fatigue Cracks at the Points of Interstrand Notching



Figure 2-11. Typical Mode 2 Fatigue Failure

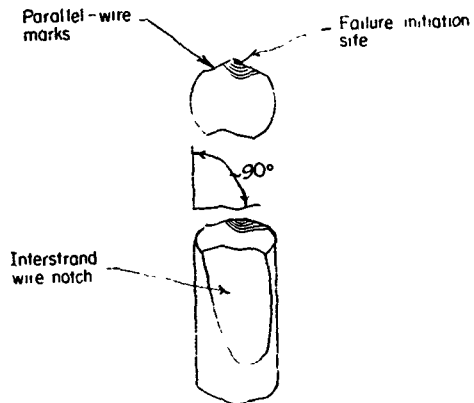


Figure 2-12. Initiation Site and Orientation of Mode 2 Fatigue Failures in Strand Outer Wires

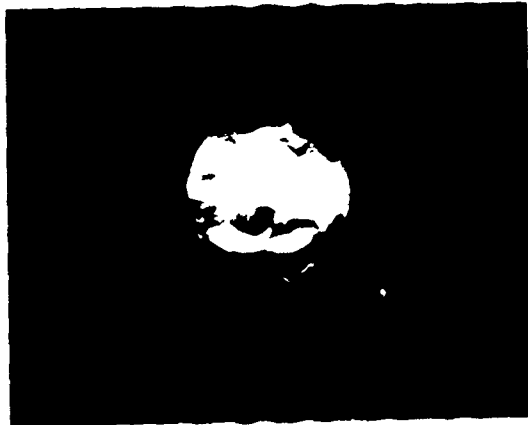


Figure 2-13. Typical Mode 2 Fatigue Failure



12X

Figure 2-14. Typical Mode 1 Tensile Failure

Sometimes rope wires that fail by tensile overload display tensile failures similar to those observed in high strain-rate overload experiments on simple tensile specimens of a ductile material. The failure differs from the low-strain-rate cup-cone failure in that a smaller reduction of metallic area is observed. Also, the fracture surface is more irregular and does not possess the symmetry of the cup-cone failure. This type of fracture is shown in Figure 2-15.



12X

Figure 2-15. Typical Mode 2 Tensile Failure

3. WIRE-ROPE SYSTEM DESIGN DATA AND TECHNIQUES

3.1. Wire-Rope Bending Fatigue Data

The primary reason for the retirement of a rope from service in most running rigging is fatigue from bending around sheaves. (Running rigging is that in which the rope moves, such as a crane-hoist rope, whereas in standing rigging the rope is stationary and usually straight as in tower guys.) Before discussing the effects of specific system parameters, certain general facts concerning the data and its use should be noted.

The data should be used qualitatively, not quantitatively. Generally, the life of a rope in the field will be longer than it is in a laboratory experiment. The reasons for this are not precisely known, but it can be speculated that rope in the field tends to rotate on its axis as it runs through the system, thus distributing fatigue damage around the circumference of the rope. Most laboratory bending-fatigue machines restrain the rope from rotation, thus confining the fatigue damage to one part of the rope circumference. Also, in most field situations, the rope is subjected to a variety of loads. It is normal engineering practice to consider the highest of these as the design load and to use this to compare field life to laboratory life. Thus, the field conditions are actually less severe in many cases than the laboratory imposed loading conditions.

Laboratory data from experiments conducted some time ago are usually quite conservative for modern ropes. Comparison of bending fatigue data from up to 50 years ago clearly shows that the relative life has significantly improved. Again, the reasons for this are not well defined but probably are due to a number of improvements in both wire quality and rope fabrication techniques. The development of preforming in particular has extended rope bending-fatigue life. In this Volume, an effort has been made to use modern data. However, in some cases, particularly where the data are not of domestic origin, the vintage is unknown.

When attempting to apply laboratory data to a field system, particular attention must be given to the wire failure modes as discussed in the previous section. The data will probably not be applicable, even qualitatively, unless the failure modes are the same as those found in the laboratory. This is generally not a problem if the operating conditions are fairly well simulated.

Laboratory bending fatigue data generated by different laboratories are not necessarily comparable. Figure 3-1 shows the results of a program recently conducted by the International Organization for the Study of the Endurance of Wire Rope (Refs. 3-1 and 3-2). This organization sent samples of a particular size and type of wire rope to a number of their members to run bending-fatigue tests under identical conditions of sheave geometry and load. The fatigue machines used were, however, quite diverse in configuration and operating principles. The numerical variation in the data from one laboratory to another is obvious. However, note that the trends are similar and most of the line slopes are about equal.

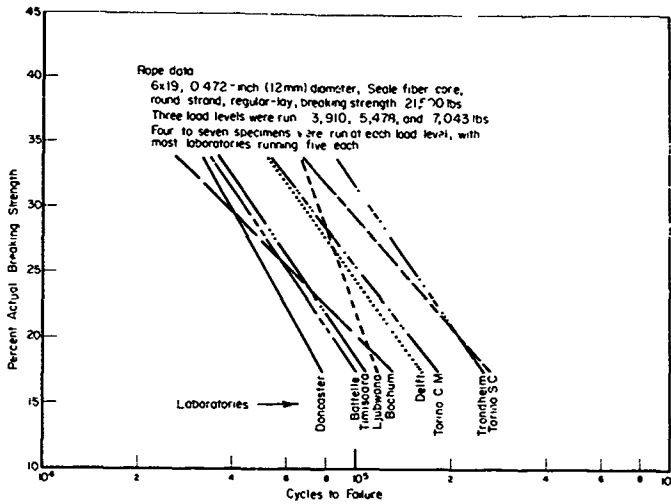


Figure 3-1. Results of Bending-Fatigue Experiments Completed in Various Laboratories

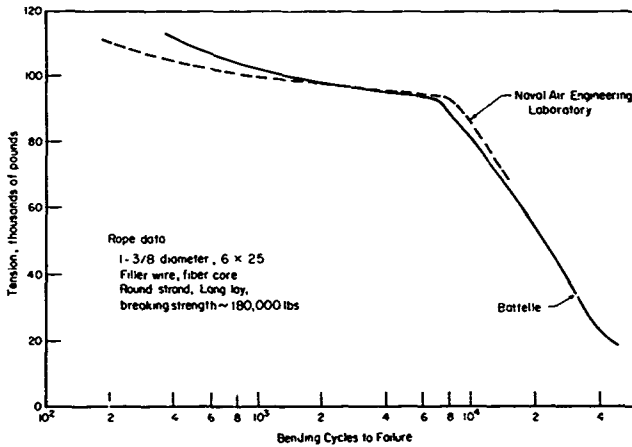


Figure 3-2. Comparison of Bending-Fatigue Data Generated in Different Laboratories on Similar Machines

Results from one laboratory can be made to match those of another, however, if care is taken to keep the test conditions and the machine configurations the same. This point is illustrated in Figure 3-2 where test results are shown from two different laboratories conducted on two machines that were built to produce interchangeable data (Ref. 3-3). The machine configuration was quite similar. The curves are nearly coincident.

3.1.1. Types of Wire-Rope Bending

There are two basic types of bending that wire ropes encounter in service--single bends and reverse bends. These are depicted in the sketches of Figure 3-3. As discussed later, they affect the rope differently. A reverse bend damages the rope more severely than two single bends in the same direction. Since bending-fatigue machines are in use that employ both types of bends, it is imperative that the presentation of all bending-fatigue data include the type of bending. In this Volume, following standard European practice, single-bend data are designated by the symbol, \surd , while reverse-bend data are designated \surd .

3.1.2. Stresses Induced by Bending Around a Sheave

The stresses induced in the wires of a wire rope when it is loaded in tension and bent around a sheave are extremely complex. (Some analytical approaches are presented and discussed later in this Volume.) The significant stresses are usually tensile, bending, and contact. The tensile stresses are caused by the tensile load, the bending stresses (tension and compression) are caused by changes in the radius of curvature of individual wires, and the contact stresses are caused by interwire contact and wire-sheave contact. Torsional stresses are usually insignificant unless the wire rope is subjected to large rotations. (For instance, to induce a shear stress of 100,000 psi in a 0.050-inch-diameter wire, a rotation of about 20 degrees per inch must be imposed.)

The relationships between the significant stresses change as the rope is subjected to different conditions. The life of a wire rope and the type and location of wire breaks are governed by the level and relative magnitude of these stresses.

3.1.3. Effects of Sheave-to-Rope Diameter Ratio, D/d

The sheave-to-rope diameter ratio (D/d), exerts a strong influence on the life of a wire rope and the mode of failure. At any given load, and with similar operating conditions, the service life of a wire rope will increase with increasing D/d values.

Most wire-rope catalogs discuss the effect of sheave size in terms of "relative service life" (RSL) for various D/d ratios. Typical curves from these sources are shown and discussed in Volume I of this handbook. To give an example of typical numbers of bending cycles-to-failure, Figure 3-4

(Ref. 3-4) shows several curves of cycles-to-failure versus D/d ratio for several values of load (in percent of actual rope breaking strength, %ABS). These safety factors and D/d ratios are fairly typical of those used in many Navy systems.

Another example of the effect of D/d ratio is shown in Figure 3-5. This plot is made from data presented by Muller (Ref. 3-5) in a paper published in 1961. Note that the trends are the same in both sets of data, even though the rope constructions are markedly different.

In most Naval installations, the D/d ratios tend to be smaller than those commonly used in many industrial applications, especially in mining. This is, of course, because of the need to conserve space and weight.

As mentioned earlier in the section on failure modes, the most common failure in normal wire-rope systems is Mode 2 fatigue on the crown wires that contact the sheave. These can be found by visual inspection. If, however, small D/d ratios are used, interstrand failures (Mode 1) can occur at high loads that may or may not be visible. Also, an even more dangerous failure location can result from very small D/d ratios and low loads. In this case the failure (Mode 2-type) can occur in the outer wires of the strand inside the rope where they contact the core. These are commonly known as "radial" breaks and are usually not visible. Both situations are dangerous and should be avoided if at all possible. Reference 3-6 shows how a change in D/d ratio can change the predominant failure mode at the same design factor. No published data or discussion of "radial" breaks is known.

3.1.4. Effects of Rope Load

Obviously, the service life of a wire rope under normal operating conditions depends strongly on the load that it carries. Several plots of cycles-to-failure versus load for some typical wire rope are shown in Figures 3-6 and 3-7. The data are from References 3-4 and 3-7. Another plot covering a much wider range of loads and D/d ratios is shown in Figure 3-8. Again, this is from Müller's work (Ref. 3-5). The curve shapes are said to be typical of that to be expected for all types of wire rope.

Figure 3-8 also illustrates another important point. While rope life is nearly always inversely proportional to load, the amount of variation can vary greatly depending on the load range. Note that in Figure 3-8, at the higher loads, the life decreases rapidly with only a small increase in load. Another good example of this is shown in Figure 3-2. These data were obtained in a series of experiments conducted for the Navy on aircraft arresting-gear rope. The actual service conditions were quite severe, and the test conditions were set up to simulate those severe conditions. A sharp decrease in rope life was evident at about 90,000 pounds tension, or about 50 percent of the rated breaking strength, and was accompanied by a change in failure mode from Mode 2 at the lower loads to Mode 1 at the higher loads. The change was fairly gradual and there were scattered Mode 1 failures in the load range just below 90,000 pounds. There were, however, few, if any, Mode 2 failures above 90,000 pounds.

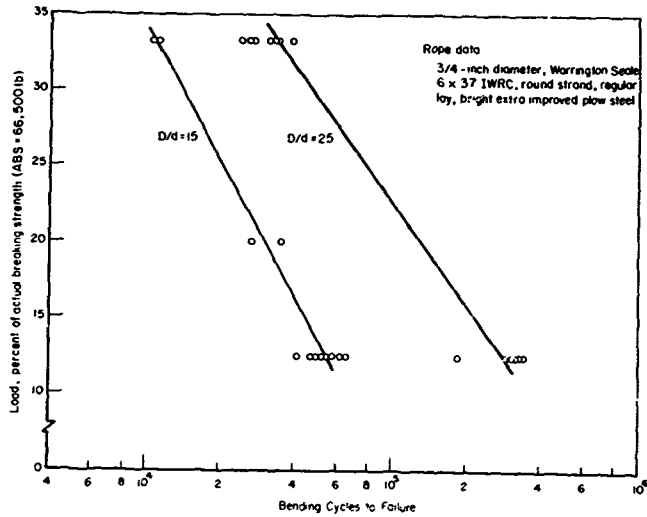


Figure 3-7. Results of Bending-Fatigue Tests on 3/4-Inch Wire Rope

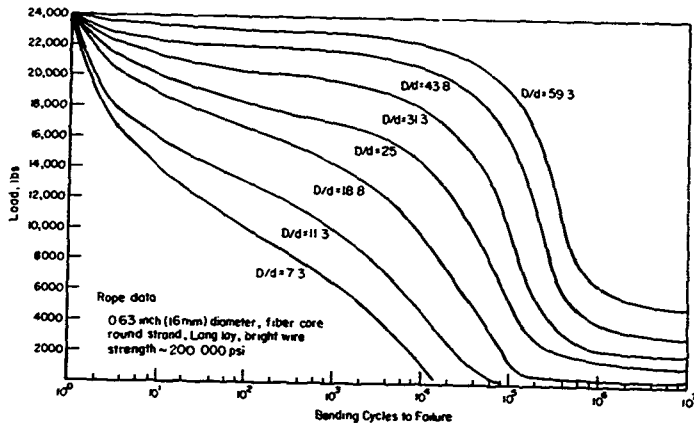


Figure 3-8. Bending-Fatigue Data for a Wide Range of Loads and D/d Ratios

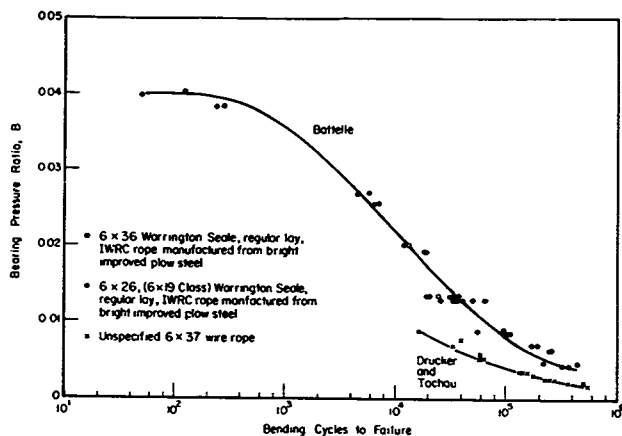


Figure 3-9. Comparison of Bending-Fatigue Data on the Basis of Bearing Pressure Ratio

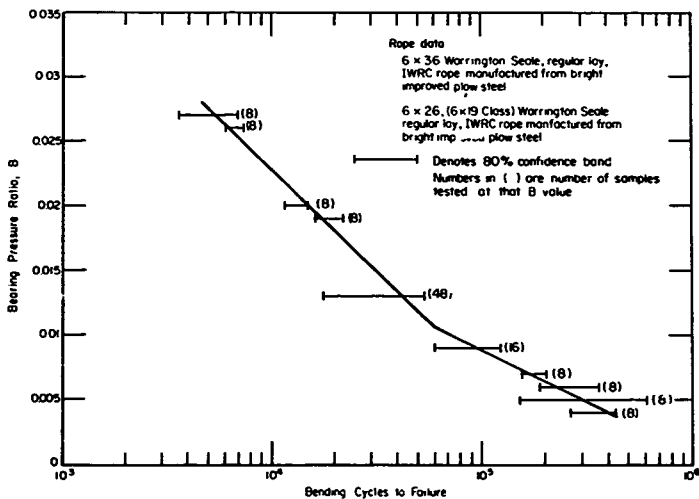


Figure 3-10. Eighty Percent Confidence Bands for Selected Bending Fatigue Data

$$\gamma = (df)(D/d) \quad , \quad (3-2)$$

where γ = life factor

(df) = design factor (actual
breaking strength/load)

D = sheave diameter

d = rope diameter.

The same Battelle data shown in Figures 3-9 and 3-10 are plotted in Figure 3-11 using γ . γ is more easily used for design than B, since it utilizes only the design factor and the D/d ratio, both normal design values. Also, it is directly, rather than inversely, proportional to rope life. The available data were approximately describable by two straight lines. Caution should be used in extrapolating these lines beyond existing data.

One drawback that B and γ both have is that neither accurately accommodate the fatigue characteristics of the wire material. The wire (or rope) ultimate strength is used in both parameters and this indicates nothing about the material's actual resistance to fatigue cycling. Some wire materials are more resistant to triaxial fatigue than others, even though they may have similar ultimate strengths. It may be advantageous in some cases to consider modifications to the B or γ factors that would include a fatigue strength parameter.

Another caution that must be observed when using either B or γ is that, even within the same rope type and strength, the resultant curves are only approximations and are valid only within limits. Significantly different rope types and strengths, and either harsh or gentle operating conditions may require development of different B or γ curves.

3.1.6 Effect of Wrap Angle

The wrap angle of a wire rope on a sheave has an almost constant effect on bending-fatigue life until the angle becomes small. At angles below a certain value, equivalent to an arc of contact of about one lay length, down to an arc equivalent of about 0.1 lay length, several investigators have reported a reduction in bending-fatigue life. Below an arc of 0.1 lay length, the sheave has virtually no effect on rope life. This is shown clearly in Figure 3-12 where data by Müller (Ref. 3-5) are shown for a rather uncommon rope construction. The same phenomenon was reported in Reference 3-14 and can be seen in Figure 3-13 (Ref. 3-7) for a more common rope. In this latter series of experiments, one section of rope was run over a sheave with a small wrap angle while another section of the same rope at the same load was run over a sheave with a 180-degree wrap angle. The number of broken wires at each location was recorded, and it was found that more external wire breakage occurred for the small wrap angles than for the 180-degree bends. These data also indicate the potential rope damaging effects of small wrap angles.

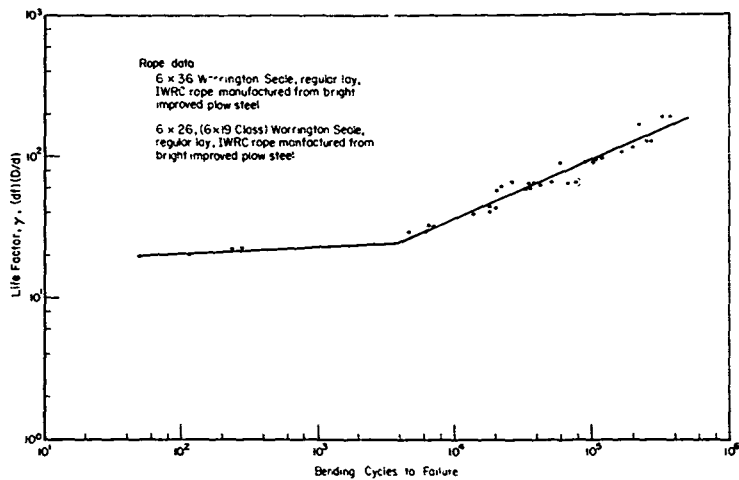


Figure 3-11. Bending Cycles to Failure Versus Life Factor, Y

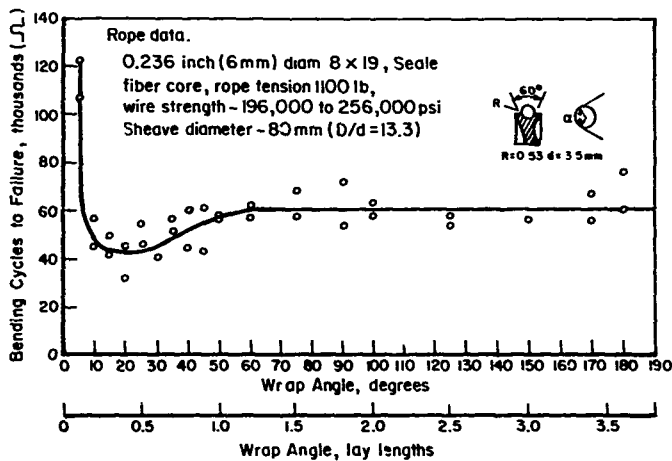


Figure 3-12. Effect of Wrap Angle on Wire Rope Bending-Fatigue Life

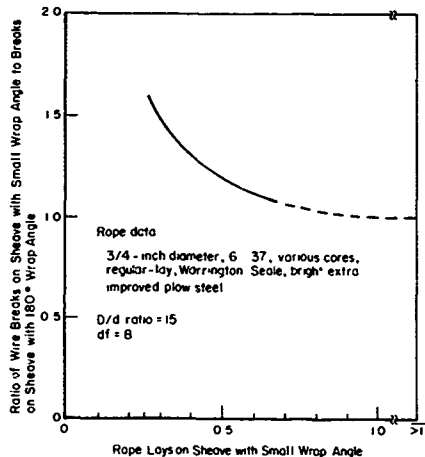


Figure 3-13. Relative Wire Breakage as a Function of Wrap Angle

3.1.7 Effect of Fleet Angle

In normal wire-rope systems using recommended fleet angles (1/2 to 1-1/2 degrees) and standard level-wind sheaves, the bending stresses induced by the rope curvature perpendicular to the plane of the level-wind sheave are insignificant. However, it is possible to induce significant bending stresses under unusual conditions--large fleet angles and/or abnormal sheave-throat shapes. The rope must bend around the lip of the sheave throat as it approaches the sheave. If this bend is long enough and the effective bending radius is small enough, this bend can affect rope life as much as inserting another sheave of that radius in the system.

If this condition is suspected, a layout should be made to check the effective bending radius and arc of contact. Then, using the material presented on the effects of wrap angle in section 3.1.6, and the material on the effects of D/d in section 3.1.5, the severity of the rope usage conditions can be assessed.

3.1.8 Effect of Rope Material

3.1.8.1 Wire Type.

By far the greatest majority of wire rope is made of plain carbon steel with a carbon content ranging between about 0.35 to 0.90 percent. Figure 3-14 illustrates the tensile strength of carbon steel wire as a function of wire diameter for various wire sizes. The common names for the various grades of wire are also shown.

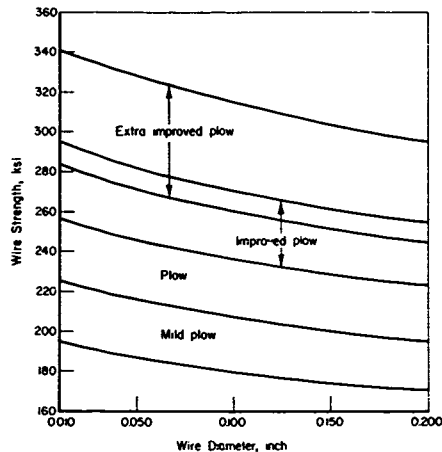


Figure 3-14. Tensile Strengths of Carbon-Steel Rope Wire as a Function of Diameter and Wire Grade.

Some wire rope is made of other metals, such as stainless steel and bronze. These are used in special situations, such as where corrosion, magnetic considerations, or high temperatures are involved. Some attempts have been made to use titanium wire with mixed success. Generally, wire ropes, made from other metals, when compared to carbon steel ropes, are weaker and/or have a lower fatigue life.

3.1.8.2. Wire Strength.

The effect of variations in carbon steel wire strength is shown in Figures 3-15 and 3-16. These figures show trends of data presented in a German wire rope publication (Ref. 3-15). According to Figure 3-15, strength of wires within a wire rope may be varied over a substantial range (at least from 200,000 to 300,000 psi), with all other factors such as load and D/d being held constant, and the bending-fatigue life will not change appreciably. On the other hand, if the design factor is held constant, as in Figure 3-16, the bending-fatigue life will decrease as the wire strength and rope load are increased. Work by other investigators on American-made rope has confirmed this trend, at least qualitatively, for higher wire strengths (Refs. 3-4 and 3-7).

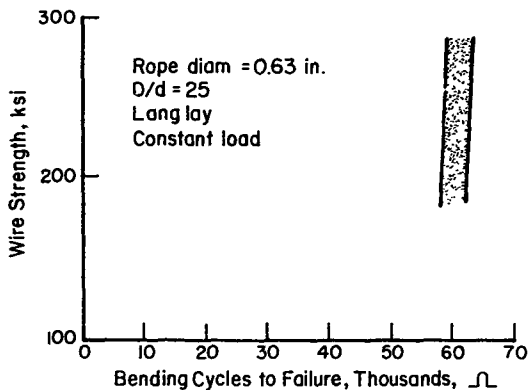


Figure 3-15. Effect of Wire Strength on Bending Cycles to Failure--All Tests Completed at Equal Rope Tensions

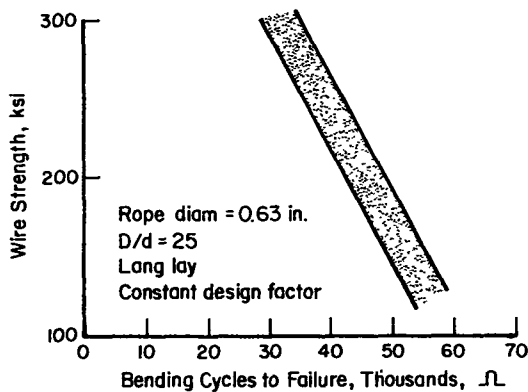


Figure 3-16. Effect of Wire Strength on Bending Cycles to Failure--All Tests Completed at Equal Design Factors

3.1.9. Effects of Swivels

No definitive data are known on the effects of swivels on the bending endurance of wire rope. Some rather inconclusive data (Ref. 3-7) indicate that swivels tend to degrade rope life, and their use should be avoided when possible. Each case, however, must be individually evaluated. The effect of swivels on the static strength of various rope constructions is discussed later in this Volume under section 3.3 on Rotation and Torque.

3.1.10. Effects of Rope Construction

There are many wire-rope constructions available. Most of these are special and are particularly useful in special applications. In this section each of the various design factors in wire-rope construction are discussed with respect to their effect on bending-fatigue life. In practice, all these factors must be considered jointly in the choice of a construction for a particular purpose.

The data that are presented cannot be used quantitatively for field applications. They all were obtained under laboratory conditions and are strictly applicable only to the specific ropes and conditions that were tested. They do, however, clearly illustrate the trends that can be expected in field use and, to a lesser degree, the amount of effect that changes in rope construction will have on the endurance of wire rope in bending.

3.1.10.1. Lay

Three different lays of wire rope are available--ordinary, Lang, and alternate. The first two are by far the most prevalent. Alternate-lay ropes are not common and, though no published data are available, are generally considered inferior to ordinary- and Lang-lay ropes in bending endurance.

Under "normal" conditions--round sheave grooves properly sized, ends restrained from rotation, no reverse bending, reasonable D/d ratio, etc.--Lang-lay rope is superior to ordinary lay in bending fatigue life. This superiority does not hold for conditions that vary from "normal". Figure 3-17 (Ref. 3-15) illustrates this observation for a variety of abnormal sheave geometries.

3.1.10.2. Number of Strands

Figure 3-18 (Ref. 3-15) shows that some constructions of eight-strand and nine-strand ropes are superior in bending fatigue to those with six strands. However, eight- and nine-strand ropes have a larger fiber core with correspondingly less metallic area and thus less strength for the same diameter. They are also less resistant to crushing.

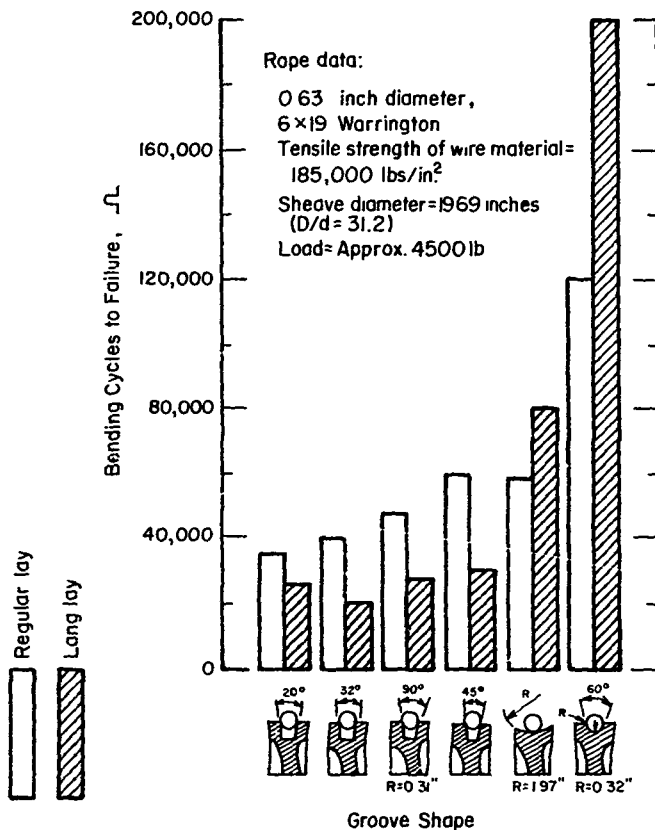


Figure 3-17. Effect of Rope Lay on Bending-Fatigue Life for Different Groove Shapes

Rope data

0 63 -inch diameter, IWRC, Lang lay

Wire strength - 220 ksi

Rope breaking strengths unspecified

Constructions (Strand construction designated in parentheses)

- | | |
|--|--|
| ① Warrington Seale, 6 × 37
(1 + 7 + (7 + 7) + 14) | ⑤ Filler wire, 8 × 19
(1 + 6 + 6F + 12) |
| ② Warrington Seale, 6 × 37
(1 + 8 + (8 + 3) + 16) | ⑥ Filler wire, 8 × 33
(1 + 8 + 8F + 16) |
| ③ Filler wire, 6 × 37
(1 + 6 + (8 + 8F) + 16) | ⑦ Filler wire, 9 × 19
(1 + 6 + 6F + 12) |
| ④ Warrington, 8 × 19
(1 + 6 + (6 + 6)) | |

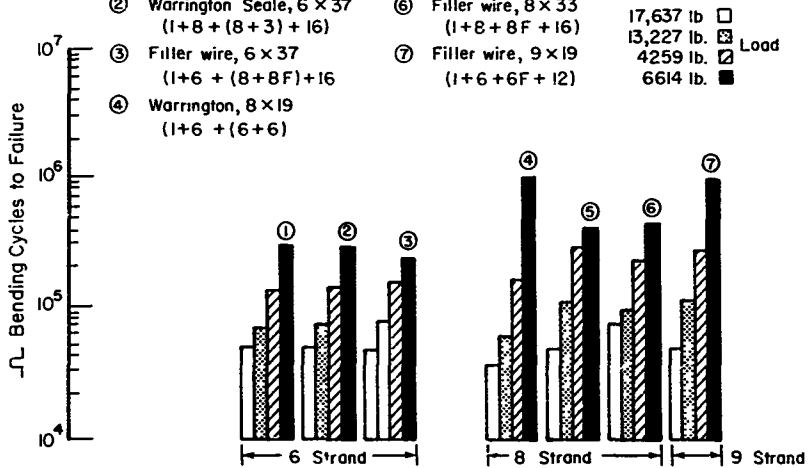


Figure 3-18. Effect of Rope Construction and Rope Load on Fatigue Life

3.1.10.3 Arrangement and Size of Wires.

Ropes with single-operation strands, such as Seale, Warrington-Seale, and filler-wire constructions, are generally superior to those with multiple-operation strands in bending endurance. Figure 3-19 (Ref. 3-16) illustrates this effect and also shows that, under those specific test conditions, the ropes with smaller wires--6 x 37--were superior to those with larger wires--6 x 19. This tendency is much less evident in other experiments conducted under different conditions and on different ropes (Ref. 3-4). Figure 3-20 shows the interaction of wire size (6 x 19 and 6 x 37) with load, while Figure 3-21 shows it with D/d ratio. Note that under these conditions and with this rope, the differences are much smaller, though the trend is still the same--the 6 x 37 rope has an equal or greater fatigue life.

3.1.10.4 Preforming.

Preformed wire ropes have significantly better bending endurance than do nonpreformed. Figure 3-22 (Ref. 3-17) shows this effect. Similar trends have been reported in Reference 3-18.

3.1.10.5 Core.

Wire ropes with a fiber core--either natural or synthetic--appear to have a somewhat greater endurance in bending than those with an IWRC when operated at the same design factor. Under this condition, for the same size rope, the load on the IWRC rope would be somewhat greater because of its inherently higher strength. If, however, the two types of rope are operated at the same load, their bending endurance is about the same, except under moderate conditions, where the fiber-core rope retains its superiority as Figures 3-23, 3-24, and 3-25 (Ref. 3-7) illustrate. Data from this same reference on differences between the various types of fiber cores--sisal, polypropylene, nylon, and Dacron--show mixed results and are not conclusive.

3.1.10.6 Special Constructions.

Innumerable special constructions of wire rope are made for particular applications. These constructions are generally inferior in bending endurance to normal round-strand wire rope. These constructions, however, may provide necessary increases in abrasion resistance, impact resistance or other factors in situations where rope usage is especially severe or unusual.

Information presented in Volume I of this Handbook on the characteristics of various rope constructions will be helpful in making a decision regarding use of special construction ropes. For example, comparisons are made between nonrotating, spin-resistant and torque balanced rope constructions (used for applications requiring special rope rotational characteristic); and smooth coil, half-locked and locked-coil track strand ropes (used for tramway and conveyer system applications).

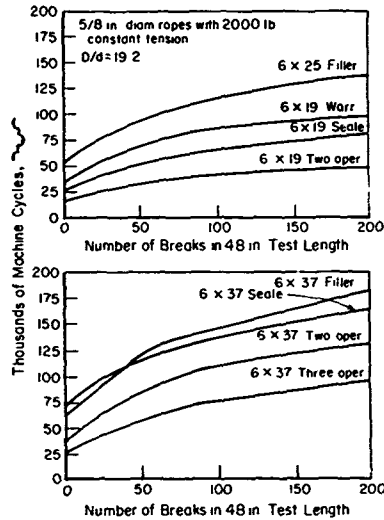


Figure 3-19. Comparative Reverse-Bend Fatigue Resistance of 6 x 19 and 6 x 37 Wire Rope

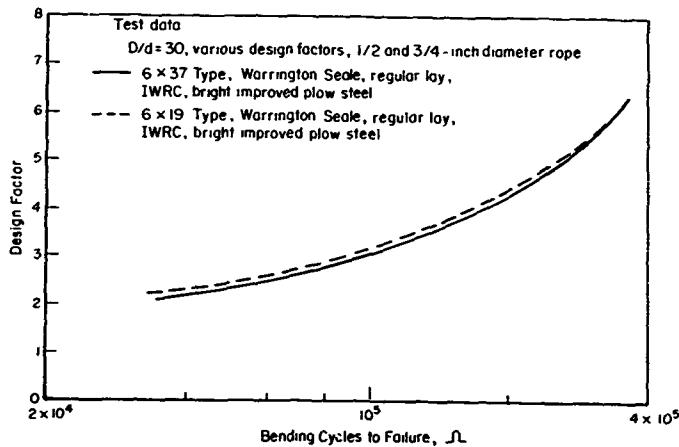


Figure 3-20. Effect of Design Factor on Bending-Fatigue Life

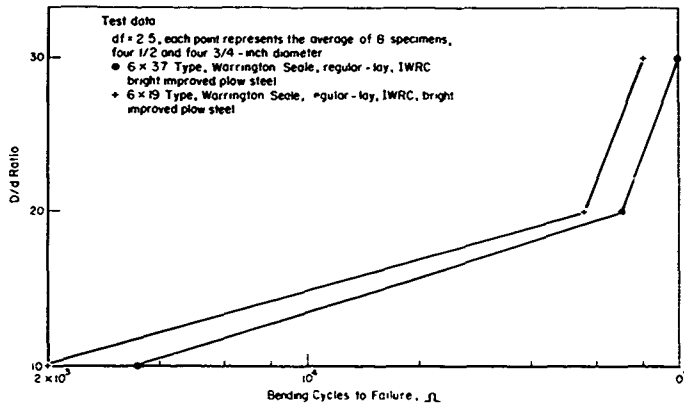


Figure 3-21. Effect of D/d Ratio on Bending-Fatigue Life

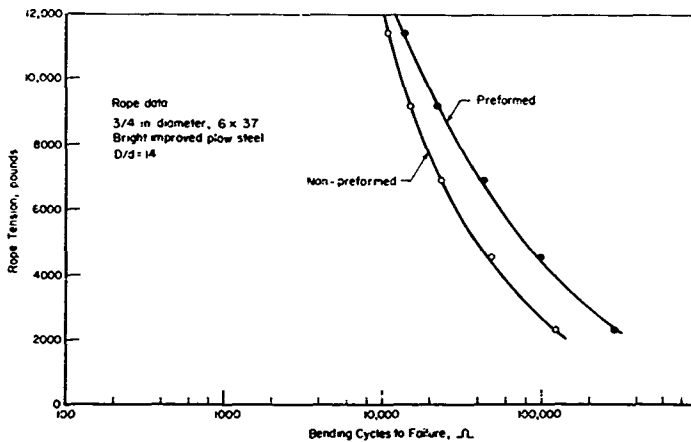


Figure 3-22. Bending-Fatigue-Life Data for Preformed and Nonpreformed Wire Rope Under Various Tensile Loads

- Notes 1 # Data extrapolated to same test load as used for fiber-core ropes
2 Rope data 6x37 Warrington-Seale, regular lay, IWRC rope manufactured from bright, improved plow steel

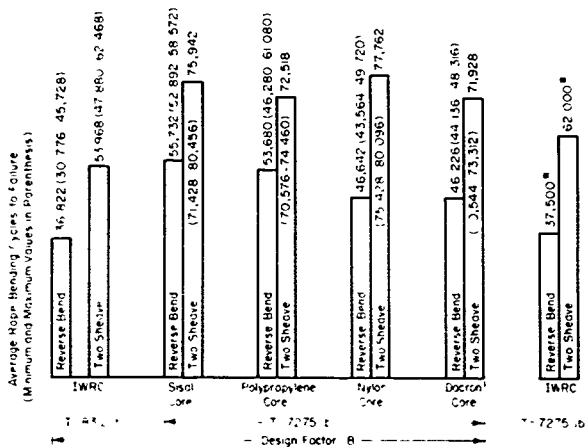


Figure 3-23. Comparison of Bending-Fatigue Data for 3/4-Inch Wire Rope With Several Core Types, D/d = 25, df = 3.

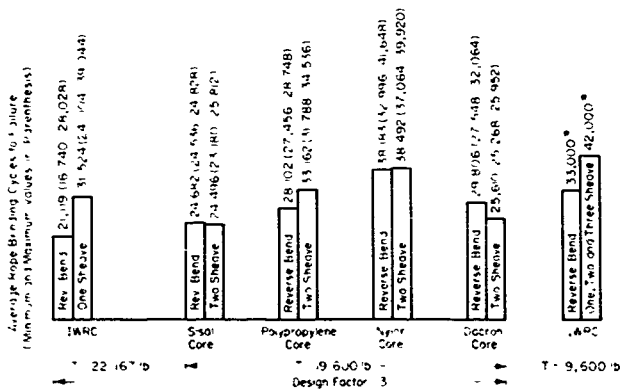
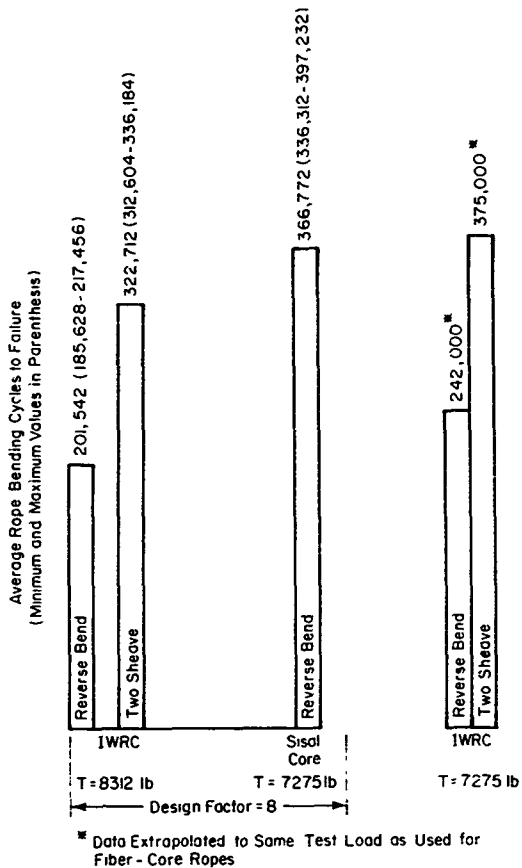


Figure 3-24. Comparison of Bending-Fatigue Data for 3/4-Inch Wire Rope With Several Core Types, D/d = 15, df = 8.



Rope Data: 6 x 37 Warrington-Seale, regular lay, IWRC rope manufactured from bright improved plow steel.

Figure 3-25. Comparison of Bending-Fatigue Data for 3/4-Inch Wire Rope With Two Rope Core Types, $D/d = 25$, $df = 8$

3.1.11. Effect of Sheave Hardness

The use of different metals in sheaves--hardened steel, cast iron, aluminum, bronze--reportedly has little or no effect on rope bending endurance (Ref. 3-15). Figure 3-26 (Ref. 3-19) also shows almost no sheave material effect in an experiment comparing aluminum and hardened steel sheaves under rather severe test conditions. However, one investigator (Ref. 3-16) has reported somewhat shorter rope life on soft metal sheaves. He surmises that this may be due to sheave throat deformation and subsequent roughness. These data are presented in Figure 3-27.

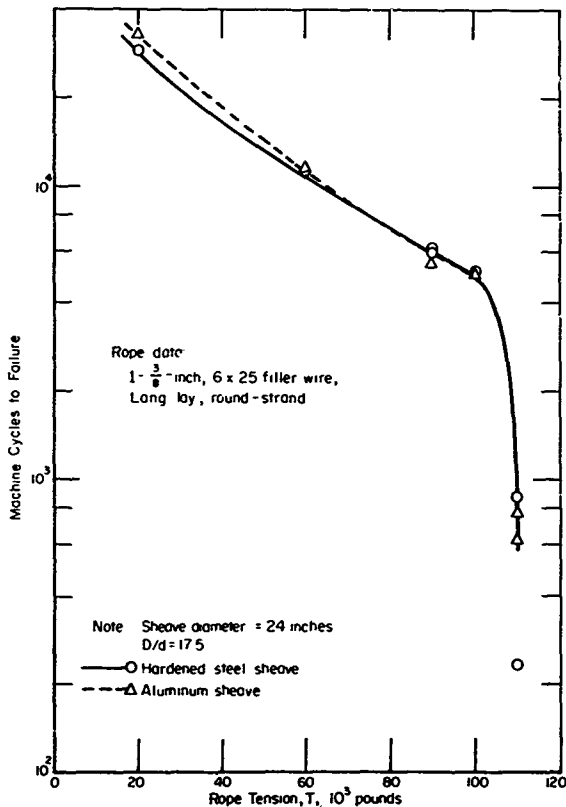


Figure 3-26. Results of Bending-Fatigue Tests on Aluminum and Hardened Steel Sheaves.

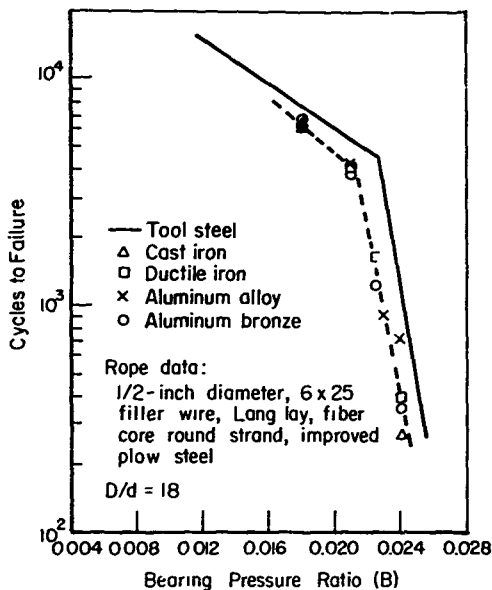


Figure 3-27. Effects of Sheave Material on Bending-Fatigue Life

Softer sheave materials such as nylon have been shown to improve bending endurance. Figure 3-28 (Ref. 3-5) compares the results of bending-fatigue experiments using cast iron and nylon-lined sheaves. It also illustrates the previously discussed superiority in bending fatigue life of eight-strand construction over six-strand.

Wooden sheaves have been used in the past for some applications, but their effect on rope life is minimal (Ref. 3-21) and their resistance to abrasion is low.

3.1.12. Effects of Sheave Throat Shape

The effects of sheave throat shape can be seen in Figure 3-17 (which was presented in an earlier section, 3.1.10 Effects of Rope Construction). Optimum bending endurance is obtained with a round groove slightly larger than the rope. Deviations from this configuration degrade rope performance in bending. As Figure 3-17 illustrates, the effect of throat shape variations on rope life is different for regular- and Lang-lay rope constructions.

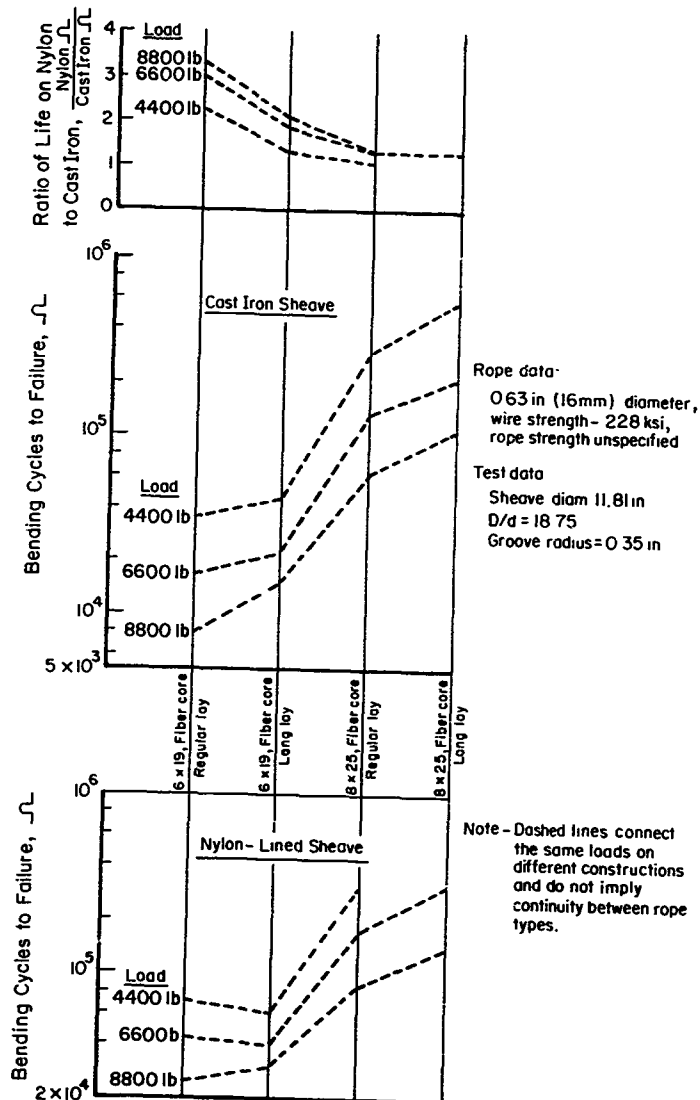


Figure 3-2 . Comparison of Bending-Fatigue Resistance of Several Rope Constructions on Nylon-Lined and Cast-Iron Sheaves

3.1.13. Effects of Corrosion, Lubrication, and Coatings

The effects of lubrication, coatings, and corrosion on the bending endurance of wire rope are highly interrelated. Ropes are lubricated for two reasons: to retard corrosion, and to reduce interwire friction which promotes interwire motion as the rope is bent over a sheave. Metallic coatings such as zinc are applied primarily to reduce corrosion but also are said to act as a lubricant between the rope wires.

3.1.13.1. Corrosion

A variety of corrosive environments are potentially detrimental to rope life. Open air, fresh water and seawater are by far the most commonly incurred. Figure 3-29 (Ref. 3-5) shows a comparison between the bending fatigue life of a wire rope previously corroded in air with an identical uncorroded rope. Note that both ropes have been degreased.

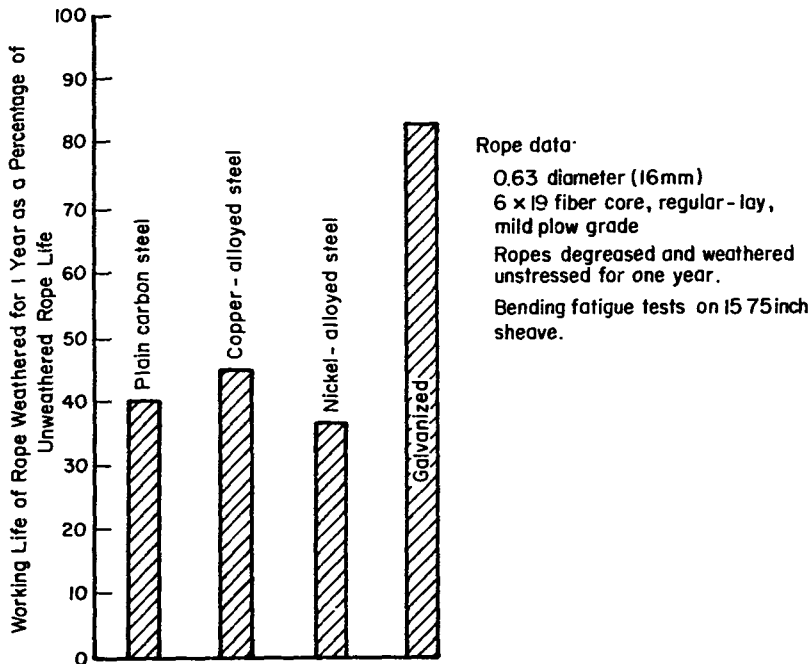


Figure 3-29. Comparison of Bending-Fatigue Resistance of Corroded and Uncorroded Wire Rope

Table 3-1 (Ref. 3-22) shows the difference between galvanized and aluminum-coated wire rope tested in air and seawater. The aluminum-coated wires were redrawn. The type of galvanized wire was not specified. Although the fatigue life of the aluminum-coated rope was reduced substantially below that of the galvanized rope for the seawater tests involving no lubrication, the bending fatigue life in seawater was about equivalent for the two ropes if the aluminum rope was lubricated periodically during cycling. No published data are known for uncoated wire rope under these conditions.

TABLE 3-1. RESULTS OF ENDURANCE LIFE TESTS ON 3/4-INCH DIAMETER ALUMINUM COATED AND GALVANIZED IMPROVED PLOW STEEL WIRE ROPES, 6 x 19--FIBER CORE.

(Aluminum-coated wires were drawn after coating.)

Wire Coating	Environment	Lubrication During Test	Direct Tensile Load (lbs)	Cycles* to First Wire Failure	Cycles to Ultimate Rope Failure	Number of Strands Broken Ultimate Failure	Average Number of Cycles to Ultimate Failure		
Galvanized (Breaking Strength 45,500 lbs)	Air	Once Daily	11,400	18,400 29,861	27,200 25,050	2 1	26,125		
			9,120	21,266 36,170	36,744 39,303	1 1	38,054		
			6,800	20,633 52,280 24,880	51,295 52,932 57,496	1 1 6	53,907		
			4,560	51,778 42,614	110,935 92,846	2 1	101,990		
	Seawater*	None	6,800	32,442 38,859 30,080	45,607 46,017 54,042	1 1 1	57,889		
	Aluminum (Breaking Strength 43,400 lbs)	Air	Once Daily	11,400	22,570 22,510	29,552 28,240	1 6	28,894	
				9,120	29,800 31,825	41,875 39,047	1 2	40,461	
				6,800	33,700 25,930 41,235	58,800 51,953 61,760	2 1 1	57,514	
4,560				50,821 51,058	81,124 72,232	6 1	76,678		
		None		6,800	17,150 19,200 13,150	24,322 27,104 19,367	1 3 1	23,578	
				Once Daily	6,800	31,145 37,355 36,716	53,902 42,831 60,473	1 2 1	52,455

*Although there is no good correlation between cycles to first wire failure and cycles to ultimate failure, the data on first wire failure are included for general information.

**Galvanized ropes were not run in seawater, with daily lubrication, because the life in seawater without daily lubrication approaches that of the rope in air with lubrication, leaving little margin for improvement.

3.1.13.2. Lubrication

Current Navy specifications (RR-W-410C) require that uncoated steel wire ropes be coated with a suitable lubricant during the process of manufacture. The lubricant must have a mineral base compounded with additives designed to provide corrosion protection and lubricating qualities during shipping, storage, handling, and the initial period of service and a suitable base for subsequent field relubrication. The lubricant must also be free from substances injurious to steel wires and fiber cores.

Proper lubrication of wire rope running on sheaves is an important factor in maximizing fatigue life. An example of the effect of lubrication is shown in Figure 3-30 (Ref. 3-15). As the figure shows, lubricated rope can have a lifetime as much as seven to eight times longer than unlubricated rope. The type and frequency of lubrication is known to influence wire-rope fatigue life, but few well-documented data are available.

3.1.13.3. Coatings

Three types of coatings are commonly available on wire rope--zinc, aluminum, and plastic. Of these, zinc is by far the most common.

Zinc-coated wire for ropes is manufactured according to three basic procedures:

1. Hot-dip galvanizing with no further processing (finally galvanized wire)
2. Hot-dip galvanizing at an intermediate stage in the drawing process (drawn galvanized wire)
3. Electrogalvanized wire.

It is generally agreed (Refs. 3-15 and 3-23) that in noncorrosive environments finally galvanized rope is somewhat weaker and less resistant to bending fatigue than rope of the same type made from bright (uncoated) wire. However, the effect of reduced bending fatigue endurance is probably less noticeable and may even be reversed in many corrosive atmospheres, especially seawater. Unfortunately, no published data are known to exist that verify these statements.

On the other hand, there is general agreement (Refs. 3-15, 3-16, and 3-23) that wire rope made from drawn-galvanized and electrogalvanized wire is equal in strength to uncoated wire rope and is superior in bending endurance in both corrosive and noncorrosive atmospheres. Figure 3-31 (Ref. 3-23) compares the bending fatigue behavior of drawn-galvanized wire rope with that of uncoated wire rope. No details describing loads or sheave sizes were given for these tests. The testing machine imposed reverse bends, and the rope was rotated during testing.

The thickness of zinc coating also appears to have an effect on bending fatigue life. Figure 3-32, which is also from Reference 3-23 and also provides no test details, shows not only the superiority of drawn galvanized

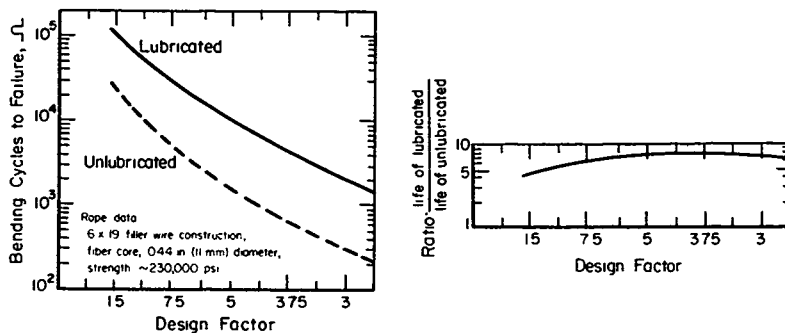


Figure 3-30. Effect of Lubrication on the Bending-Fatigue Life of a Rope for Various Design Factors.

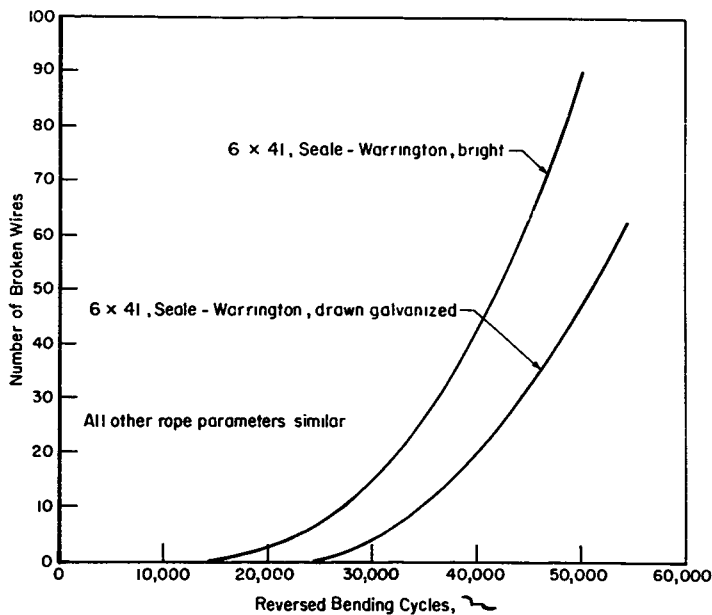


Figure 3-31. Comparison of Bending Endurance of Wire Ropes Made From Bright (Uncoated) and Drawn Galvanized Wire.

and electrogalvanized wire rope, but also indicates a substantial increase in fatigue resistance for rope made with wire with thicker zinc coatings. No American data are known on this subject.

Aluminum-coated wire for wire rope has been used infrequently. Few data are available for this type of rope, especially in bending fatigue. The data shown in Table 3-1 represent most of the available published information.

Plastic-coated wire rope is widely used in light service operations and in special applications such as food-handling equipment. Figure 3-33 (Ref. 3-24) shows comparative fatigue life data for bare and nylon-jacketed ropes. Although the sizes of the ropes are not given, they are believed to be quite small. Larger plastic-coated ropes are being used with increasing frequency. No published bending-fatigue data are known to be available for the larger plastic-coated sizes.

A major difference in the type of corrosion resistance provided by the metallic coatings, as compared to the plastic, is the wire behavior after the coating has been pierced. Both zinc and aluminum coatings protect the steel wire galvanically, and small holes do not adversely affect the corrosion protection provided by the coating. However, once a plastic coating has been penetrated, it no longer protects the steel and may even serve to retain corrosive fluids within the cable.

3.1.14. Effect of Reversed Bends

Figures 3-34 and 3-35 (Ref. 3-5) show the adverse effect of reverse bending for Lang-lay and regular-lay ropes under various loads and sheave ratios. Note that Lang-lay ropes are more affected than regular-lay. Table 3-2 (Ref. 3-7) also illustrates the fatigue life reduction due to reversed bends.

Table 3-2. FATIGUE LIFE REDUCTION DUE TO REVERSE BENDS

Rope Data: 3/4-inch diameter, regular lay, IWRC, 6 x 37, extra improved plow steel

Rope Diameter, inch	D/d	Design Factor	Life Reduction Factor*
1/2	15	3	0.807
1/2	15	8	0.740
1/2	25	3	0.527
1/2	25	8	0.556
3/4	15	3	0.697
3/4	15	5	0.848
3/4	15	8	0.793
3/4	25	3	0.670
3/4	25	8	<u>0.819</u>
Average			0.717

$$*\text{Life reduction factor} = \frac{\text{Reverse-bend cycles}}{\text{Single-bend cycles}}$$

- A Finally galvanized (zinc deposit 0.47 oz/sq ft)
 B Drawn galvanized (zinc deposit 0.28 oz/sq ft)
 C Drawn galvanized (zinc deposit 0.48 oz/sq ft)
 D Electro galvanized (zinc deposit 0.52 oz/sq ft)
 All other rope and test parameters similar

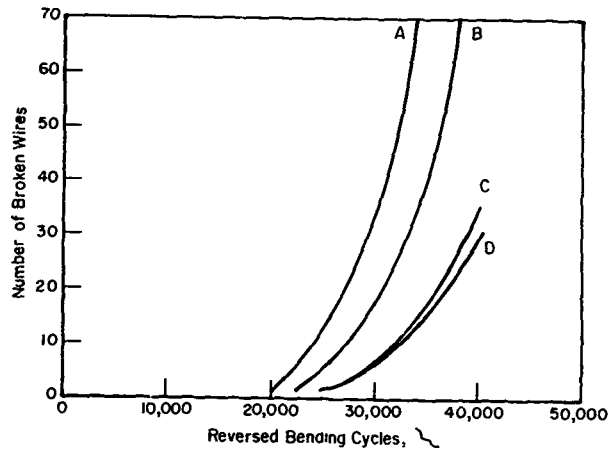


Figure 3-32. Comparison of Bending Endurance of Various Galvanized Wire Ropes

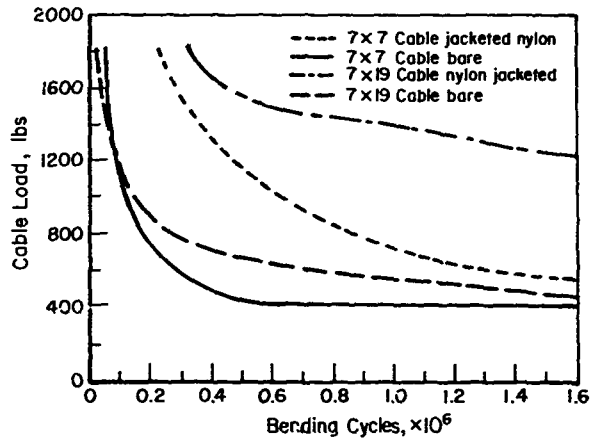


Figure 3-33. Bending-Fatigue Data for Uncoated and Nylon-Jacketed Cable

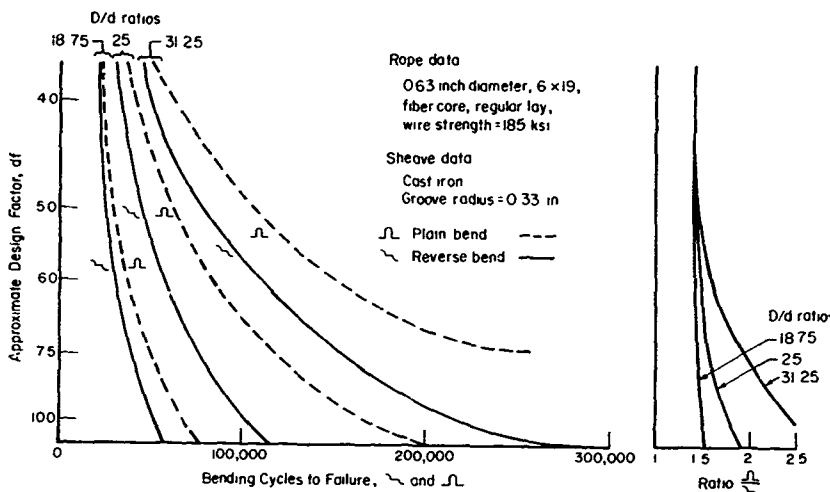


Figure 3-34. Effect of Plain and Reverse Bending on the Fatigue Life of Regular-Lay Wire Rope.

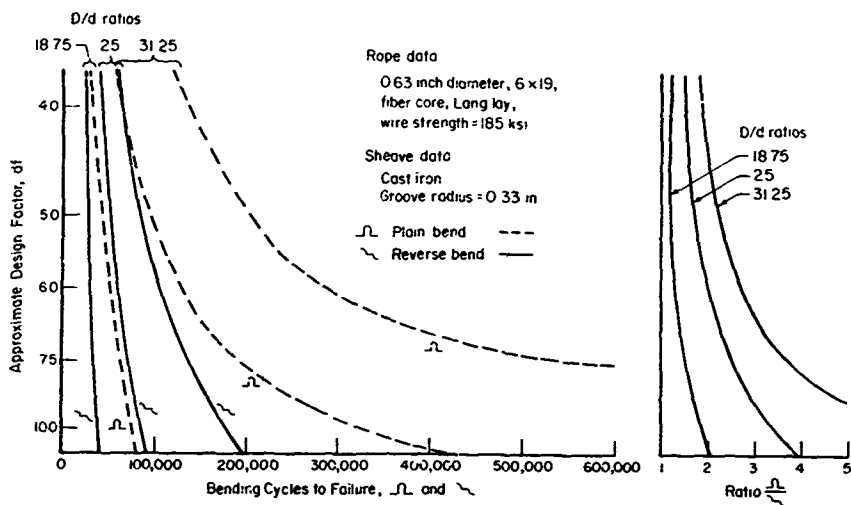


Figure 3-35. Effect of Plain and Reverse Bending on the Fatigue Life of Lang-Lay Wire Rope.

Although no data are known, it has been stated that long distances between reverse bends alleviate their adverse effect on rope life because of the natural tendency of a wire rope in a field system to rotate slightly as it moves through the system.

3.2. AXIAL FATIGUE OF WIRE ROPE

Many of the effects noted in bending endurance of wire rope can also be found in axial fatigue except, of course, those in which the sheave plays a part. Generally, axial fatigue data are less available in the literature and, as with bending data, must be interpreted with care.

3.2.1. Effect of Cyclic Axial Loads on Wire Rope Fatigue

Several load-cycle characteristics must be considered in axial fatigue of wire rope--the maximum load, the mean load, and the load range. These are illustrated in Figure 3-36 (Ref. 3-25). Of these, the load range has the most effect on fatigue life. An illustration of the qualitative effect of load range is shown in Figure 3-37 (Ref. 3-26) for one specific wire rope construction. The investigator who produced these data indicates that mean load has little or no effect on the axial fatigue life of wire rope. This is

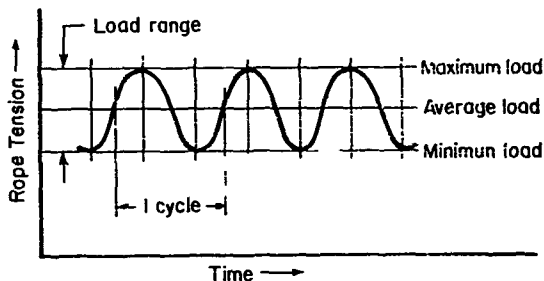


Figure 3-36. Characteristics of Load Cycle Pattern Used in Axial Fatigue Tests

illustrated in Figure 3-38 (Ref. 3-27). Figure 3-39, from Reference 3-28, also illustrates that axial fatigue life data for wire strand are ordered only when plotted versus load range and not maximum or mean load.

3.2.2. Effect of Cyclic Axial Loads on Steel Strand Fatigue

The effect of cyclic axial loads on the fatigue behavior of steel strands of various configurations is shown in Figure 3-40 (Ref. 3-29). Wire sizes and strengths were not specified for these data.

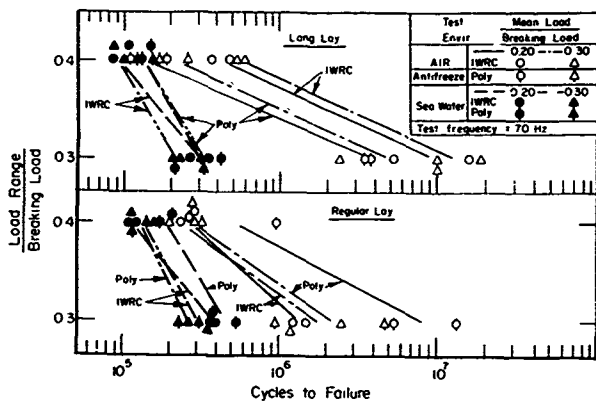


Figure 3-37. Axial Fatigue Test Data for 1/2-Inch Diameter, 6 x 25 Polypropylene Core and IWRC, Bright Improved Plow Steel, Wire Rope.

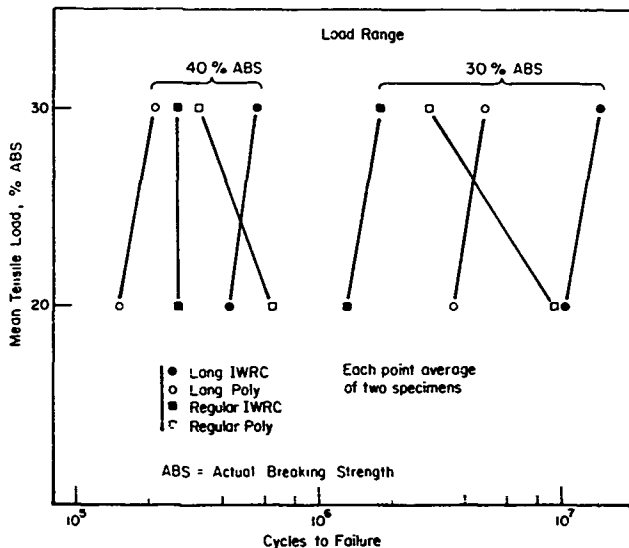
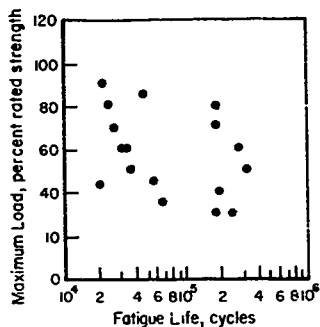
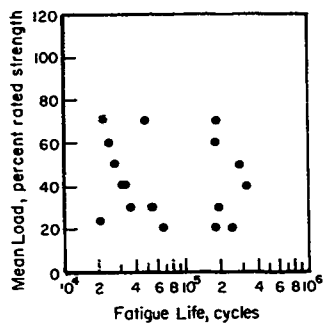


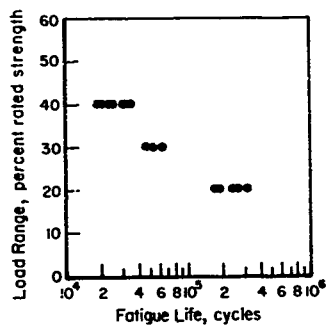
Figure 3-38. Effect of Mean Load on the Axial Fatigue of IWRC and Polypropylene Core Wire Rope.



a Maximum Load Versus Cycles to Failure



b Mean Load Versus Cycles to Failure



c. Load Range Versus Cycles to Failure

Figure 3-39. Effect of Maximum, Mean and Range of Load on the Axial Fatigue Life of 1-Inch, 1 x 19 Galvanized Strand

3.2.3. Effects of End Fittings

Unlike results for bending fatigue, available axial fatigue data indicates that the type of end fitting used to anchor the rope has a significant effect on the fatigue resistance of that wire rope. This can be seen in Figures 3-40 and 3-41 (Ref. 3-29). In every case, the swaged sockets produced greater axial fatigue lives than cast zinc sockets. Care must be taken during swaging, however; if such care is not taken, the swaged fittings will perform no better than zinc sockets.

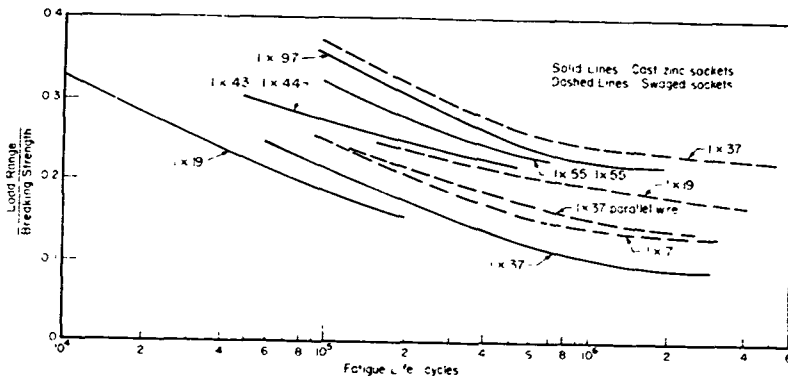


Figure 3-40. Effect of Construction and Socketing Technique on the Axial Fatigue Life of Steel Strand.

3.2.4. Effects of Core

Figure 3-41 also shows (at least for the experimental conditions tested) that fiber-core rope exceeds IWRC rope in fatigue life when tested at the same design factor. This difference in fatigue resistance is reportedly due to complete degradation of the wire rope core after only a small number of axial load cycles (Ref. 3-29).

3.2.5. Effects of Lay

The difference in fatigue behavior of Lang-lay and regular-lay rope subjected to axial loads is not completely clear. The only published data known are shown in Figure 3-38 (Ref. 3-27). According to this source, it appears that for IWRC rope, Lang-lay is superior, while for polypropylene-core rope, regular-lay is better in its resistance to axial fatigue. However, the conditions under which the data were generated are sufficiently different, that any conclusions are only speculative.

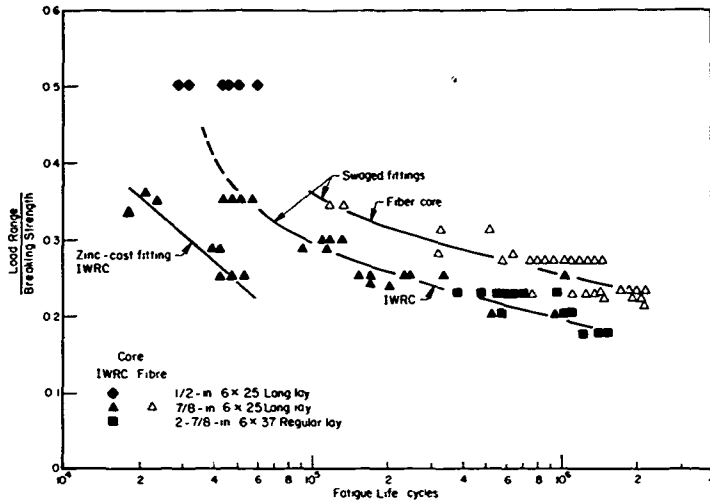


Figure 3-41. Effect of Diameter, Core Material, Construction, and Socketing Technique on the Axial Fatigue Life of Steel Wire Rope

3.2.6. Effects of Rope Construction and Material

The results of a series of cyclic tension tests on different constructions are shown in Table 3-3 (Ref. 3-30). These experiments were conducted in air with the ends fixed to prevent rotation. Figure 3-42 (Ref. 3-29) shows the effect of wire material on axial fatigue life of wire rope. At the higher load ranges, rope behaves the same in axial fatigue as in bending--operating at the same design factor, the rope made from the stronger wire has a shorter life. However, at the lower load ranges the difference almost disappears and ropes made from different strength wires behave similarly.

3.2.7. Effect of Frequency

The effect of cyclic frequency on axial fatigue life is believed to be small so long as reasonable rope temperatures are maintained. There is, however, no trustworthy published data to firmly substantiate this belief. Of course, if the frequency is high enough to raise the rope temperature to a point where the rope material properties are affected, the fatigue life will be changed.

Table 3-3. RESULTS OF CYCLIC TENSION TESTS

Test Number	Specimen	Ultimate Breaking Strength (U.B.S.-lbs)	Load Range		Cycle Period (Sec.)	No. of Cycles to Failure	
			Low ? L.B.S.	High ? L.B.S.		One Wire	Whole Rope
1	20' - 1/4" 1 x 19 GAC (Bare)*	10,700	27.5	52.5	8	30,733	--
2	20' - 1/4" 1 x 19 GAC (Bare)	10,700	27.5	52.5	8	29,392	--
3	20' - 1/4" 1 x 19 GAC (Bare)	10,700	20.0	40.0	7	74,640	--
4	20' - 1/4" 1 x 19 GAC (Bare)	10,700	20.0	40.0	7	65,374	--
5	20' - 1/4" 1 x 19 GAC (Bare)	10,700	12.5	27.5	6	103,836	--
6	20' - 1/4" 1 x 19 GAC (Bare)	10,700	12.5	27.5	6	110,138	--
7	20' - 1/4" 1 x 19 GAC (Bare)	10,700	5.0	15.0	5	118,727	--
8	20' - 1/4" 1 x 19 GAC (Bare)	10,700	5.0	15.0	5	187,587	--
9	20' - 1/4" 1 x 19 GAC (Bare)	10,700	5.0	15.0	5	99,233	--
10	20' - 1/4" 1 x 42 Galv. IPS Strand**	10,880	27.5	52.5	8	--	57,056
11	20' - 1/4" 1 x 42 Galv. IPS Strand	10,880	27.5	52.5	8	--	53,909
12	20' - 1/4" 1 x 42 Galv. IPS Strand	10,880	27.5	52.5	8	--	40,842
13	20' - 1/4" 1 x 42 Galv. IPS Strand	10,880	27.5	52.5	8	--	31,844
14	20' - 1/4" 1 x 42 Galv. IPS Strand	10,880	27.5	52.5	8	--	48,416
15	20' - 1/4" 1 x 42 UHS Strand***	13,000	27.5	52.5	8	--	71,482
16	20' - 1/4" 1 x 42 UHS Strand	13,000	27.5	52.5	8	--	40,938
17	20' - 1/4" 1 x 42 UHS Strand	13,000	27.5	52.5	8	--	40,309
18	20' - 1/4" 1 x 42 UHS Strand	13,000	27.5	52.5	8	--	41,891
19	20' - 1/4" 1 x 42 UHS Strand	13,000	27.5	52.5	8	--	39,770
20	20' - 9/32" 1 x 50 Aluminized and Swaged IPS Rope	9,900	27.5	52.5	8	--	106,051
21	20' - 9/32" 1 x 50 Aluminized and Swaged IPS Rope	9,900	27.5	52.5	8	--	118,867
22	20' - 9/32" 1 x 50 Aluminized and Swaged IPS Rope	9,900	27.5	52.5	8	--	109,156
23	20' - 9/32" 1 x 50 Aluminized and Swaged IPS Rope	9,900	27.5	52.5	8	--	96,444
24	20' - 9/32" 1 x 50 Aluminized and Swaged IPS Rope	10,500	27.5	52.5	8	--	90,805
25	20' - 5/16" 3 x 19 Gal. IPS Torque Balanced Rope	10,500	27.5	52.5	8	--	No Failure After 622,208 cycles
26	20' - 5/16" 3 x 19 Gal. IPS Torque Balanced Rope	10,500	27.5	52.5	8	--	No Failure After 261,366 cycles

* GAC = Galvanized aircraft cable (wire rope).

** Galv. IPS = Galvanized improved plow steel.

*** UHS = Ultra-high strength.

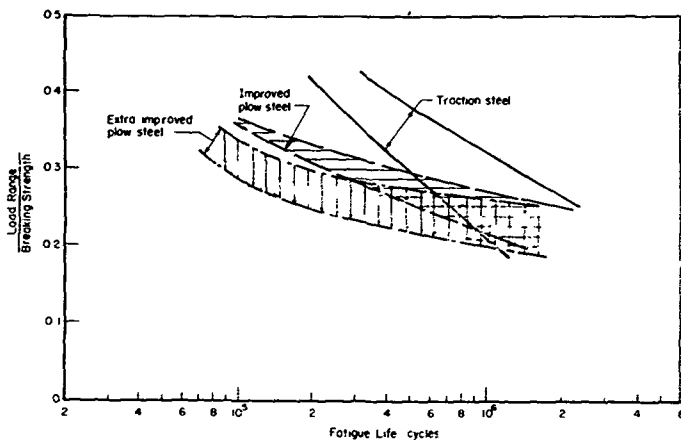


Figure 3-42. Effect of Wire Strength on the Axial Fatigue Behavior of a Steel Wire Rope (Unknown Construction).

3.2.8. Effect of Corrosion

As in bending fatigue, corrosion has a detrimental effect on the axial fatigue life of wire rope. Figure 3-37 (Ref. 3-26) illustrates the difference in fatigue lives of wire rope cyclically tensioned in corrosive and noncorrosive environments. The ropes tested in seawater were degreased and exposed to flowing seawater for 48 hours before testing and were kept immersed in flowing seawater throughout the testing. The specimens cycled in the noncorrosive environment exhibited significantly longer lifetimes. It is pertinent that these experiments were conducted at a very high frequency of approximately 70 cycles per second. Consequently, it was necessary to cool the noncorroded specimens with the polypropylene cores with a "noncorrosive" antifreeze rather than cycling them in air. The effect of this is unknown. Also, because of the high frequency, the exposure to seawater was short, so the actual cycle values are probably not indicative of what might be expected at a lower frequency and longer exposure times. A later report (Ref. 3-31) on a continuation of this program, tends to confirm this; however, this work was completed with the same equipment limitations and high frequencies.

3.2.9. Effect of Diameter

The effect of diameter on the axial fatigue resistance of wire rope is discussed briefly in Reference 3-13. It is stated there that axial fatigue life tends to decrease as the rope size increases, for the same construction and wire strength. Data presented in Figure 3-41 tend to contradict this conclusion, however. If rope size is a factor in axial fatigue resistance, the effect is probably relatively small and due primarily to the decrease in ductility of larger wires at equivalent strengths.

3.2.10. Effects of Lubrication and Coating

Figure 3-43 (Ref. 3-29) shows that lubrication and coatings have an effect on the axial fatigue behavior of steel wire strand. No similar data are known for wire rope, but the trends would quite likely be similar.

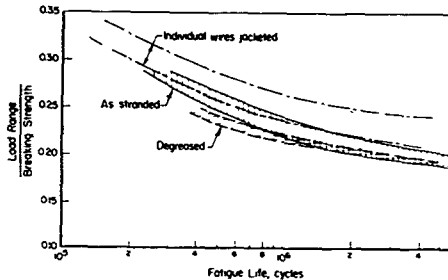


Figure 3-43. Effect of Wire Coating and Lubrication on the Axial Fatigue Life of 3/4-Inch, 1 x 37 Steel Wire Strand.

It has also been stated (Ref. 3-29) that zinc coating of rope wires (presumably drawn after coating) may cause slight improvement in the axial fatigue endurance of wire rope, but no data have been found in support of this conclusion.

3.3. ROTATION AND TORQUE

A characteristic of wire rope that must be considered in all systems, especially those in which both ends are not fixed against rotation, is the tension-induced torque and resulting rotation. The construction of nearly all wire ropes is such that a tension load induces torque in the rope. Certain three-strand constructions are very nearly torque-balanced, but in some other constructions the torque build-up is surprisingly high. Lang-lay rope is particularly prone to rotation and should never be used with an end free to rotate. This rotation can be very troublesome in several respects.

3.3.1. Kink Formation

If the load on a rotated rope is suddenly removed (or even decreased substantially) the rope may loop, and then, as the load is reapplied, form a tight kink which will drastically lower the rope breaking strength. This behavior was successfully simulated in a laboratory investigation (Ref. 3-32) conducted to determine the tension-rotation, torque and kink characteristics of several types of low-torque oceanographic tension members, contrahelically wrapped strands and two types of three-strand wire rope. Kinks were induced by suspending a length of rope, applying a low tensile load with a free-hanging weight, and then rotating the rope manually. Applied torque was measured intermittently, until a kink formed. A brief summary of the results is shown in Table 3-4.

Table 3-4. TORSIONAL CHARACTERISTICS OF VARIOUS CONSTRUCTION

Property	Cable Type					
	1 x 19 GAC, 1/4" Diameter, Jacketed	1 x 42 UHS, 1/6" Diameter, Torque Balance	1 x 43 Gal., 1PS, 1/4" Diameter, Torque Balance	1 x 41 Gal., 1PS, 9/32" Diameter, Torque Balance	1 x 19 Aluminized, Sogged, 9/32" Diameter	3 x 19 Gal., 1PS, 3/16" Diameter Torque Balance
Rated breaking strength, lb	8,200	13,000	9,000	9,000	9,900	10,300
Measured average breaking strength, ends fixed, lb	10,700		10,880	10,100	9,400	10,500
Torsional spring constant per unit length at 0 turns, lb/turn	14	30	20	50	5.0	7.9
) + Turns		16	20	50	5.8	7.0
) - Turns						
) (+/-) lb/turn						
Torque balance at zero turns, ft-lb/ft	4.75 x 10 ⁻⁴	3.75 x 10 ⁻⁴	10.5 x 10 ⁻⁴	3.75 x 10 ⁻⁴	24.5 x 10 ⁻⁴	Approximately zero
) + Turns	--	--	5.40 turns	3.40 turns	26.0 turns	24.2 turns
) at kink	--	--	2.5 ft-lbs	9.0 ft-lbs	5.4 ft-lbs	6.5 ft-lbs
) + Torque	--	--	-14.75 turns	-3.90 turns	-13.20 turns	-24.20 turns
) formation	--	--	-4.30 ft-lbs	-3.90 ft-lbs	-3.15 ft-lbs	-8.25 ft-lbs
) properties for	--	--				
) length = 17 ft	--	--				
) tension = 4.5 lb	--	--				
) at kink	--	--				
) Torque	--	--				
) at kink	--	--				

* GAC = Galvanized aircraft cable.

** UHS = Ultra-high strength.

*** 1PS = Improved plow steel.

In another experiment (Ref. 3-33) on an unidentified rope (presumably a three-strand construction) the tension member was loaded with a free-hanging weight. After the rope had stabilized and rotation had ceased, the weight was rapidly lowered to the ground. No kinks were formed. Though no published data are available, it is generally assumed that other rope constructions (such as 6 x 37, 18 x 7, etc.) would kink under a similar test.

3.3.2. Breaking Strength

Another potential problem with suspended ropes allowed to rotate freely is a degradation of breaking strength. This is particularly a problem in most types of low-rotation wire-rope constructions, such as 18 x 7 nonrotating and 8 x 19 spin resistant. Some illustrative data are presented in Table 3-5 (Ref. 3-34). Figures 3-44 and 3-45 (Ref. 3-34) show the torque and rotational properties of the 18 x 7 ropes described in Table 3-5. No published data are available for other constructions; however, proprietary tests have shown similar behavior for 18 x 7 nonrotating and 8 x 19 spin-resistant ropes. In comparative tests regular-lay, six-strand rope rotated substantially, but its strength was not degraded; in fact, it increased slightly.

Table 3-5. INFLUENCE OF ROTATION ON ULTIMATE STRENGTH OF 1½-INCH, 18 x 7 NONROTATING WIRE ROPE

Manufacturer	Ultimate Strength Ends Fixed, lbs.	Ultimate Strength One End Free, lbs.	Reduction in Strength, Percent
A	132,800	100,500	24.3
B	121,500	80,000	34.2
C	132,600	97,000	26.9
D	128,400	91,000	29.1

3.3.3. Torque Calculation

Reference 3-34 presents the derivation of equations for computing the torque which develops due to loading for most common wire-rope constructions. In general, a wire rope is made up of a layer or layers of strands helically wrapped around a metallic or fiber rope core. The strand itself comprises a layer or layers of wires helically wrapped around a wire or fiber-strand core. The basic assumptions that are used in this analysis include the following:

1. The rope is loaded in tension only with the ends held fixed to prevent twisting or unlaying of the strands.
2. All stresses in the wires remain below the elastic limit of the material and the material obeys Hooke's Law.

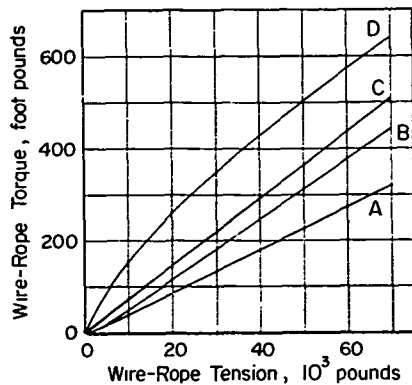


Figure 3-44. Typical Torque Characteristics of 18 x 7 Nonrotating Wire Rope

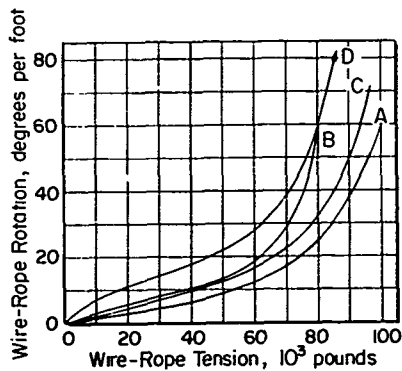


Figure 3-45. Typical Rotational Characteristics of 18 x 7 Nonrotating Wire Rope

3. Radial dimensions for the cross section of the unloaded rope are assumed to remain constant under load; the interwire contact deformations and rope-core compression are neglected.
4. All strands in each layer are the same length and are formed into perfect helices.
5. All wires in all strands are made of the same material.
6. All wires in each layer of each strand are the same length and are formed into perfect helices before closing the strands into a rope.
7. Values for the tensile stresses in the individual wires and the torque developed by the wires as calculated for straight strands are assumed to be valid for strands helically wrapped to form a wire rope.

Basically, the analysis developed below shows the total wire-rope torque to be the summation of strand torque and wire torque, with the direction of twist of the strands and wires providing the appropriate sense of the signs for the summation.

3.3.3.1. General Theory for Analysis of Wire-Rope Torque

Consider first the simple wire-rope geometry shown in Figure 3-46 where N strands are wrapped in a right-hand helix around a fiber core. As shown in Figure 3-47, the tensile load on each strand is

$$T_s = T / (N \cos \epsilon) \quad (3-3)$$

The tensile load, T , on the wire rope produces for each strand a driving force,

$$F = T_s \sin \beta \quad (3-4)$$

which acts to unlay the strand. The total moment produced in the rope owing only to the helical wrap of the strands is then

$$M_s = N F R \quad (3-5)$$

as determined by Figure 3-48. Substitution of Equations 3-3 and 3-4 into Equation 3-5 yields

$$M_s = T R \tan \theta \quad (3-6)$$

which is positive for a right-hand rope lay.

Equation 3-6 is valid for any rope with a single layer of strands wrapped around a fiber core. This includes flattened-strand as well as round-strand

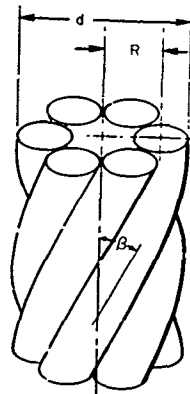


Figure 3-46. Geometry of a 6-Strand Wire Rope

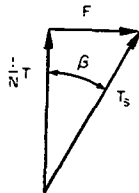


Figure 3-47. Wire Rope Force Triangle

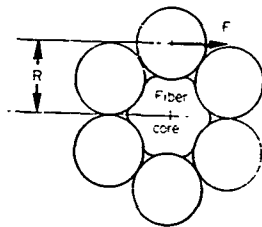


Figure 3-48. Force Contributing to Wire Rope Torque

ropes. For a rope with more than one layer of strands or a rope with a strand core, the calculation becomes only slightly more complicated as will be discussed later.

Consider now a single strand under a tensile load T_s . This strand is composed of m layers of wire wrapped around either a fiber core or a wire core, all wires being made of the same material. Hruska (Ref. 3-35) has shown that the tensile stress in the core wire may be calculated using the equation,

$$\sigma_c = T_s / \left(\sum_{i=c}^m N_i A_i \cos^3 \alpha_i \right) \quad (3-7)$$

The tensile stress on the wires in any layer may then be found by

$$\sigma_i = \sigma_c \cos^2 \alpha_i \quad (3-8)$$

If the strand has a fiber core rather than a metallic core, Equation 3-7 may still be applied by setting A_c equal to zero. The resulting numerical value, although it has no physical meaning, may then be used with Equation 3-8 to determine the actual stress in the other wires. In general, the tensile stress in the wires in the i^{th} layer is related to the tensile stress in the wires in the j^{th} layer by

$$\sigma_i = \sigma_j (\cos^2 \alpha_i / \cos^2 \alpha_j) \quad (3-9)$$

Equation 3-8 is a special case of Equation 3-9 where $\alpha_c = 0$.

The torque induced in the strand by the tensile load may be calculated using the same procedure as outlined in Equations 3-3 through 3-6. The force acting to unlay one wire is

$$f_i = T_{w_i} \sin \alpha_i \quad (3-10)$$

as determined by Figure 3-47. The total moment contribution of one complete layer of strands due only to the helical wrap of the wires is then

$$M_w = N \cos \beta \sum_{i=c}^m f_i r_i \quad (3-11)$$

or, by substitution of Equation 3-10,

$$M_w = N \cos \beta \sum_{i=c}^m r_i A_i \sigma_i \sin \alpha_i \quad (3-12)$$

which is positive for a right-hand-strand lay.

The total torque developed in a simple wire rope with a fiber core may now be expressed as the sum of the contributions of the helically wrapped strands and the helically wrapped wires, or

$$M = TR \tan \beta + N \cos \beta \sum_{i=c}^m n_i A_i \sigma_i r_i \sin \alpha_i \quad (3-13)$$

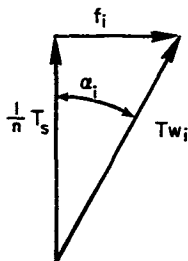


Figure 3-49. Strand Force Triangle

For a wire rope with more than one layer of strands, the above equations for torque and wire stress must be solved by taking one layer of strands at a time. The torque produced by the helically wrapped strands is calculated using an expanded version of Equation 3-6,

$$M_s = \sum_{i=c}^m T_i R_i \tan \beta_i \quad (3-14)$$

where T_i is the portion of the rope tension that is carried by the i^{th} layer of strands.

To calculate T_i , Equation 3-7 must be solved for each layer of strands to find the core-wire stress in terms of the tension carried by that layer of strands. Then, if all core wires are made of the same material, Equation 3-9 applied to the strand-core wires yields, as a special case,

$$\sigma_{c_i} / \sigma_c = \cos^2 \beta_i / \cos^2 \beta_j \quad (3-15)$$

Simultaneous solution of Equations 3-3, 3-7, and 3-15 gives the desired values for T_i . This same analysis applies to ropes with a strand core, ropes with an independent wire-rope core, or multiple-layer nonrotating ropes.

If the strand wires are not all of the same material, Equation 3-9 must be further modified to include the appropriate elastic moduli,

$$\sigma_i / \sigma_j = (E_i / E_j) (\cos^2 \alpha_i / \cos^2 \alpha_j) \quad (3-16)$$

Calculation of the torque contribution of the helically wrapped wires in a complex rope requires the application of Equation 3-12 to each layer of strand. Again, all values of torque are positive for right-hand lay.

This same analysis may be applied to flattened-strand ropes, although the wires in such ropes do not have constant pitch radii. By assuming an average value for the pitch radius of the wires in each layer, fairly accurate results are obtained.

The analysis presented in this paper applies only to wire ropes having the ends fixed to prevent twisting or unlaying of the strands. Any amount of rotation drastically alters the stress distribution in the rope, especially in nonrotating rope constructions.

The above equations provide a method of determining the magnitude of the wire stresses and torque that will be developed by almost any wire rope. However, these calculations are time consuming, especially for ropes containing strands with several layers of wires. A simplification that provides a more convenient method for calculating wire stress and wire-rope torque is discussed below.

3.3.3.2. Simplified Equations for Wire Ropes With Single-Operation Strands

A majority of the wire ropes in common use are composed of single-operation strands, that is, strands that are fabricated in one pass through the stranding machine so that all wires have the same lay length or pitch. The following analysis applies to ropes with single-operation strands.

In Equation 3-7, $(n_i A_i)$ equals the total area of all wires in the i^{th} layer of the strand. This may be replaced by $k(2\pi r_i)d_{w_i}$ wide as shown in Figure 3-50, and k is a constant used to account for the fact that a layer of wires has a smaller total area than a ring of the same width. Equation 3-7 then becomes

$$\sigma_c = T_s / \left[\sum_{i=c}^m k(2\pi r_i)d_{w_i} \cos^3 \alpha_i \right] \quad (3-17)$$

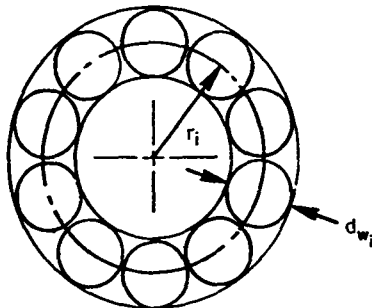


Figure 3-50. One Layer of Wires in a Strand

Now suppose the number of wires in the strand is allowed to become very large, and at the same time the size of each wire is allowed to become very small. For a strand in which all wires have the same lay length, Equation 3-17 may

be expressed as

$$\sigma_c = T_s / \int_0^{d_s/2} k(2\pi r) \cos^3 \alpha dr \quad (3-18)$$

From the strand geometry, it is found that $2\pi = l \tan \alpha$. Also $dr = (l/2\pi) \sec^2 \alpha d\alpha$. Substitution of these relationships into Equation 3-18 gives

$$\sigma_c = 2\pi T_s / (kl^2 \int_0^\lambda \sin \alpha d\alpha) \quad (3-19)$$

where

$$\lambda = \tan^{-1} (\pi d_s / l) \quad (3-20)$$

The solution to Equation 3-19 is

$$\sigma_c / T_s = 2\pi [kl^2 (1 - \cos \lambda)] \quad (3-21)$$

This equation may be used to calculate the tensile stress in the core wire for any single-operation strand in which all wires have the same lay length, l . It has been found that a value for k of 0.80 provides a good approximation for most common strands. The stress in the i^{th} layer of wires may then be found using Equation 3-8.

A similar technique may now be used to evaluate the torque provided by the helically wrapped wires in one layer of strands. In Equation 3-12, let

$$n_1 A_1 = k(2\pi r_1) d_{w1}$$

$$r_1 = (l/2\pi) \tan \alpha_1$$

$$\text{and } \sigma_1 = \sigma_c \cos^2 \alpha_1$$

The total torque developed by the wires in one layer of strands is then

$$M_w = (kl^3 N \cos \beta \sigma_c / 4\pi^2) \int_0^\lambda \sin \alpha \tan^2 \alpha d\alpha \quad (3-22)$$

The solution of Equation 3-22 is

$$M_w = (kl^3 N \cos \beta \sigma_c / 4\pi^2) [(1 - \cos \lambda)^2 / \cos \lambda] \quad (3-23)$$

Substitution of Equations 3-3 and 3-21 into Equation 3-23 gives the total torque contribution of all wires in one layer of strands,

$$M_w = (l/2\pi) (\sec \lambda - 1) T \quad (3-24)$$

It has been found that for common wire-rope geometries, Equation 3-24 yields values of wire torque approximately 10 percent higher than the torque calculated using Equation 3-12. This influences the value of the total wire-rope torque by only about 2 percent.

Now the total torque developed by a simple fiber-core wire rope under tensile load T may be expressed as

$$M = M_s + M_w = [(2\pi R^2/L) + (L/2\pi) (\sec \lambda - 1)] T \quad (3-25)$$

Again, if a complex (multiple-layered) wire rope is being considered, simplified Equations 3-20, 3-21, and 3-24 must be applied to each separate layer of strands as was discussed earlier with regard to Equations 3-6, 3-7, and 3-12.

3.3.3.3. Simplified Equations Applied to Six-Strand Wire Ropes

Probably the most common wire-rope construction consists of six strands wrapped around a fiber core. The simplified equations may be conveniently expressed graphically for this type of wire-rope construction. For either round-strand or flattened-strand ropes, a good value for the pitch radius of the strands is

$$R = 0.34 d \quad (3-26)$$

Accordingly, the strand diameter is about

$$d_s = 0.32 d \quad (3-27)$$

The use of Equation 3-26 in conjunction with Equation 3-6 yields the torque contribution of the helically wrapped strands in a six-strand rope as

$$M_s/T = 2\pi R^2/L = 0.726 d^2/L \quad (3-28)$$

Figure 3-51 provides a graphical representation of Equation 3-28 and includes values for the strand lay angle, λ . Logarithmic coordinates are used in this figure to provide reasonable accuracy over a wide range of wire-rope geometries. Equation 3-28 or Figure 3-51 may be used for six-strand ropes with either single-operation or multiple-operation strands.

The tensile stress in the core wires of a six-strand wire rope may be calculated using Equation 3-27 together with Equations 3-20 and 3-21. This yields

$$\sigma_c/T_s = 2\pi/[(Ld^2 (1 - \cos \lambda))] = 7.854/[L^2 (1 - \cos \lambda)] \quad (3-29)$$

where

$$\lambda = \tan^{-1} (\pi d_s/L) \approx \tan^{-1} (d/L) \quad (3-30)$$

The tensile stress in any other wire in the strand may be calculated using Equation 3-8. The tensile stress is highest in the core wire and it is lowest in outer wires of the strand. For most common ropes, the outer wires are stressed to at least 90 percent of the stress in the core wire.

Equation 3-30 may now be used with Equation 3-24 to evaluate the total torque contribution of the helically wrapped wires in a six-strand wire rope composed of single-operation strands. The result is shown graphically in Figure 3-52.

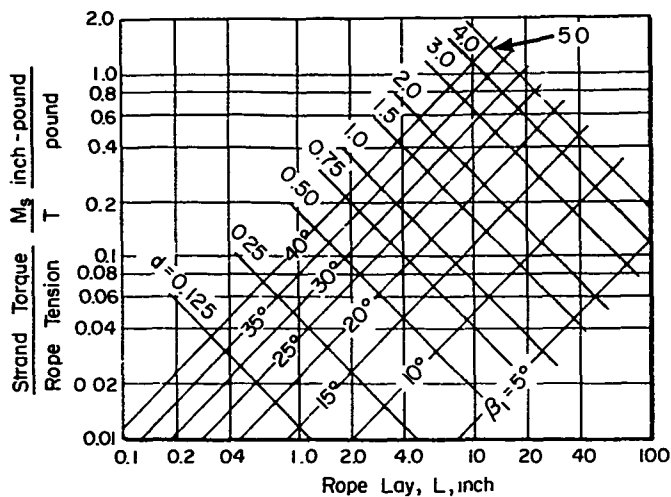


Figure 3-51. Torque Developed by Helically-Wrapped Strands in a Six-Strand Wire Rope

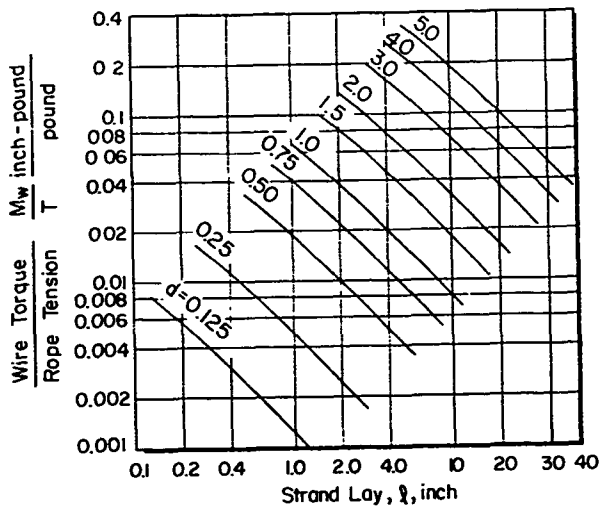


Figure 3-52. Total Torque Developed by Helically Wrapped Wires in a Single-Operation Strand of a Six-Strand Wire Rope

The data displayed in Figures 3-51 and 3-52 may now be used directly as indicated by Equation 3-25 to evaluate with suitable accuracy the total torque developed by a simple wire rope containing six single-operation strands.

3.3.3.4. Sample Calculations for Simple Wire Rope

As an example of how the simplified equations may be used to advantage, consider the wire-rope geometry shown in Figure 3-53. A 1-3/8-inch-nominal-diameter, Lang-lay rope of this design was tested to determine the torque developed as the specimen was loaded with the ends restrained from rotation. A sensitive strain-gage load cell was used to monitor both tension and torque as the rope was loaded a number of times to 100,000 pounds or about 60 percent of its breaking strength. The torque curve was found to be linear with 0.204 inch-pounds of torque developed per pound of applied tension.

The actual diameter of this preformed rope was $d = 1.41$ inches, the rope lay was $L = 8.80$ inches, and the strand lay was $l = 3.74$ inches. These are the only three parameters for which values must be known to make use of the simplified equations developed above.

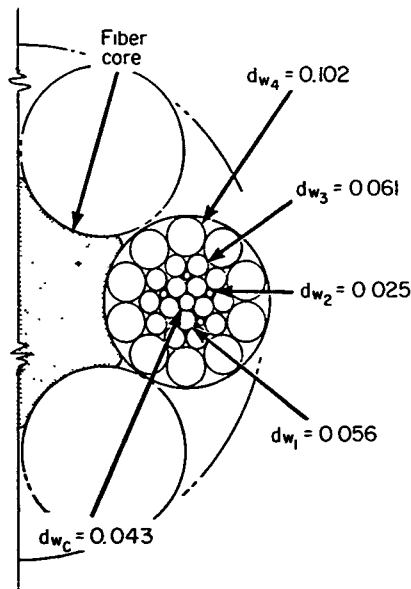


Figure 3-53. Cross Section of a 6 x 31 Fiber-Core Wire Rope

From Equation 3-28 or Figure 3-51, the torque contribution of the helically wrapped strands is found to be $M_s = 0.164 T$ inch-pounds. Using Equations 3-29 and 3-30, the stress in the core wire is found to be $\sigma_c = 8.73 T_s$ psi. Equations 3-24 and 3-30 or Figure 3-52 gives the total torque contribution of the helically wrapped wires as $M_w = 0.041 T$ inch-pounds. The total torque produced in the wire rope is then $M = M_s + M_w = 0.205 T$ inch-pounds, which is essentially identical to the measured value of 0.204 T inch-pounds.

If the same calculations are attempted using the longer method of analysis, it is necessary to first make the measurements and calculations indicated in Table 3-6. Here the wire stress is determined using Equations 3-7 and 3-8. The value obtained in this way for core-wire stress is within 2 percent of the value calculated using the simplified analysis.

Table 3-6. MEASUREMENTS AND CALCULATIONS FOR
EXAMPLE WIRE-ROPE CONSTRUCTION

$d = 1.41$ inches

$L = 8.80$ inches

$l = 3.74$ inches

Layer	Number of Wires, n	Wire Diameter, d_w , inch	Wire Area, A, inch ²	Pitch Radius, r, inch	Lay Angle, α , degrees	σ_c / T_s , inch ⁻²
Core	1	0.043	0.001452	0	0	8.61
1	5	0.056	0.002463	0.0495	4.75	8.55
2	5	0.025	0.000491	0.0690	6.61	8.49
3	10	0.061	0.002922	0.1040	9.91	8.35
4	10	0.102	0.008171	0.1745	16.34	7.93

Using Equation 3-12, a value for the torque contribution of the helically wrapped wires is found to be $M_w = 0.037 T$ inch-pounds. This is approximately 10 percent lower than the value obtained using the simplified analysis. The total torque produced in the wire rope is then $M = M_s + M_w = 0.201 T$ inch-pounds, which is within 2 percent of the measured value.

These sample calculations indicate that both methods of analysis provide accurate values for wire-rope torque. The real value of the simplified analysis is that it may be used to determine the torque characteristics of a working six-strand wire rope by measuring only the rope diameter, d ; the rope lay, L ; and the strand lay, l .

3.3.3.5. Measurement of Rope Lay and Strand Lay

Measurement of the rope lay can be done quite accurately by following one strand along the rope for a number of turns and then dividing that length of

the rope by the number of the strand. Measurement of the strand lay can also be made quite accurately if the number of outer wires in each strand is known. This may be done by placing a length of tape helically on the rope so that it follows along one strand for exactly one turn around the rope. If the tape is then rubbed with a pencil lead or other marker, an image of each wire will be left on the tape.

This tape-measuring technique for determining strand lay may be expressed as follows:

$$l = CS' (n_o/n_t \pm n_o) \quad (3-31)$$

where

$$C = \cos \beta' / \cos \beta / \cos \beta$$

$$\beta' = \tan^{-1} (\pi d/L)$$

$$\beta = \tan^{-1} (2\pi R/L)$$

In Equation 3-31 the positive sign is used for Lang-lay wire rope and the negative sign is used for regular-lay wire rope.

The correction factor, C, used in Equation 3-31 is required for the following reason. In one rope lay, the true length of the strand as measured at the strand centerline is $S = L/\cos \beta$, where $\beta = \tan^{-1} (2\pi R/L)$. The strand length as determined by the tape-measuring technique will be $S' = L/\cos \beta'$, where $\beta' = \tan^{-1} (\pi d/L)$. The value of S' is larger than the value of S. Therefore, any physical measurement of strand length using the tape must be multiplied by $C = S/S' = \cos \beta' / \cos \beta$ to obtain values for true strand length.

3.4. RELATIVE STRAND MOTION IN A WIRE ROPE ON A SHEAVE

Wire rope is a complex machine element in which several important geometric changes take place as a result of applied loads and bending around a sheave or winding drum. The major changes in geometry of a straight wire rope in tension have been investigated and are fairly well understood.

The geometric changes occurring in a wire rope on a sheave are less well understood. Among these changes are bending of the wires, shape distortion of the cable due to the bearing load on the sheave, and relative motion between adjacent strands and wires. An analysis of the relative motion between strands in a wire rope on a sheave (Ref. 3-3) is considered below.

The equation defining the strand length around the sheave for a given wrap angle, ψ , is:

$$s = \int_0^{\psi} R_p \left\{ \left[1 + \frac{R}{R_p} \cos \left(-\frac{R_p \tan \beta}{R} \psi + \theta_0 \right) \right]^2 + \tan^2 \beta \right\}^{\frac{1}{2}} d\psi \quad (3-32)$$

where

R_p = pitch radius of sheave

R = pitch radius of strand, measured from rope to strand centerline, inches

- ψ = sheave reference angle, degrees
 θ = angle defining the position of a strand in a wire rope, degrees
 β = strand lay angle, degrees
 θ_0 = initial angular position of a strand, degrees
 s = true length of one strand as measured from the point of rope-to-sheave tangency through any specified angle, ψ , inch.

In the above equation, θ_0 determines which strand is being considered. Figure 3-54 shows the graphical result of Equation 3-32 for a six-strand rope construction. The mathematical analysis of this problem is presented in detail in Reference 3-3.

3.4.1. Graphical Results of Strand-Motion Solution

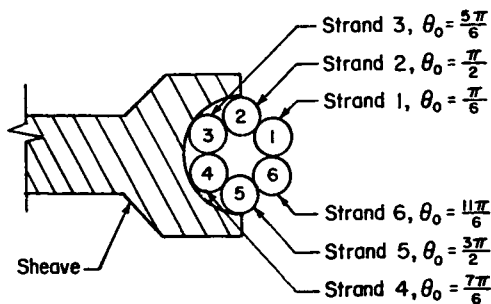
The results of the analysis are presented in generalized form here. The parameters necessary in evaluation of the magnitude of the motion between adjacent strands are the ratio of the rope lay length to the rope diameter, l/d ; the ratio of the sheave pitch diameter to the rope diameter, D/d ; and the rope diameter, d . The rope lay length is the distance required for each strand to complete one turn of its helix about the axis of the rope. Once these parameters are known for a particular rope and sheave, Figure 3-55 can be used to determine the maximum relative strand motion, Δs_{\max} . This is done by finding the point on the left half of the figure which corresponds to the particular values of l/d and D/d . This point is then projected horizontally to the right until the line corresponding to the rope diameter, d , is intersected. Then the corresponding value of Δs_{\max} is read on the right horizontal axis.

For a 1-3/8-inch, 6 x 25 filler-wire, round-strand wire rope on a 24-inch sheave, the interstrand motion is found as shown below. The actual diameter of a typical rope is 1.46 inches, and the lay length is 9.5 inches. Thus the ratio of lay length to rope diameter, l/d , is 6.50, and the sheave-to-rope diameter ratio D/d is 16.4. This gives a maximum strand motion, Δs_{\max} of about 0.11 inch.

In Reference 3-3 an attempt was made to measure experimentally the strand motion for the 1-3/8-inch rope mentioned above. No valid results were obtained because of the high rope friction and because of distortion in the free end of the cable where the measurements were being made.

3.4.2. Discussion and Further Implications of the Strand-Motion Solution

Six-strand wire ropes are of greatest current interest to the Navy, therefore, the graphs in this section are plotted only for six-strand wire-rope constructions. The results are also valid for single strands having six wires over a core. However, it should be emphasized that the solution presented in Reference 3-3 is perfectly general and, therefore, is applicable to any construction. It should also be noted that a slight error results if Figure 3-55 is applied to flattened-strand constructions. This error



Note: Bracketed numbers refer to the relative motion between the two strands whose numbers are noted. Unbracketed numbers refer to the length of the strand noted relative to the average length of all six strands.

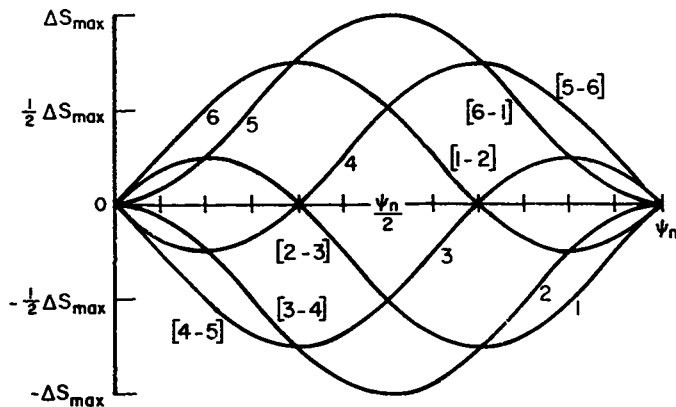


Figure 3-54. Relative Strand Motion Between Nodal Planes in a Wire Rope Wrapped on a Sheave

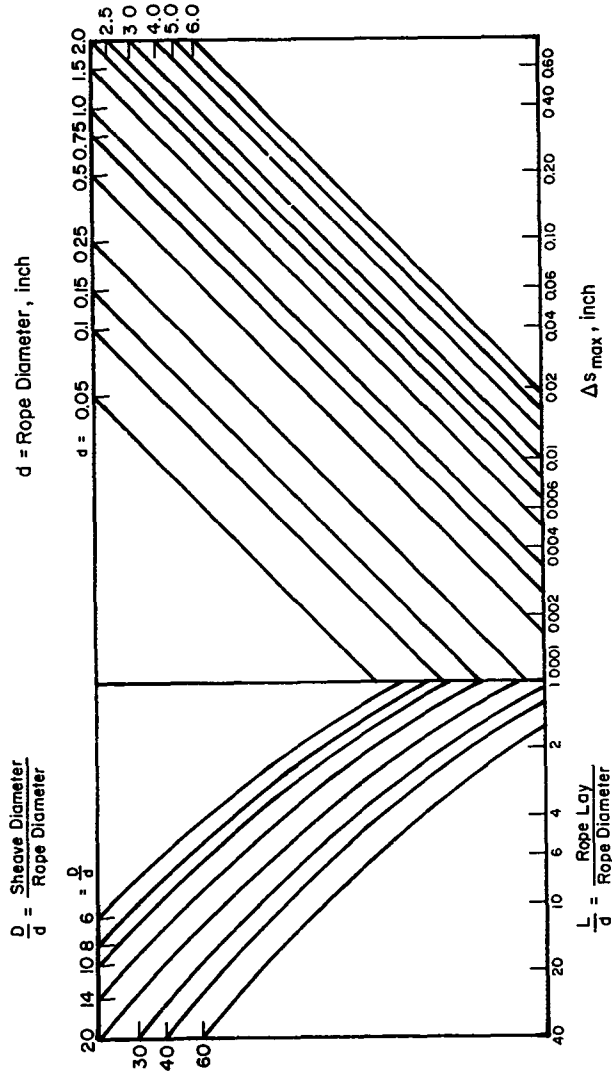


Figure 3-55. Influence of Rope and Sheave Geometry on the Relative Strand Motion of a Six-Strand Wire Rope

arises because of small differences in the helical geometry of the strands in round-strand and flattened-strand wire ropes. Nonetheless, Figure 3-55 can still be used for flattened-strand cables to get a good indication of the magnitude of the motion expected.

One result of the strand-motion solution is the prediction of what will be referred to as the nodal angle, ψ_n . Consider a wire rope on a turning sheave. There are certain discrete planes through the rope where all the strands are aligned just as they were in the straight rope. The arc length on the pitch line of the sheave between two such planes is one rope lay, and the angle subtended by this rope lay is the nodal angle, ψ_n . Figure 3-56 shows this relationship pictorially. Thus, ψ_n can be defined in terms of the sheave diameter, D , and the rope lay, l , as

$$\psi_n = \frac{360}{\pi} \frac{l}{D} \quad (3-33)$$

Now that the nodal angle has been defined it is possible to show the amount of slip between any two strands at any point on the sheave in terms of the maximum slip which occurs, Δs_{\max} , and fractions or multiples of the nodal angle, ψ_n . Figure 3-54 shows this relationship. This plot shows only one cycle since the Δs function is periodic in ψ_n .

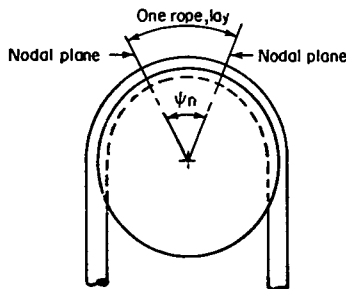


Figure 3-56. Schematic Illustration of Nodal Angle on a Sheave

The existence of the nodal angle has been known for some time among users and manufacturers of wire rope. There has been some speculation that it might be desirable to match the sheave size to the rope size in a manner which would make the rope wrap angle some integer multiple of ψ_n . The reasoning behind this speculation is that if the above condition is met, then all strands contained on the sheave are of exactly the same length, and, hence, there is no resulting tensile stress variation among the strands. This reasoning is correct for a completely frictionless cable. However, since a rope is not at all frictionless, as is discussed in more detail

below, the strand motion actually takes place in the straight portion of the rope adjacent to the sheave, and the strands are stationary once they are on the sheave. Therefore, there is no means available to communicate from one end of the rope what the conditions are at the other end. In other words, once the rope is on the sheave and interstrand motion is stopped, it does not matter how far the rope travels before it leaves the sheave. Thus, it can be concluded that the condition that the rope wrap angle be some integer multiple of the nodal angle has an insignificant effect on operation and expected life.

It is desirable, however, to reduce the magnitude of relative strand motion for several reasons. This motion causes the wires in the cable to wear at the contact points. Recalling that these contact points are the same points at which the very high contact stresses occur illustrates the importance of minimizing the motion. Another result of the motion is friction-induced heating. At high tensile loads and high rope velocity, the rope may become quite hot and melt off the protective lubricant, thus interfering with proper rope lubrication. With the lubricant gone from the contact points the wear problem is compounded. Preliminary calculations show that most of the energy required to cycle a rope around a sheave can be accounted for by considering only the friction-induced heat energy released as a result of the predicted interstrand motion.

Reference to Figure 3-55 indicates the important parameters involved from a design standpoint in reducing interstrand motion. It is easily seen that a reduction in the ratio of rope lay to rope diameter, l/d , produces a corresponding reduction in Δs_{max} . It should also be noted that a reduction in this ratio is beneficial from the standpoint of wire-bending stress. However, there is a design trade-off here in that the smaller l/d becomes, the lower are the ultimate strength and elastic modulus of the rope. This indicates that there may be some optimum value of l/d for a given application. An increase in the ratio of sheave diameter to rope diameter, D/d , also decreases Δs_{max} . The only upper limit on this ratio is one of space availability. Although a change in the coefficient of friction in the rope will affect Δs_{max} very little, lower friction would alleviate some of the undesirable effects such as cable and sheave heating associated with strand motion. Heating in a properly aligned sheave is actually a result of heat transfer from the rope to the sheave.

Since friction is inherent in all wire rope, and since it is one factor which complicates the experimental determination of relative strand motion, the question arises as to the effect of friction on relative strand motion in a wire rope in actual service. Two things can be said in general about a working wire rope in this respect.

Observations of wire rope tested on a Battelle wire-rope fatigue machine (Ref. 3-3) have shown that a very large part of the interstrand motion takes place in the straight section of the rope quite near the point of rope tangency on the sheave. Also, due to the bearing loads of the rope on the sheave, the interstrand contact force and, thus, the internal rope friction increases considerably as the rope wraps onto the sheave.

The friction forces in the straight section of a 1-3/8-inch wire rope were computed and compared to the forces that would be required to prevent the

4. WIRE ROPE STRESS ANALYSIS

A number of investigators (Refs. 3-8, 3-15, and 4-1) discuss the difficulty or even the impossibility of accurately computing the stresses in a wire rope. (Some of these same investigators then attempt the analysis themselves with no better apparent success than those that preceded them.) Nevertheless, efforts to derive equations that will permit a wire-rope designer to rationally predict the relationship between the conditions imposed on a rope, the stresses produced, and the resultant rope life continue. No one has succeeded to date primarily because of the complex nature of the stress field present in the wires of a rope and its sensitivity to external factors that are extremely difficult to identify accurately, such as friction and wire surface condition.

The induced stresses that are normally present in a loaded wire rope are tensile, bending, shear, compressive, contact or "Hertzian", and torsion. To further complicate the problem, there are normally residual stresses which have been introduced in the manufacturing process. Both the construction of the rope and its usage conditions dictate which of the stresses predominate.

In this presentation no attempt is made to give the derivation of the equations or all of the assumptions that were made with the single exception of the bending stress analysis. The interested reader should consult the cited references for more detailed analyses.

4.1. TENSILE STRESS

The tensile stress in an individual wire in a straight wire rope, neglecting radial contraction of the rope under axial loading and internal friction, is given by (Refs. 3-35 and 4-2):

$$\sigma_1 = \sigma_c \left(\frac{\cos^2 \alpha_1}{\cos^2 \beta} \right) \quad (4-1)$$

$$\sigma_c = T_s / \left[A_c \cos \beta + \frac{1}{\cos^2 \beta} (n_1 A_1 \cos^3 \alpha_1 + \dots + n_i A_i \cos^3 \alpha_i) \right] \quad (4-2)$$

$$T_s = T / m_s \cos \beta \quad (4-3)$$

Combining:

$$\sigma_1 = \frac{T \cos^3 \alpha_1}{m_s \cos \beta (A_c \cos^3 \beta + n_1 A_1 \cos^3 \alpha_1 + \dots + n_i A_i \cos^3 \alpha_i)} \quad (4-4)$$

where

σ_1 = tensile stress in wires in layer i , lb/in²

σ_c = tensile stress in core wires, lb/in²

α_1 = lay angle of wire layer i , degrees

4. WIRE ROPE STRESS ANALYSIS

A number of investigators (Refs. 3-8, 3-15, and 4-1) discuss the difficulty or even the impossibility of accurately computing the stresses in a wire rope. (Some of these same investigators then attempt the analysis themselves with no better apparent success than those that preceded them.) Nevertheless, efforts to derive equations that will permit a wire-rope designer to rationally predict the relationship between the conditions imposed on a rope, the stresses produced, and the resultant rope life continue. No one has succeeded to date primarily because of the complex nature of the stress field present in the wires of a rope and its sensitivity to external factors that are extremely difficult to identify accurately, such as friction and wire surface condition.

The induced stresses that are normally present in a loaded wire rope are tensile, bending, shear, compressive, contact or "Hertzian", and torsion. To further complicate the problem, there are normally residual stresses which have been introduced in the manufacturing process. Both the construction of the rope and its usage conditions dictate which of the stresses predominate.

In this presentation no attempt is made to give the derivation of the equations or all of the assumptions that were made with the single exception of the bending stress analysis. The interested reader should consult the cited references for more detailed analyses.

4.1. TENSILE STRESS

The tensile stress in an individual wire in a straight wire rope, neglecting radial contraction of the rope under axial loading and internal friction, is given by (Refs. 3-35 and 4-2):

$$\sigma_1 = \sigma_c \left(\frac{\cos^2 \alpha_1}{\cos^2 \beta} \right) \quad (4-1)$$

$$\sigma_c = T_s / \left[A_c \cos \beta + \frac{1}{\cos^2 \beta} (n_1 A_1 \cos^3 \alpha_1 + \dots + n_i A_i \cos^3 \alpha_i) \right] \quad (4-2)$$

$$T_s = T / m_s \cos \beta \quad (4-3)$$

Combining:

$$\sigma_1 = \frac{T \cos^3 \alpha_1}{m_s \cos \beta (A_c \cos^3 \beta + n_1 A_1 \cos^3 \alpha_1 + \dots + n_i A_i \cos^3 \alpha_i)} \quad (4-4)$$

where

σ_1 = tensile stress in wires in layer i , lb/in²

σ_c = tensile stress in core wires, lb/in²

α_1 = lay angle of wire layer i , degrees

- β = lay angle of strands, degree
 A_i = area of individual wires in layer i , in²
 A_c = area of core wire, in²
 T = tensile force on rope, lb
 T_s = tensile force on strand, lb
 m_s = number of strands
 n_i = number of wires in layer i .

4.2. BENDING STRESS

Over the years, many attempts have been made to compute (or estimate) the bending stresses in a wire rope. These analyses have ranged from simplistic to extremely complex. Many wire-rope manufacturers and users regard the problem as insolvable. Indeed, until the advent of large computers, the problem was nearly so. To illustrate the diverse formulas that have been suggested in the past, Table 4-1 (Ref. 4-1) presents some of them and compares their results.

Currently, several attempts are in progress to solve the problem using finite-element analysis techniques. Another analysis involving methods of vector analysis and strength of materials has been completed (Ref. 4-3) and is reproduced here.

To analyze the bending stresses in the wires of a rope, it is first necessary to determine the radii of curvature of the wires prior to and after bending the rope. The wire-bending stress can then be calculated from the change in wire curvature. The purpose of the following analysis is to present a procedure for computing the radii of curvature of the wires both in a straight rope and in a rope wrapped on a sheave and determining the resultant bending stresses.

The complexity of the equations generated in the analysis requires numerical results in order to be viewed meaningfully. Therefore, all numerical results were obtained using the parameters of a 1-3/8-inch-diameter, 6 x 25 filler wire, Lang-lay, round-strand wire rope, which is referred to hereafter as the Standard Rope.

4.2.1. Analysis of a Straight Wire Rope

4.2.1.1. Wire-Rope Geometry

Figure 4-1 shows a typical Lang-lay, wire-rope construction in which both the wire and strand wraps conform to a right-hand rule. Another common configuration is regular-lay construction which differs from Lang-lay only in that the wire wrap is opposite the strand wrap. The analysis presented below is specifically for a Lang-lay rope but can easily be adapted to regular-lay by noting the change in geometry.

Table 4-1. COMPARISON OF BENDING STRESS FORMULAS*

Key	Formula	Notation	Bending Stress, lbs/in ²	% of Formula "A"
A	$\sigma_b = \frac{Ed_o}{D}$	σ_b = Bending Stress (lbs/in ²) E = Modulus of Elasticity of Wire (lbs/in ²) d _o = Diameter of Outside Wire D = Sheave Tread Diameter (ins)	24,555	100
B	$\sigma_b = \frac{Ed_o}{D} \cos^2 \alpha \cos^2 \beta$	σ_b , E, d _o , and D = Same as in "A" α = Wire Lay Angle, degrees β = Strand Lay Angle, degrees	19,595	80
C	$\sigma_b = \frac{Ed_o}{D} \cos^2 \alpha \cos^2 \beta$	Same as in "B"	21,935	89.5%
D	$K = \frac{FA_m}{2.06 \frac{R_b}{d_o} + c_o}$ and $\sigma_b = \frac{K}{A_m}$ which may also be expressed as $\sigma_b = \frac{0.485 Ed_o}{R_b}$	E, σ_b , and d _o = Same as in "A" K = Total Bending Force on a Rope (lbs) A _m = Metallic Area Rope (in ²) R _b = Radius of Bend to $\frac{1}{2}$ of Rope (in) c _o = 14.1 (Constant for this Rope Construction)	23,635	96.3%
E	$\sigma_b = \frac{0.44 Ed_o}{D}$	Same as in "A"	10,805	44
F	$\sigma_b = \frac{0.667 Ed_o}{D} \cos^2 \alpha \cos^2 \beta$	Same as in "B"	13,070	53.2%
G	$\sigma_b = \frac{F_r d_o}{2R_b}$	σ_b , d _o , and R _b = Same as in "D" F _r = Modulus of Elasticity of Rope (lbs/in ²)	10,270	41.8%
H	$P_o = \frac{(d_w)^2 EG_r}{8 R_{ds} [2G_r (1 + \sin^2 \gamma_o) + E \cos^2 \gamma_o]}$ and $\sigma_b = \frac{\sum P_o}{A_m}$	σ_b , E, A _m , and R _b = Same as in "D" P _o = Loss in Strength per Wire (lbs) d _w = Diameter of Individual Wire (in) G _r = Modulus of Rigidity of Wire (lbs/in ²) d _s = Diameter of Strand (in) γ_o = Complement of Angle between Individual Wire and $\frac{1}{2}$ of Rope, degrees	2,100	8.5%

*Rope used: 1" \pm 6 x 21 Filler wire construction, Lang lay; Head sheave: 10' 6" tread diameter.

An analysis by Stein and Bert (Ref. 4-4) correctly defined the geometry of a wire rope as presented here, but failed to correctly compute the radii of curvature. Figure 4-2 shows the arrangement of the rectangular coordinate systems defining the rope. The nomenclature used in the analysis is as follows:

- R = pitch radius of strand, measured from rope centerline to strand centerline, inch
- r = pitch radius of wire, measured from strand centerline to wire centerline, inch
- β = lay angle of strand in rope, measured between rope and strand centerlines, degrees
- α = lay angle of wire in strand, measured between strand and wire centerlines, degrees

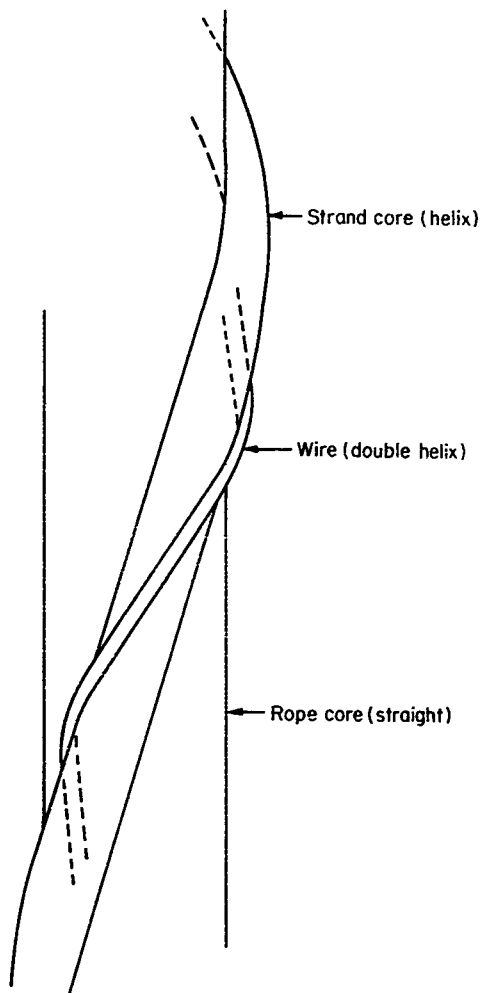


Figure 4-1. Typical Lang-Lay Wire Rope Construction

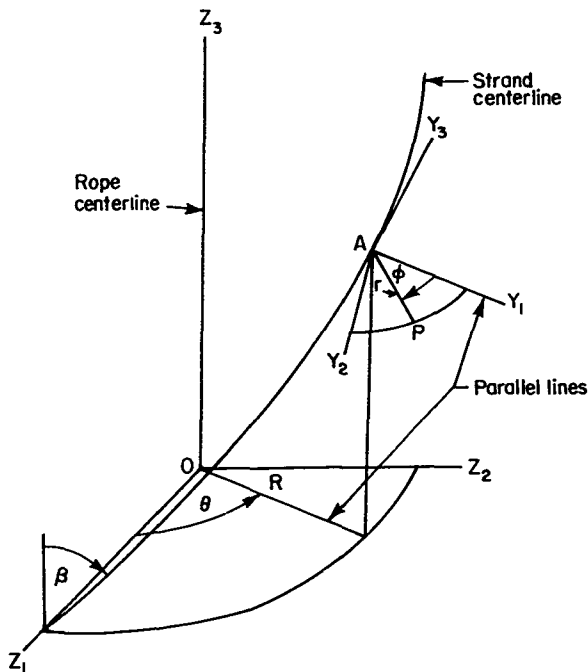


Figure 4-2. Straight-Rope Geometry

θ = angle defining position of strand, degrees (see also Figure 4-14)

ϕ = angle defining position of wire, degrees (see also Figure 4-14).

For this analysis it is assumed that the centerline of each of the strands of the wire rope forms a true helix. Therefore, R and β are constants, and for the Standard Rope discussed herein, $R = 0.47$ inch and $\beta = 17.75$ degrees. Further, it is assumed that r has a constant value equal to 0.19 inch for the Standard Rope.

In Figure 4-2, the principle system, Z_1, Z_2, Z_3 is oriented such that Z_3 forms the centerline of the rope. Point A, located at $(R \cos \theta, R \sin \theta, R \theta \cot \beta)$ in the Z system, is on the strand centerline and denotes the origin of the Y_1, Y_2, Y_3 system. The Y_3 axis is tangent to the strand centerline, while the Y_1 axis is parallel with the radial vector component specifying A. Point P, the point on the wire about which the radius of curvature is computed, is restricted to lie in the $Y_1 - Y_2$ plane and is located at $(r \cos \phi, r \sin \phi, 0)$ in the Y system.

4.2.1.2. Derivation of Equations

Using matrices to rotate and translate the coordinates of P into the Z system (see Section 5.1.) gives

$$\{Z\} = \begin{bmatrix} ((R + r \cos \theta) \cos \phi - r \sin \theta \cos \phi \sin \epsilon) \\ ((R + r \cos \theta) \sin \phi + r \sin \theta \cos \phi \cos \epsilon) \\ (R \epsilon \cot \epsilon - r \sin \theta \sin \epsilon) \end{bmatrix} \quad (4-5)$$

The radius of curvature, ρ , of the wire at Point P can be expressed as (Ref. 4-5)

$$\rho = \frac{(\bar{Z}' \cdot \bar{Z}')^{1.5}}{|\bar{Z}' \times \bar{Z}''|} = \frac{|\bar{Z}'|^3}{|\bar{Z}''|} \quad (4-6)$$

where the numerator is the magnitude of the first geometrical derivative of $\{Z\}$, squared, and the denominator is the magnitude of the second geometrical derivative of $\{Z\}$, where primes denote differentiation with respect to ζ . By computing the derivatives and substituting into Equation 4-6, it is found that ρ is a function of θ , ϕ , θ' , and θ'' . Solution of the equations, then, requires that a (θ, ϕ) relationship be derived.

At this point it is desirable to point out certain geometrical considerations pertinent to the development of the required (θ, ϕ) relationship. Consider first a single straight strand prior to closing the strand into a rope. Each wire of the strand forms a true helix, such that at any point on the wire the tangent to the wire is at a constant angle, α , to the strand centerline. Note that if a point moves along the wire at a constant velocity, its velocity component along the strand axis and its velocity component in the plane perpendicular to the strand axis also will be constant. Therefore, a simple helix may be defined either by the constant lay angle or by the uniform-motion consideration.

The two methods of defining the helix produce identical geometrical results. However, in defining the geometry of the wires in the straight rope, a perplexing problem is encountered; namely, how does one define the double-helix configuration of the wires? Physically, the rope is formed by first wrapping the wires helically on a core, to form a strand, and then wrapping the strand helically on a central core, to form a rope. The wires in the straight strand can be defined as outlined above. After wrapping the strand helically on the rope core, though, it is difficult to predict exactly how the wires behave. A constant angle between a tangent to the wire and a tangent to the strand centerline may exist, and, if assumed, a radius-of-curvature solution may be obtained. Assuming a combination of uniform motions, i.e., uniform motion along the strand centerline combined with uniform circular motion in the plane perpendicular to the strand, then a different, though similar, radius-of-curvature solution can be derived. It will be shown that both conditions do not exist simultaneously. Thus, assuming constant lay angle, then the motion is not uniform and vice-versa.

It is possible, perhaps probable, that both varying angle and nonuniform motion conditions exist simultaneously in a real rope; however, making this assumption does not lend enough constraints for solving the problem. Of the possible combinations of angle and motion assumptions, then, only two are acceptable for analysis, and, since either of these seems equally likely to occur, the problem will be solved for each case.

The required (ϕ, θ) relationships for the two solutions may be derived as follows. Note that, in the Z-system, the tangent to the wire double-helix curve at P and the tangent to the strand simple-helix curve at A have between them the wire lay angle, α . Thus, the scalar dot product of the two tangents is

$$\bar{Z}' \cdot \bar{A}' = |\bar{Z}'| |\bar{A}'| \cos \alpha \quad (4-7)$$

where

\bar{Z}' = tangent to double-helix curve

\bar{A}' = tangent to helix curve.

Substituting derivatives yields the differential equation,

$$\phi' + \cos \beta = \frac{R \tan \alpha}{r \sin \beta} + \tan \alpha \sin \beta \cos \phi \quad (4-8)$$

Refer to Section 5.2. for the details of obtaining Equation 4-8 from 4-7.

4.2.1.2.1. Constant Angle Assumption.

First, consider the constant-angle assumption. If α is constant, then Equation 4-8 may be written as

$$\phi' + c = a + b \cos \phi \quad (4-9)$$

where a, b, c are the appropriate constants. Of the several solutions to Equation 4-9 (Ref. 4-9), only one case, $(a - c)^2 > b^2$, satisfies the physical situation for real wire-rope parameters (α, β, R and r) and, thus, the correct relation is

$$\theta = \frac{2}{\sqrt{(a - c)^2 - b^2}} \tan^{-1} \left(\frac{a - c - b \cos \phi}{\sqrt{(a - c)^2 - b^2}} \tan \frac{\phi}{2} \right) + K_1 \quad (4-10)$$

where K_1 may be evaluated per initial conditions. Also,

$$\phi'' = -b\phi' \sin \phi \quad (4-11)$$

follows readily from Equation 4-9.

Figure 4-3 displays graphically the (ϕ, θ) relationship given by Equation 4-10. It is important to notice that the slope is not constant, but fluctuates about the "average slope" line as shown. The magnitude of the fluctuation is small, but the important consideration is that many terms in the second derivatives of the equations for radius of curvature take on significant magnitudes.

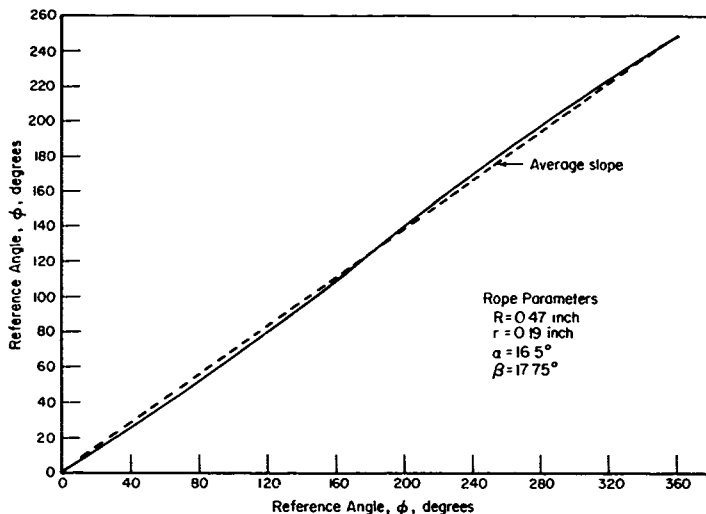


Figure 4-3. Reference-Angle Relationship Assuming Constant Wire Lay Angle, α

Substituting Equations 4-9, 4-10, and 4-11 into \bar{Z}' and \bar{Z}'' (see Sections 5.2. and 5.3.) and then into Equation 4-6 yields the radius of curvature of the wire for the constant-angle assumption. Because of the length of the equations, they were programmed on a computer (see Section 5.4.) to provide a digital solution.

4.2.1.2.2. Uniform-Motion Assumption.

Now consider the uniform-motion assumption. Assuming uniform motion means geometrically that $\theta = k\theta$, where k is a constant. Substituting $\theta' = k$ into Equation 4-8 and rearranging yields

$$\alpha = \tan^{-1} \frac{k + \cos \beta}{\frac{R}{r \sin \beta} + \sin \beta \cos \theta} \quad (4-12)$$

The constant, k , may be determined by assuming α fluctuates about the average of α for the Standard Rope. The solution was obtained by an iterative computer approximation, where k was varied until α was the desired value for the Standard Rope. (See Section 5.4.) The value of k and the reciprocal of the "average slope" of the constant angle (θ, θ) relationship were found to be equal within the accuracy of the numerical integration.

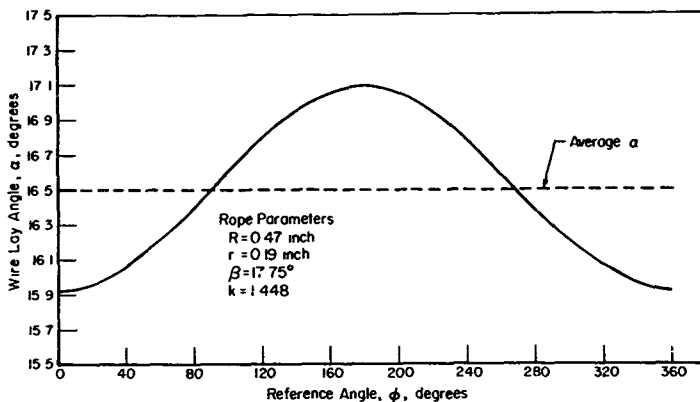


Figure 4-4. Variation in Wire Lay Angle, α , in a Straight Wire Rope Assuming Uniform Wire Motion

Knowing k , the variation of α is displayed in Figure 4-4, where it can be seen that α varies about the average of α used in the constant-angle analysis. Note also that this relation is purely illustrative, in that once k has been determined, α does not appear in the equations for computing the radius of curvature of the rope wire.

Substitution of $\theta = k\phi$ into \bar{Z}' and \bar{Z}'' and then into Equation 4-6 yields the radius of curvature for the uniform motion assumption.

4.2.1.3. Results.

Figure 4-5 gives the results of the double-helix solutions together with an available approximation for the Standard Rope. It is convenient at this time to refer to a plane section of a strand as shown in Figure 4-6. Points of interstrand contact should be noted as well as the values of θ corresponding to each wire. The Starkey and Cress (Ref. 4-7) approximation was made by assuming that the value of the radius of curvature of a wire in a rope is approximately the same as that for the radius of curvature of a wire in a straight strand, i.e., the radius of curvature for a simple helix. This value, expressed mathematically as $r/\sin^2\alpha$, was used for approximating the radius of curvature of the real wires at the points of interstrand contact. Figure 4-5 shows that this approximation is very close to both the constant-angle solution and the uniform-motion solution at the points of interstrand contact (Positions 5 and 9). Since the Starkey and Cress value is for a simple helix, it seems reasonable that the double-helix solutions would fluctuate about this constant value as, indeed the solutions do.

Both curves in Figure 4-5 can be interpreted in two ways. Consider first a moving point on one wire making one complete revolution around a strand, i.e., going from the extreme outside of the rope at $\theta = 0$, around to the inside of

the rope and passing next to the rope core at $\theta = 180$ degrees, and then completing the revolution by appearing again on the extreme outside of the rope at $\theta = 360$ degrees. The graph shows the magnitude of the radius of curvature, ρ , at any position along this length of wire (usually termed one lay length). It is noted that the value of ρ is periodic in 360 degrees of θ and is symmetrical about $\theta = 180$ degrees in both solutions.

The second interpretation of the curves in Figure 4-5 involves an imaginary plane cutting through a strand as shown in Figure 4-6. This interpretation gives the value of ρ for each of the wires at the point at which it passes through the plane.

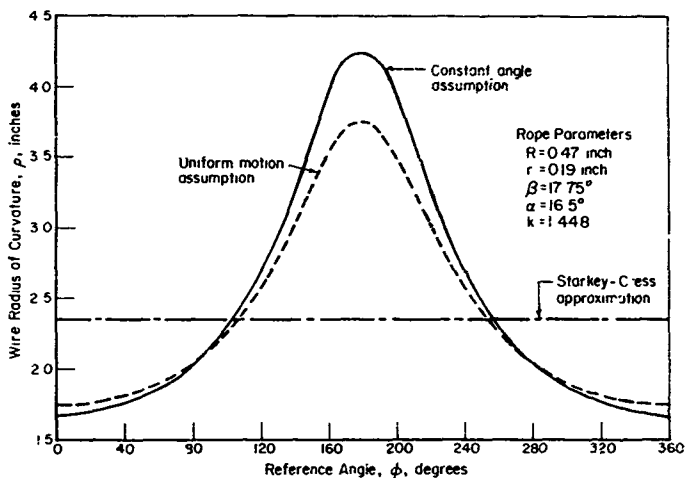


Figure 4-5. Variation in Wire Radius of Curvature Within a Wire Rope

The values of ρ given by each curve in Figure 4-5 were compared to the physically measured values of ρ for the real wire. First, arcs were drawn on paper using the radii predicted by each of the solutions for the same common value of θ . Then a preformed wire, removed from a rope, was placed over the arcs and its curvature, at the same known value of θ , was compared to each. This procedure was repeated for several locations along the wire. It was found that the radius of curvature of the wire predicted by the two double-helix solutions gave good results when compared to the radius of curvature

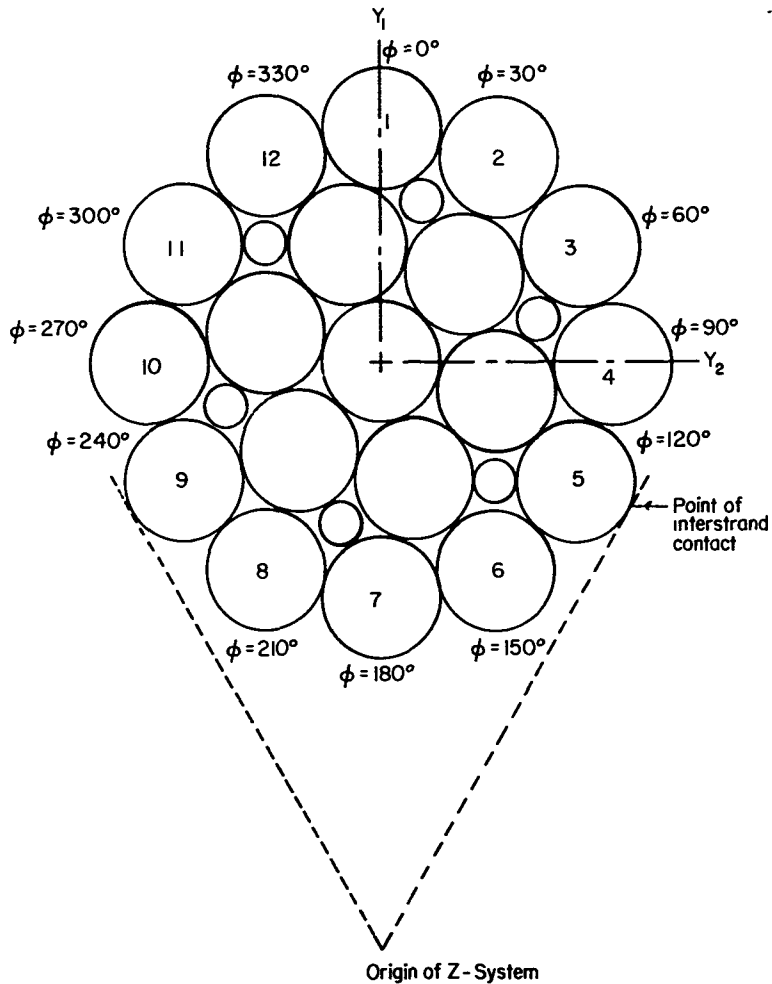


Figure 4-6. Plane Section of a 6 x 25 Filler-Wire Strand

of real wire at all points along the length of the wire, but that it was not possible to make measurements with the accuracy required to determine the correct solution.

An interesting demonstration of the validity of the assumed wire-rope geometry can be made by observing the geometric pattern that a wire projects onto the $Z_1 - Z_2$ plane, and comparing it with the pattern seen by looking along the Z_3 axis of a wire removed from a preformed wire rope. The values used for these coordinates (Z_1, Z_2) can be obtained from either double-helix solution. Figure 4-7 represents the $Z_1 - Z_2$ plot for the Standard Rope. In this construction, both the wires and the strands are wrapped in right-hand

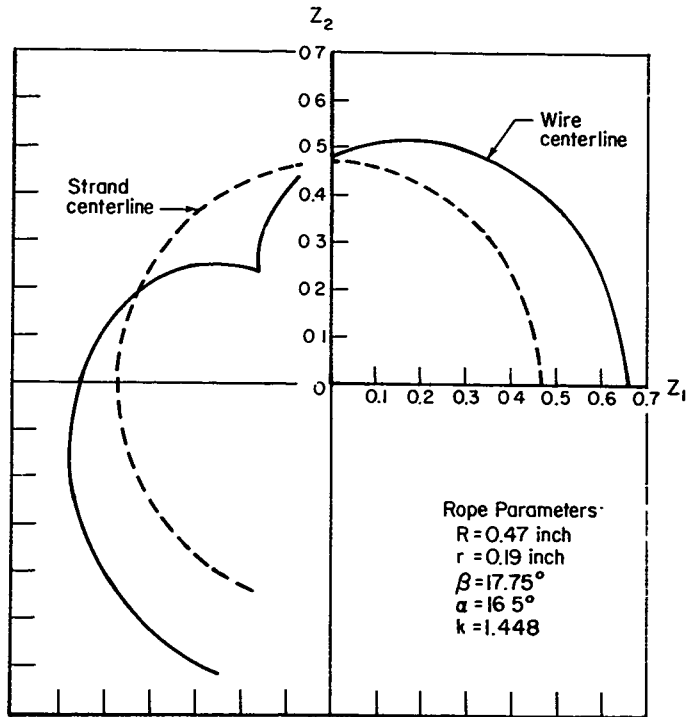


Figure 4- . Illustration of Wire Position in the Standard Rope Relative to the $Z_1 - Z_2$ Coordinate System

helices. It was noted that upon looking down the length (along the Z_3 axis) of a preformed Lang-lay wire, the same geometric pattern as shown in Figure 4-7 was observed. Further, for measurement purposes, there is no appreciable difference in the geometries generated by application of the constant-angle and uniform-motion assumptions. In other words, the difference in the geometries cannot be measured on an actual rope, thus eliminating actual measurement as a method of determining which solution provides the results most nearly matching a real rope.

As a further check on the validity of the solutions, the wire lay angle, α , was varied to confirm that as α approaches some small finite value, the wire geometry becomes that of a simple helix. Considering first the uniform-motion solution, substituting $k = 0$ into the appropriate equations will yield the geometry of a simple helix. This can be seen most easily by referring to the straight rope geometry, Figure 4-2. Physically, letting $k = 0$ produces a rope geometry such that any outer wire maintains its same position in the strand along the length of the rope.

On first thought, it might seem that for $k = 0$ the wire lay angle, α , is also zero and that both the wire and strand centerlines are at angle β to the rope centerline. However, setting k equal to zero in Equation 4-12 yields a value for α of approximately 6.45 degrees for the outer wire at $\theta = 0$ in the Standard Rope. That such a small, nonzero α actually exists for $k = 0$ can be easily verified by viewing the simple-helix geometry. The strand centerline lies at angle β to the rope centerline and has pitch radius R . The lay length of the strand is defined as the distance that the strand covers along the rope centerline for one revolution of θ , and is equal to $R\theta/\tan \beta$ as shown in Figure 4-8. With the wire parallel with the strand centerline, the wire also takes the geometry of a simple helix with a pitch radius of $R + r$ for the outer wire at $\theta = 0$. For any given θ , the lay lengths of wire and strand are equal, and β' can be written as

$$\beta' = \tan^{-1}\left(\frac{R+r}{R}\right) \quad (4-13)$$

For the Standard Rope, $\beta' = 24.20$ degrees. The wire lay angle, α , can be found by noting that $\alpha = \beta' - \beta$, at $\theta = 0$. This yields $\alpha = 6.45$ degrees, which equals the value of α predicted by the uniform-motion solution for $k = 0$.

Also, the value of radius of curvature, ρ , predicted by the uniform motion solution, at $\theta = 0$, $k = 0$, exactly equals the ρ calculated for a simple helix of radius $R + r$ and lay angle β' . This value of ρ is computed as $(R + r)/\sin^2 \beta'$ and is equal to 3.93 inches.

As α is varied in the constant-angle solution, a singularity occurs in the (θ, β) relationship. The $(a - c)^2 > b^2$ condition used to determine Equation 4-10 does not hold true between 6.45 degrees and 6.95 degrees, thus changing the form of the relationship (Ref. 4-6). The arc tangent in Equation 4-10 becomes either the inverse hyperbolic tangent or cotangent depending on whether the magnitude of its argument is more or less than one. When the magnitude of the argument is one, then the inverse hyperbolic grows infinite, something which is not consistent with rope geometry.

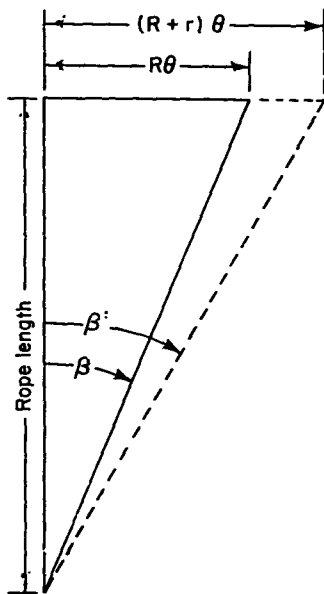


Figure 4-o. Illustration of the Interrelationship Between Strand Lay Angle and Strand Length as Compared to Rope Length

It should be noted, however, that this singularity in the (θ, θ') relationship does not affect the predicted radius of curvature for the constant-angle solution, since all the information about θ and θ' necessary for computing ρ is contained in Equation 4-9. Furthermore, the wire becomes a simple helix at $\alpha = 6.45$ degrees, where "average slope" k is zero, and this is just the value of α predicted by simple helix-geometry considerations above. The significance of this value of α , which corresponds to the lower limit of the singularity region, has yet to be realized. The value of ρ at $\theta = 0$, predicted by the constant-angle solution, is again 3.93 inches.

Another check of the constant-angle solution is possible by letting α equal 90 degrees. For this case the computed radius of curvature equals r , the pitch radius of the wire. This is the expected result since for this lay angle the wires form circles. Similarly, as k approaches infinity in the uniform-motion solution, a radius of curvature equal to r also results. Thus, both solutions reduce to expected results for extreme cases of α and k and remain possible solutions.

As was stated earlier in this report, the analysis is presented specifically for a Lang-lay rope. However, it is now simple to obtain the solutions for a regular-lay construction by noting a sign change.

For the constant-angle solution, substituting a negative α into Equations 4-7 through 4-11 makes them correspond to equations for a regular-lay rope. Thus, the (θ, θ) relationship is modified slightly, but is still the same general form as in Figure 4-3. The most interesting aspect, though, is that the radius-of-curvature plot is unchanged from that displayed in Figure 4-5.

Similarly, a solution for regular-lay rope may be obtained by substituting $\theta = -k\theta$ into the uniform-motion-solution equations for radius of curvature. Again, the same radius-of-curvature plot is obtained for both Lang-lay and regular-lay ropes provided that the two values for k are chosen to correspond to the same magnitude of average α . Note that for the same magnitude of average α for Lang-lay and regular-lay ropes, the magnitudes of the k 's are different. For example, when average α in the regular-lay rope $k = -3.355$. This is true since zero k occurs at nonzero α . Figure 4-9 displays the

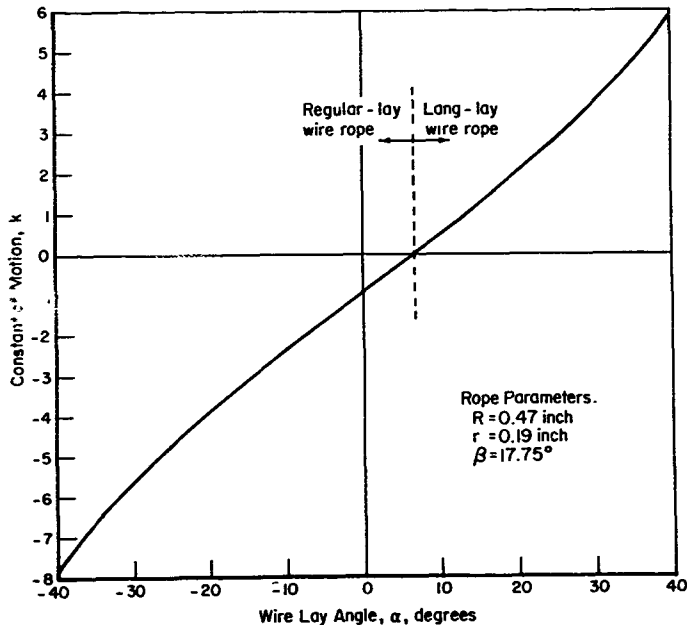


Figure 4-9. Relationship Between Wire Lay Angle and the Constant of Motion.

relationship of k to α for both regular-lay and Lang-lay ropes. The curve is valid for either the uniform-motion solution (k versus average α).

While varying α to make the preceding checks on the radius of curvature solutions, an unexpected sensitivity to α was noted in ρ . Figure 4-10 shows a family of curves for radius of curvature from the constant angle solution as a function of the wire lay angle, α , for various values of θ . When it is realized that α is the most difficult parameter in the rope to measure, the importance of Figure 4-10 becomes apparent. For instance, a one-degree error in measuring α for the Standard Rope can result in as much as a 27 percent error in the value of ρ at $\theta = 180$ degrees.

A similar family of curves for the uniform-motion solution is shown in Figure 4-11. Both the constant-angle and uniform-motion solutions predict a singularity at $\theta = 180$ degrees for α approximately 11 degrees, or k approximately 0.5. Since the singularity predicts a straight segment of wire at this point, this seems entirely reasonable.

Since the radius-of-curvature plots, Figure 4-5, are the same for both regular-lay and Lang-lay, it should be expected that Figure 4-10 is the mirror image of the same family of curves for negative values of α . (The curves are symmetrical about $\alpha = 0$.) This is true even though the transition from Lang-lay to regular-lay occurs at $\alpha = 6.45$ degrees. Also, for the uniform-motion solution, Figure 4-11 would be the same mirror image of the curves with the curves being symmetrical about $k = -0.95$.

4.2.2. Analysis of a Wire Rope Wrapped on a Sheave

The analysis to determine radii of curvature of the wires in a rope wrapped on a sheave (triple helix) proceeds in an analogous manner to the analysis of the straight rope (double helix). First, the rope geometry must be defined. Then, reference-angle relationships must be derived. Once the angle relationships are determined, then simple substitution of geometrical derivations into Equation 4-6 yields the desired result.

4.2.2.1. Wire-Rope Geometry

The rectangular coordinate systems which define the rope-on-sheave configuration are a modification of the straight rope coordinate systems, Figure 4-2. With one exception, the desired coordinate system involves laying the Figure 4-2 coordinate system at right angles and at sheave radius, R , to a central coordinate system, X_1, X_2, X_3 . In Figure 4-12, the Y-coordinate system has been reduced to lie in the $Z_1 - Z_2$ plane such that the Y_1 axis is collinear with the radial vector component ($R \cos \theta, R \sin \theta, 0$). This alteration is dictated by the curvature of the rope since, for example, beginning at the origin of the Z system, the desired point of the strand centerline, A in Figure 4-2, is no longer vertically oriented above the $Z_1 - Z_2$ plane as it was in the straight rope analysis. Justification for this change is that reference angle θ is now dependent on the sheave reference angle, ψ , and the Z system is now rotating in order to follow the wire geometry.

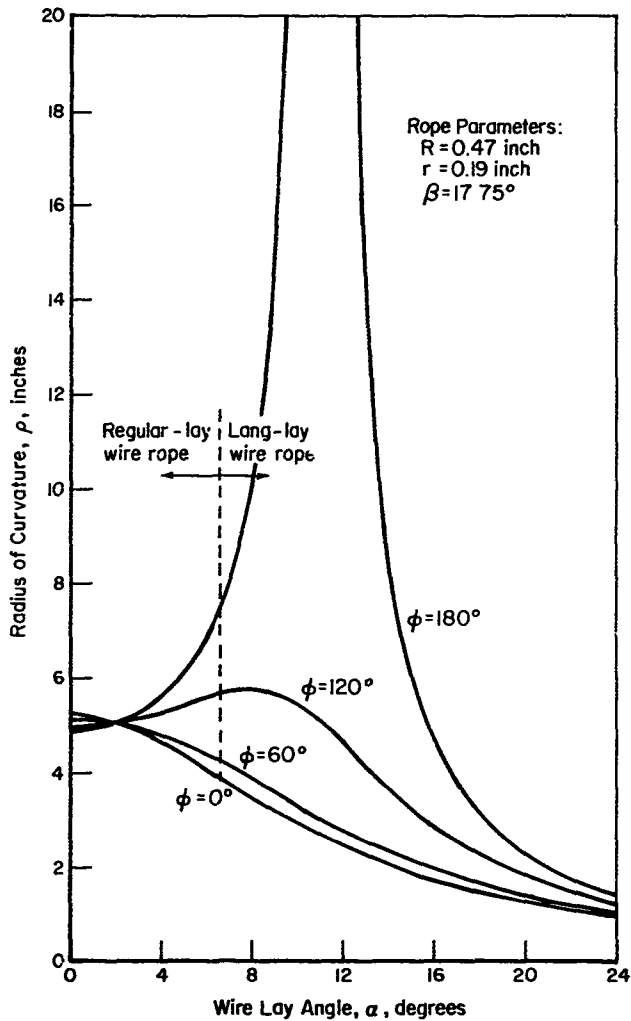


Figure 4-10. Sensitivity of Radius of Curvature to Wire Lay Angle - Constant Angle Assumption

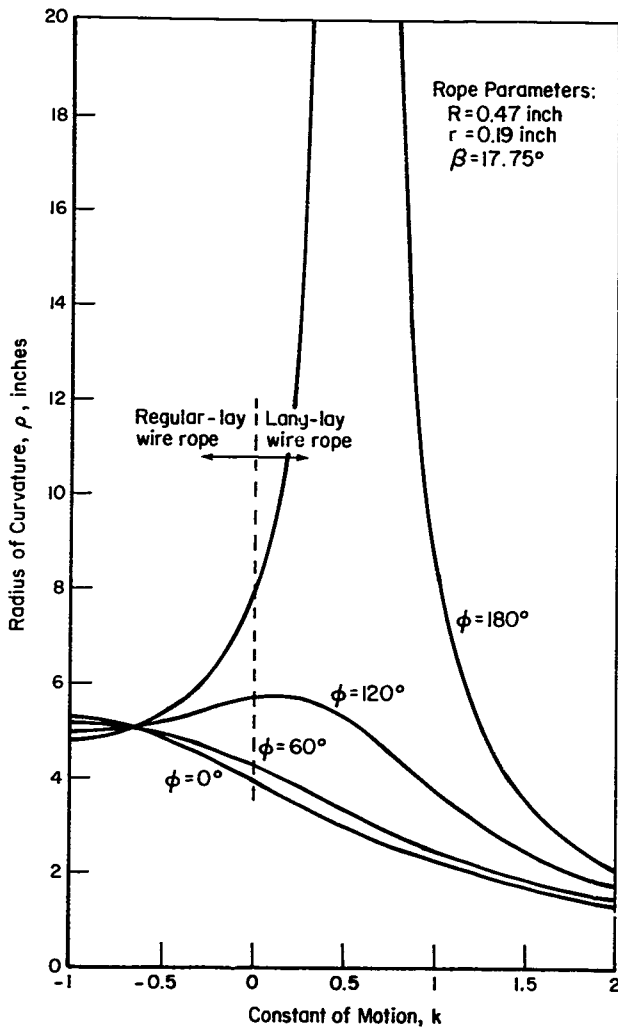


Figure 4-11. Sensitivity of Radius of Curvature to Constant of Motion - Uniform-Motion Assumption.

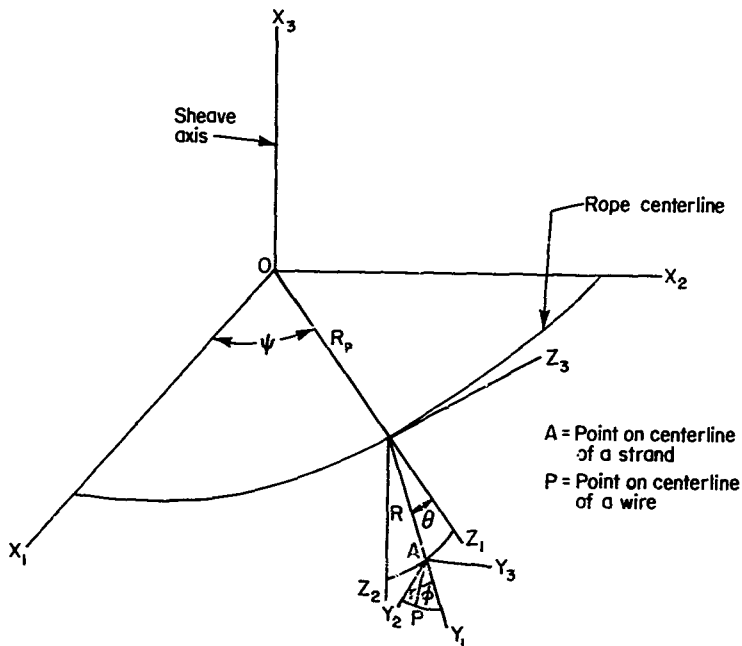


Figure 4-12. Geometry of a Wire Rope Wrapped on a Sheave

It might be noted at this point that the present analysis could be made perfectly general by wrapping the rope helically on a drum at a prescribed lay angle instead of wrapping it on a sheave at the specific lay angle of ninety degrees. However, the complexity of the geometrical derivatives even with this simplification will soon substantiate the decision to consider just the sheave. Physical intuition also indicates that the sheave presents the most interesting case since, given any drum of radius, R_p , maximum bending stresses in the rope occur at the ninety-degree rope lay angle.

Due to the above-mentioned complexity, the derivation of the geometrical-position equations and their associated derivatives will be performed through the strict utilization of matrices (see Section 5.1) and no attempt is made to expand the results in this report. Expansion of the matrices is contained in the digital computer solution, Section 5.6.

4.2.2.2. Derivation of Equations

In Figure 4-12, the coordinates of the point, P, on the wire centerline under consideration, can be related to the Z system by

$$[Z] = [\theta] [\beta] [Y] + [A'] \quad (4-14)$$

where $[\theta]$, $[\beta]$, and $[Y]$ retain their definitions as given in Section 5.1. $[A']$ must be, because of the previously mentioned coordinate alteration,

$$[A'] = \begin{bmatrix} R \cos \phi \\ R \sin \phi \\ 0 \end{bmatrix}$$

The coordinates in the Z system can be related to the X system as,

$$[X] = [\psi] [\chi] [Z] + [C] \quad (4-15)$$

where, by analogy with the straight-rope analysis,

$$[\chi] = \begin{bmatrix} 1 & 0 & 0 \\ 0 & 0 & 1 \\ 0 & -1 & 0 \end{bmatrix}$$

$$[\psi] = \begin{bmatrix} \cos \psi & -\sin \psi & 0 \\ \sin \psi & \cos \psi & 0 \\ 0 & 0 & 1 \end{bmatrix}$$

$$[C] = \begin{bmatrix} R_p \cos \psi \\ R_p \sin \psi \\ 0 \end{bmatrix}$$

Combining Equations 4-14 and 4-15 yields the X-system coordinates of point P,

$$[X] = [\psi] [\chi] ([\theta] [\beta] [Y] + [A']) + [C] \quad (4-16)$$

Expansion of Equation 4-16 yields the desired results.

It was at this point in the straight-rope analysis that the unresolvable problem of assuming a uniform-motion or a constant-angle configuration for the wires became apparent. A similar problem presents itself here in determining reference-angle relationships, but it is easily resolved.

First, consider that the strands in the bent rope assume the role of the wires in the straight rope (they, therefore, form a double helix). Then, considering the possible configurations of the strand, the uniform-motion and constant-angle assumptions with associated equations present themselves as possible solutions to determining a (ψ, θ) relationship of the constant-angle assumption.

Next, a (ψ, θ) relationship must be determined. To solve this problem, in general, the first derivative of $[X]$ might be dotted with the first derivative of the Point A, Figure 4-12, where, denoting $[AX]$ as the X system coordinates of A,

$$[AX] = [\psi] [\chi] [A'] + [C] \quad (4-17)$$

and, then, analogous to the straight rope analysis, the dot product is written,

$$[X'] \cdot [AX'] = |\bar{X}'| |\overline{AX}'| \cos \alpha$$

where α retains its straight rope analysis definition of the lay angle of the wire in strand. This procedure could be used to determine the new constant (ψ, θ) relationship of the uniform-motion assumption or the varying relationship of the constant-angle assumption. Note that β , the strand lay angle, is not constant in the uniform-motion solution when taking derivatives, but is governed by the relation analogous to Equation 4-13

$$\beta = \tan^{-1} \left(\frac{K_1}{\frac{R}{R_p} + \cos \theta} \right) \quad (4-18)$$

where K_1 is the relationship of (ψ, θ) .

However, when this technique is employed, the resultant equations are very complex. The constant-angle solution for a new (ψ, θ) relationship appears impossible to solve in closed form. The uniform-motion solution must be numerically integrated for average α , and this is an equally forboding task.

Further, even if this analysis were successfully performed, it is doubtful that the resultant (ψ, θ) relationship would be correct owing to the assumptions involved. The above analysis assumes a frictionless rope, i.e., all strands and wires are free to move as warranted to retain a constant-angle or uniform-motion configuration. An actual rope, however, exerts friction forces on the strands and wires which tend to maintain its configuration as the rope is bent. In fact, over the entire length of the rope, the average (ψ, θ) relationship for the straight rope must remain true for the bent rope since, upon bending of the rope, the strands and wires do not shift position at the ends of the rope. Thus, the average relative wire-to-strand (ψ, θ) relationship holds.

Therefore, the analysis will proceed considering the uniform-motion assumption since if uniform motion does exist, then the relationship is already known. The difficulty of assuming a constant angle is that the analysis becomes very complex and thus, for simplicity, this assumption is abandoned.

One further point deserves mention in the determination of the (ψ, θ) and (θ, θ) uniform-motion relationships. In discussing Figure 4-9 in the straight rope analysis section of this report, the relationship of lay angle α to constant of motion K , it was noted that the curve was valid either for the uniform-motion solution (constant K versus average α) in which a numerical integration was performed, or for the constant-angle solution (average K versus constant α). Therefore, it is apparent that α needn't be integrated to find the constant of motion, but the direct method of using average K from the constant angle solution can be utilized. This average K is simply one-half the reciprocal of the leading coefficient of Equation 4-10,

$$K = \sqrt{(a - c)^2 - b^2} \quad (4-19)$$

where, for the (\emptyset, θ) relationship $\emptyset = K_1 \theta$,

$$\begin{aligned} a &= \frac{R \tan \alpha}{r \sin \beta} \\ b &= \tan \alpha \sin \theta \\ c &= \cos \theta \end{aligned}$$

and, for the (ψ, θ) relationship $\theta = K_2 \psi$,

$$\begin{aligned} a &= \frac{R_p \tan \beta}{R} \\ b &= \tan \theta \\ c &= 0 \end{aligned}$$

Equation 4-16, the X system coordinates of Point P, can now be differentiated twice with respect to ψ to obtain \bar{X}' and \bar{X}'' . This task is accomplished in Section 5.5. without expanding the matrices of Equation 4-16, not because the matrix differentiation is easier than differentiation of the expanded equations, but because the results are easier to check for error and because the matrix results translate to computer-program statements simply. Finally, substitution of \bar{X}' and \bar{X}'' into Equation 4-6 yields the radii of curvature for the assumption of uniform motion in the rope bent over a sheave.

4.2.2.3. Results

The results of radii-of-curvature calculations for Standard Rope bent over a 12-inch sheave are displayed in Figure 4-13. The family of curves represent radii of curvature as a function of \emptyset , the position of the wire in the strand, and, for discrete values of θ , the position of the strand on the sheave.

Interpretation of the curves is quite straightforward. Referring to Figure 4-12, it can be seen that reference angle θ is measured from a line emanating from the X system origin, the sheave center, and passing through the rope centerline and is always measured in the perpendicular plane of the rope. Thus, $\theta = 0^\circ$ is the outside strand position, and $\theta = 180^\circ$ corresponds to the strand on the side of the rope in direct contact with the sheave. Figure 4-14 illustrates this relation. The various curves for discrete θ in Figure 4-13, therefore, represent the relative position of strand to sheave.

Similarly, reference-angle θ is measured in the perpendicular plane of the strand, which is tilted at lay angle β and oriented such that the line at angle θ locating Point A in Figure 4-12 forms its axis of tilt and is the reference line for \emptyset . Hence, Figure 4-14 can only show the true plane of the rope and the projected planes of the strands.

Interpretation of Figure 4-13 is now clear. Given any value of θ , simply rotate a line from the rope centerline in the clockwise direction to locate the strand. For any specific value of \emptyset at this strand position, simply rotate a line from the strand centerline in the tilted plane again in the

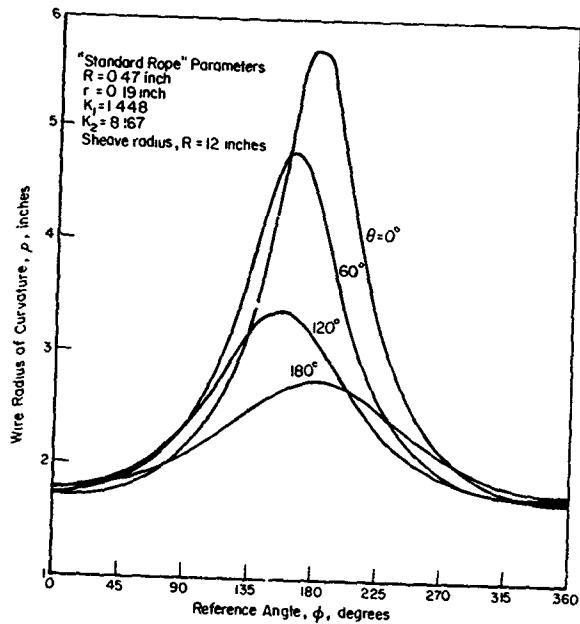


Figure 4-13. Radius of Curvature of Wires in a Rope Wrapped on a Sheave

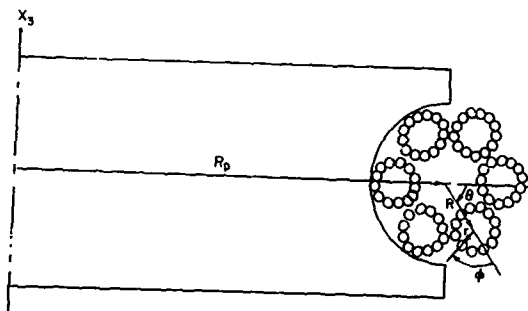


Figure 4-14. Plane Section of A Rope Wrapped on a Sheave

clockwise direction to locate a specific wire. Figure 4-13 shows the values of radii of curvature for all wire positions, all values of θ , and at unique strand positions, discrete values of θ .

Comparing curves of Figure 4-13 with the uniform-motion curve for the straight rope in Figure 4-5, it is readily apparent that maximum changes in radius of curvature occur at the $\theta = 180^\circ$ wire position on the $\theta = 0^\circ$ and the $\theta = 180^\circ$ strand position. An increase in radius of curvature corresponds to "back-bending" or straightening of the wire, as should be expected at position $\theta = 180^\circ$, $\theta = 180^\circ$.

It should be noted that Figure 4-13 displays only radii of curvature for θ between 0° and 180° . This is due not only to crowding of the curves, making them difficult to read for small values of θ , but also the curves' symmetry about $\theta = 180^\circ$. Mathematically, this relation is

$$\rho(\theta, \theta) = \rho(2\pi - \theta, 2\pi - \theta) \quad (4-20)$$

4.2.3. Analysis of Bending Stress

The above analysis of radii of curvature for the straight rope and the rope bent over a sheave have yielded the basic components for computing change in wire stress when the rope is bent.

However, in computing bending stress in the wires, it is apparent that simple bending occurs only at discrete positions in the rope. Simple bending refers to the case in which all bending occurs in one plane and the radius-of-curvature vectors for the wire, before and after the rope is bent, have no included angle between them. Observation of a wire rope reveals that most wires are not oriented such that their curvature aligns parallel with the plane of bending in the sheave and, thus, simple bending is an exception.

4.2.3.1. Derivation of Equations.

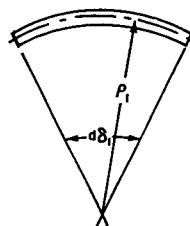
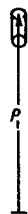
Therefore, a stress relation for complex bending must be derived. Figure 4-15a displays a segment of wire in the initially straight rope, where ρ_1 is the radius of curvature. The same segment of wire, after bending of the rope, Figure 4-15b, has radius of curvature ρ_2 . Figure 4-15c shows the relation between the initial and final positions of the wire, and Point N, the maximum stress position in the new configuration. Denoting r_w as the wire radius and ξ as the angle between ρ_1 and ρ_2 , and assuming $r_w \ll \rho_1$ or ρ_2 , which allows use of simple beam considerations in computing stress, the strain due to bending can be written as

$$\epsilon = \frac{l_2 - l_1}{l_1} \quad (4-21)$$

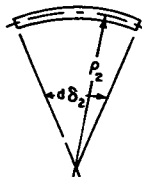
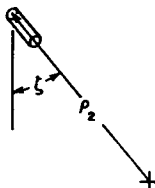
where

$$l_1 = (\rho_1 + r_w \cos \xi) d\delta_1 \quad (4-22)$$

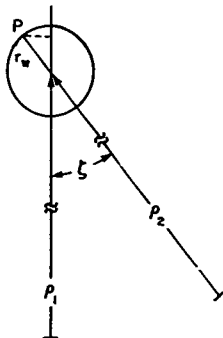
the length of the wire segment at Point P as viewed by ρ_1 , and



a.



b.



c.

Figure 4-15. Illustration of Wire Segments in Complex Bending

$$l_1 = (\rho_2 + r_w) d\delta_2 \quad (4-23)$$

the length of that same segment as viewed by ρ_2 .

Since the length of wire centerline in this segment is unchanged,

$$\rho_2 d\delta_2 = \rho_1 d\delta_1 \quad (4-24)$$

Then, assuming the linear Hooke's Law stress-strain relation such that

$$\sigma_b = E\epsilon \quad (4-25)$$

where

σ_b = bending stress, psi

ϵ = strain, inch/inch

E = Young's Modulus, 30×10^6 psi

and substituting Equations 4-22 and 4-23 into 4-25, the result is

$$\frac{\sigma_b}{E} = \frac{(\rho_2 + r_w) d\delta_2 - (\rho_1 + r_w \cos \xi) d\delta_1}{(\rho_1 + r_w \cos \xi) d\delta_1} \quad (4-26)$$

Then utilizing Equation 4-24,

$$\frac{\sigma_b}{E} = \frac{r_w d\delta_2 - r_w \cos \xi d\delta_1}{(\rho_1 + r_w \cos \xi) d\delta_1} \quad (4-27)$$

or finally,

$$\frac{\sigma_b}{E} = \frac{r_w}{\rho_1 + r_w \cos \xi} \frac{d\delta_2}{d\delta_1} - \frac{r_w \cos \xi}{\rho_1 + r_w \cos \xi} \quad (4-28)$$

Assuming $r_w \cos \xi \ll 1$, an assumption justified by Figure 4-5, and knowing that r_w is on the order of 0.05 inch, the result is,

$$\sigma_b = E r_w \left(\frac{1}{\rho_2} - \frac{\cos \xi}{\rho_1} \right) \quad (4-29)$$

The final point in the stress analysis concerns determination of angle ξ , the angle between ρ_1 and ρ_2 . Noting that the radius of curvature is directed along the second geometrical derivative (Ref. 4-8), then the coordinates of the straight rope and the bent rope must be aligned such that the angle between the second derivatives can be evaluated.

An easy method to align coordinates involves realizing that once values for ψ and θ have been specified in the bent rope, then ρ is independent of ψ , the reference angle in the sheave. This should be expected since no unique values of ψ exist, although all values of θ and θ in the bent rope are unique. For example, a wire at position $\psi = 0^\circ$, $\theta = 30^\circ$, $\theta = 60^\circ$, has the same radius of curvature as every other ψ position where $\theta = 30^\circ$, $\theta = 60^\circ$. Thus, ψ need not vary in the computer program, but a specific convenient value such as $\psi = 0$ can be chosen as the permanent sheave position. This value of ψ not only shortens the computer statements, but it also allows the straight rope

coordinate system to be placed at $(R_p, 0, 0)$ such that the straight rope is always tangential to the bent rope, Figure 4-16.

The coordinates are now aligned such that the Z coordinates of the straight rope correspond to the X coordinates of the bent rope as

$$\begin{aligned} Z_1'' &= X_{n1}'' \\ Z_2'' &= X_{n3}'' \\ Z_3'' &= X_{n2}'' \end{aligned} \quad (4-30)$$

where X_{n1} , X_{n2} , X_{n3} are the new X coordinates of the straight rope. Now as ϕ and θ are varied, the point whose radius of curvature is being considered is essentially always located in the $X_1 - X_3$ plane. Therefore, points in the $X_1 - X_3$ plane located by the same values of ϕ and θ are identical points. Dotting \bar{X}'' and \bar{X}_n'' , the cosine of ξ can be found as

$$\cos \xi = \frac{\bar{X}'' \cdot \bar{X}_n''}{|\bar{X}''| |\bar{X}_n''|} \quad (4-31)$$

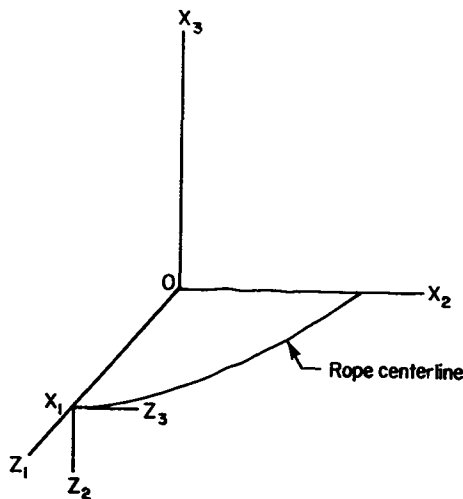


Figure 4-16. Coordinate Alignment Used for Comparing Radii-of-Curvature Results

It should be noted that since the plane in which θ is measured is tilted at angle θ to the $X_1 - X_3$ plane, the point under consideration can be as far as $r \sin\theta$ out of the plane. Then when the rope is bent, the same point will not be at the same location and a slight error in ξ is incurred. However, since for real rope and sheave parameters, $R_p \ll R + r$, the error is so slight that it can be completely ignored without loss of accuracy.

4.2.3.2. Results.

The results for straight rope, bent rope, and stress were programmed using Standard Rope parameters on a 24-inch-diameter sheave (see Section 5.6.). The results of stress calculations are displayed in Figure 4-17. Corresponding to maximum change in curvature, maximum stress change occurs at $\theta = 180^\circ$ on the $\theta = 0$ and $\theta = 180^\circ$ strands. Positive stress indicates tension on the side of the wire furthest from its associated center of curvature. Negative stress, of course, then indicates compression. A number of strand positions are displayed in Figure 4-17, and stress, as is radii of curvature, is symmetrical about $\theta = 180^\circ$ by the relation,

$$\sigma(\theta, \theta) = \sigma(2\pi - \theta, 2\pi - \theta) \quad (4-32)$$

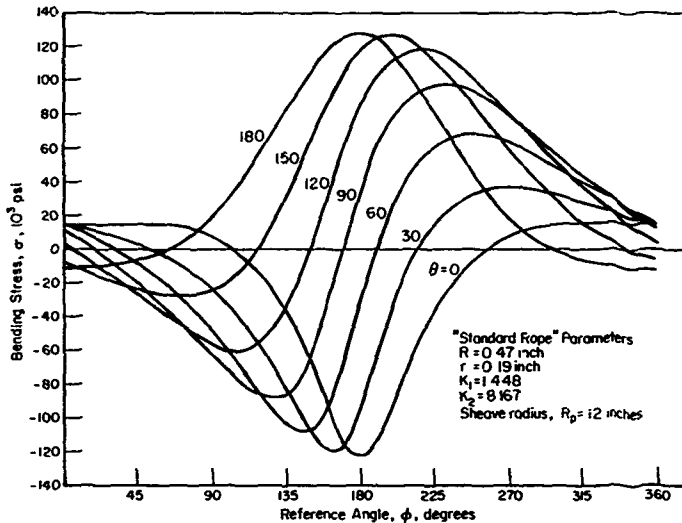


Figure 4-17. Bending Stress in Rope Wires Resulting From Bending of the Standard Rope Around a 24-Inch Diameter Sheave.

Although the magnitude of the stress at $\theta = 180^\circ$, $\theta = 180^\circ$ is slightly greater than that at $\theta = 180^\circ$, $\theta = 0$ this should not be construed as a general result. The important consideration, though, is that maxima always occur at these two positions and at these points $\xi = 0$. Therefore, substitution of $\theta = 180^\circ$ at $\theta = 0^\circ$ and $\theta = 180^\circ$ into the radius of curvature equations greatly simplifies them for future work which will include evaluation of the influence of various rope and sheave parameters on rope-wire bending stress.

4.3. CONTACT STRESSES

Contact stresses in a wire rope are one of the most important determinants of its fatigue life and are, by far, the most difficult to analyze. To date, no reliable and accurate analysis has been completed, primarily because these stresses, even under low rope tensile loads, are so high that the wires yield, changing the geometry and thus invalidating the elastic force-geometry-stress relationships normally used for stress computation.

There are four areas in a normal wire rope where contact stresses can be induced:

1. At the wire-sheave interfaces
2. At the interfaces between wires in a strand
3. At the interfaces between wires in adjacent strands
4. At the interfaces between the wires in the strands and the wires in the core of an IWRC rope.

4.3.1. Wire-Sheave Interface

No published analysis is known for the contact stresses induced at the wire-sheave interface. This represents a major gap in wire-rope analysis since, for many common rope systems, this is the area where wire failures first start.

One investigator (Ref. 4-9) has published a derivation of the standard formula for the average contact pressure. It is written as follows:

$$p = \frac{2T}{Dd} \quad (4-33)$$

where

- p = average contact pressure, lb/in²
- T = tensile force on rope, lb
- D = sheave diameter, in
- d = rope diameter, in.

This derivation is based on a static analysis only, and the investigator goes on to derive equations for the average pressure that include the effects of rope weight, friction, differential sheave-rope rotational velocity, and a

differential tension in the rope between first and last rope-sheave contact. The resulting equations are quite complex, and, except for unusual conditions, the average pressure changes only slightly.

No analytical work on actual wire-sheave contact pressures is known. One investigation (Ref. 4-10) did experimentally determine the "footprint" of a wire rope wrapped around a sheave-like radius for the quite unusual condition of an aircraft arresting-gear cable wrapped around an arresting hook point.

4.3.2. Wire Interfaces in a Strand

The radial force on an infinitely thin wire helically wrapped on a cylinder is (Ref. 4-11)

$$F_w = T_w \frac{\sin^2 \alpha}{\rho} \quad (4-34)$$

where

- F_w = force between wire and cylinder (core wires), lb
- α = lay angle of wire in strand, measured between strand and wire, degrees
- T_w = tensile force on wire, lb
- ρ = radius of curvature of wire, in

The individual radial forces must then be combined to relate to the strand tension, T_s . For a simple seven-wire strand with wires of equal diameter, the relation is (Refs. 4-7 and 4-12)

$$F_w = \frac{T_s \cos^2 \alpha \sin^2 \alpha}{d_w (1 + 6 \cos^2 \alpha)} \quad (4-35)$$

where, in addition to the terms above:

d_w = diameter of wire, in

No published relation for more complex strands is known, although its formulation would be a relatively simple extension of the work described above.

The contact stresses between the parallel wires are (Ref. 4-13)

$$\sigma_x = -2\mu \left\{ \left[1 + \left(\frac{z}{b} \right)^2 \right]^{\frac{1}{2}} - \frac{z}{b} \right\} \frac{b}{\Delta} \quad (4-36)$$

$$\sigma_y = - \frac{\left\{ \left[1 + \left(\frac{z}{b} \right)^2 \right]^{\frac{1}{2}} - \frac{z}{b} \right\}^2}{\left[1 + \left(\frac{z}{b} \right)^2 \right]^{\frac{1}{2}}} \frac{b}{\Delta} \quad (4-37)$$

$$\sigma_z = - \frac{b}{\Delta} \left[1 + \left(\frac{z}{b} \right)^2 \right]^{-\frac{1}{2}} \quad (4-38)$$

where b is the half-width of the rectangular area of contact between the wires and is given by

$$b = \left(\frac{2R_w \Delta}{\pi} \right)^{\frac{1}{2}} \quad (4-39)$$

For parallel wires,

$$\Delta = \frac{d_w (1 - \mu^2)}{E} \quad (4-40)$$

In these equations

E = modulus of elasticity, lb/in²

μ = Poisson's ratio

σ_x = stress in axial direction, lb/in²

σ_y = stress in direction tangential to the wire, lb/in²

and

σ_z = stress in direction radial to the wire, lb/in²

In more complex strand configurations, parallel wire contact is not achieved. (See Volume I of this Wire-Rope Handbook for a discussion of strand constructions.) When this is the case, the simplified equations presented above cannot be used, and the more complex methods discussed in the next section must be applied.

4.3.3. Interstrand Wire Contact

In general, the contact forces and stresses induced between the wires of adjoining strands must be computed using the geometry of the particular rope under consideration and the general contact-stress formulas, which are far too complex for the scope of this handbook. Once the forces are known, the stresses can be computed using the methods presented in Reference 4-13. Several general comments on the problem and several solutions for specific rope geometries are, however, in order.

In computing the interstrand contact force, it is necessary to know (or assume) the amount of support contributed by the core, since this governs the interstrand spacing and, thus, the force. Most investigations, when analyzing synthetic-core ropes, assume a worst-case condition--no core support at all. This, of course, produces the highest interstrand forces. It is, however, not a particularly realistic assumption, especially when a rope is new and subjected to only moderate forces. The actual interstrand force is an extremely complex function involving core material, core hardness, core condition, core size, length and type of rope service, and many other variables. In view of this, the assumption of no core support seems the only one practical for general rope analysis. (Of course, for specific situations the amount of core support can be determined, at least roughly, by measurements.)

Another fact which makes the calculation of interstrand contact stresses unrealistic is that they are so high, even for relatively low rope tensile loads, that the yield strength of the material is exceeded. All of the equations are based on elastic behavior. No complete analysis attempting to account for the actual plastic behavior is known. (One incomplete attempt is discussed later.)

Even with these drawbacks, evaluation of the stresses is of value because they can be used to qualitatively evaluate various constructions.

4.3.4. Interstrand Contact Forces

For any six-strand rope, the maximum interstrand contact force per unit of rope length is (Ref. 3-3)

$$F_s = \frac{T}{6R} \sin \beta \tan \beta \quad (4-41)$$

where F_s = interstrand contact force, lb
 T = tensile force on rope, lb
 R = pitch radius of strand, measured from rope centerline, in
 β = lay angle of strand in rope, measured between rope and strand centerlines, degrees.

This interstrand force is actually imposed at discrete points along the length of the strand where the outer wires touch. The distance between these contact points is

$$L_c = \frac{2\pi r_o}{n_o \tan \alpha_o} \quad (4-42)$$

where L_c = distance between interstrand contact points, in
 r_o = pitch radius of outer wires measured from strand centerline to wire centerline, in
 n_o = number of outer wires in a strand,
 α_o = lay angle of outer wires, degrees.

Combining equations 4-41 and 4-42 gives the interstrand force at each contact point:

$$F_s = \left(\frac{2\pi \sin \beta \tan \beta}{6n_o \tan \alpha_o} \right) \left(\frac{R}{r_o} \right) T \quad (4-43)$$

For a 1-3/8-inch-diameter, 6 x 25, filler-wire, Lang-lay, round-strand wire rope (exact dimensions given in Reference 3-3), the interstrand force is

$$F_s = .0123T \quad (4-44)$$

4.3.5. Interstrand Contact Stresses

As noted above, the equations defining all of the interstrand contact stresses are extremely complex, involving the evaluation of several elliptic integrals. (They must, however, be used if a solution to the combined stress problem is attempted.) It is possible and fairly simple to compute the maximum interstrand contact stresses. They can be found by solving the following simplified equations (Ref. 4-13):

$$A = \frac{1}{2} \left(\frac{1}{r_w} + \frac{1}{\rho} \right) - \frac{1}{2} \left(\frac{1}{r_w} - \frac{1}{\rho} \right) \cos \theta_c \quad (4-45)$$

$$B = \frac{1}{2} \left(\frac{1}{r_w} + \frac{1}{\rho} \right) + \frac{1}{2} \left(\frac{1}{r_w} - \frac{1}{\rho} \right) \cos \theta_c \quad (4-46)$$

$$\Delta = \frac{2}{A+B} \left(\frac{1-\mu^2}{E} \right) \quad (4-47)$$

where

θ_c = wire crossing angle, degrees.

Then, using charts from Reference 4-13 to find the values of the terms C_b , C_σ , C_τ , C_G , and C_{ZS} from the value of B/A , the stresses can be found as follows:

$$b = C_b (F_c \Delta)^{1/3} \quad (4-48)$$

$$\sigma_{\max} = C_\sigma \left(\frac{b}{\Delta} \right) \quad (4-49)$$

$$\tau_{\max} = -C_\tau \left(\frac{b}{\Delta} \right) \quad (4-50)$$

$$\tau_{G\max} = C_G \left(\frac{b}{\Delta} \right) \quad (4-51)$$

$$Z_S = C_{ZS} b \quad (4-52)$$

where

b = semiminor axis of ellipse of contact, in
 σ_{\max} = maximum normal stress, lb/in²
 τ_{\max} = maximum shear stress, lb/in²
 $\tau_{G\max}$ = maximum octahedral shear stress, lb/in²
 Z_S = distance below wire surface at which τ_{\max}
 and $\tau_{G\max}$ occur, in.

The maximum compressive contact stress always occurs at the surface in the z direction.

Using the same 6 x 25 rope referenced above, and utilizing the approximate radius of curvature of the outer wires discussed in the section on bending stress ($\rho = r_w / \sin^2 \alpha$, which introduces only a negligible error), the maximum contact stresses computed using the formulas above are

$$\sigma_{\max} = -(5.51 \times 10^4) T_R^{1/3}$$

$$\tau_{\max} = (1.76 \times 10^4) T_R^{1/3}$$

$$\tau_{C\max} = (1.58 \times 10^4) T_R^{1/3}$$

To illustrate the magnitude of these stresses, only 183 pounds of rope tension would induce a maximum shear stress of 100,000 psi, which is about the yield point of some rope wire. The tension in the rope is higher than this when it is being manufactured. Thus, any meaningful stress analysis of even a straight rope must account for core support and plastic behavior of the wires.

4.3.6. Core-Strand Interface Stresses

No analysis of the contact stresses at the core-strand interface in an IWRC rope is known. The stresses here, however, are probably even higher than those between the strands because the wires in the core rope are generally small. Some confirmation of this assumption has been found when IWRC ropes that have been cycled in the laboratory for only a small percentage of their fatigue life are dissected. Frequently, the core wires are found in small pieces.

4.3.7. Elastic-Plastic Analysis

Obviously, the absurdly high values of contact stress that are predicted for low rope loads, assuming elastic behavior of the wire, make any such numerical results useless except as a starting point for an elastic-plastic analysis. One investigator (Refs. 4-14 and 4-15) attempted such an analysis but did not complete it.

4.4. TORSIONAL AND SHEAR STRESSES

No published analysis of torsional stresses in a wire rope is known. One investigator (Refs. 4-16 and 4-17) has derived equations for torsional stresses in strands but has not extended these to rope.

The importance of directly induced shear stresses, either torsional or longitudinal, is questionable when the rope ends do not rotate (ends fixed or torque-balanced) thus preventing significant rotational strain. As pointed out in the section on Failure Modes in Wire Rope, one characteristic wire failure mode is a typical 45-degree shear-type failure, but this type can be (and probably is) induced by the complex combination of tension, bending, and compressive contact stresses at the point of wire failure.

4.5. WIRE ROPE DYNAMICS

In almost all wire-rope systems, the rope is subjected to dynamic loads to a greater or smaller degree. In most of these cases, these dynamic loads are

either small enough to be ignored or can be accounted for by simply adding the forces due to acceleration to the design loads. The dynamic action of the rope itself is not considered.

However, in some systems, the dynamic effects of the rope are of such importance that they must be considered. Examples are mooring systems, tow ropes (and cables) in both water and air, and aircraft arresting-gear systems. Many groups have studied and solved these problems, at least to a degree sufficient for engineering accuracy. These solutions are typically quite complex and require a computer for their use. A complete coverage of this subject is beyond the scope of this handbook. Each subject is covered briefly, and the interested reader is provided with reference for more complete discussion and mathematical detail.

Generally, a survey of the literature available indicates that there is a distinct lack of published experimental and field data by which the analytical approaches can be validated. Field data are particularly lacking in the open literature. This is clearly an area in which more work is needed. One exception is a report (Ref. 4-18) on a series of experimental ocean lifts during which records were made of dynamic loads and frequencies.

4.5.1. Longitudinal Forces

Various techniques for computing dynamic longitudinal loads are surveyed in References 4-19, 4-20, 4-21, and 4-22. Of these, Reference 4-20 is particularly useful since it incorporates the information contained in the other surveys and also indicates if there was any experimental verification of the analysis. This report also lists a large number of references, both reports and articles, on this subject.

Snap loading, when the cable tension goes to zero then snaps to high value, is a special and very damaging case of dynamic longitudinal loading. It is examined both analytically and experimentally in Reference 4-13 for both a wire rope and a wire rope with a short length of nylon rope attached. As might be expected, the nylon had a substantial mitigating effect on the peak loads. Another group analyzed the problem using an analog computer (Ref. 4-24). Also, more recently, a series of experiments (Ref. 3-30) was conducted where the rope--in this case a strand--load was varied from a very low value (50 pounds) to from 25 to 50 percent of its breaking strength. The cycling rate was 3 and 6 seconds per cycle, something less than true impact, but not unreasonable for the loading rate that might be expected in a long wire rope. The results are shown in Table 4-2. Especially at the higher maximum load conditions, the lifetimes are quite short.

A computer program to solve transient, dynamic, and snap-load responses to surface excitations is presented in Reference 4-25. It was published subsequent to Reference 4-20, and has not been validated experimentally.

Table 4-2. CYCLIC IMPACT TEST DATA

($\frac{1}{2}$ " 1 x 19 galvanized aircraft cable (bare) rated breaking strength 8,200 pounds.)
(Specimen Length--12', 8")

Test Number	Static Load	Load Range (lbs)	Sec/Cycle	Total Cycles ^a	Time	Remarks
1	2,000	50 - 4,000	6	1,700	3.0 hours	Eight wire failures inside end fitting.
2	2,000	50 - 4,000	6	1,000	2.0 hours	One outer-wire failure outside end fitting
3	2,000	50 - 4,000	6	800	1.6 hours	One wire failure inside end fitting
4	1,500	50 - 3,000	3	8,300	7.0 hours	One wire failure inside end fitting.
5	1,500	50 - 3,000	3	4,200	3.5 hours	One wire failure inside end fitting
6	1,500	50 - 3,000	3	11,200	9.0 hours	One wire failure inside end fitting
7	1,300	50 - 2,000	3	48,800	41.0 hours	One wire failure inside end fitting
8	1,000	50 - 2,000	3	29,200	25.0 hours	Three wires failed outside end fitting.
9	1,000	50 - 2,000	3	16,300	14.0 hours	One wire failure at edge of end fitting.

^aTo the nearest 100 cycles

4.5.2. Transverse Forces

Normally, wire rope is not subjected to transverse forces except when it goes around a sheave, not usually considered a dynamics problem. There are, however, at least two cases where dynamic transverse forces are important--strumming induced by vortices when a rope is in a moving fluid (usually air or water), and impact on aircraft arresting-gear rope. (Another case of transverse vibrations, but in this case excited by a sudden increase in tensile force in a suspended rope span, is treated analytically in Reference 4-26.)

4.5.2.1. Strumming

When a wire rope (or cable) is subjected to crossflow at Reynold's numbers from about 10^3 to 10^6 , vortices are formed that produce a fluctuating pressure. This causes the rope to vibrate in a plane normal to the direction of flow. The phenomenon is known as "galloping" when produced in overhead tension lines by winds and "strumming" when produced in a towed wire rope or mooring rope in a current. The discussion in this handbook will be confined to strumming. Reference 4-20 discussed the problem and points out that it causes cable fatigue, high acoustic noise levels, and increased drag. It also summarizes the status of analytical attempts to predict and describe the strumming phenomenon. Equations are presented and reproduced here that will provide rough design approximations and, at least, predict

when strumming is likely to be a problem. These were developed by a group of investigators at the Naval Air Development Center (Refs. 4-27 and 4-28).

Experimental studies have shown that flexible cylinders and cables are induced to vibrate by vortex shedding at frequencies approximated by the String Equation. The string equation for vibration in water is:

$$f_n = (n_f/2H) (T/m_c)^{1/2} \quad (4-53)$$

where

- f_n = natural frequency, Hz
- n_f = mode number, 1, 2, 3 ...
- H = cable length, in
- T = cable tension, lb
- m_c = virtual mass of cable, slug/in³

It has also been shown that the approximate frequency of vortex shedding from relatively short* cylinders and cables perpendicular to flow may be characterized by the Strouhal Equation which is given as:

$$f_s = S_s V_o / d \quad (4-54)$$

where

- f_s = Strouhal frequency, Hz
- S_s = Strouhal number ≈ 0.2 when
 $2 \times 10^3 < R_r < 1 \times 10^6$
- V_o = free stream velocity, in/sec
- d = diameter of cable, in
- R_r = Reynolds Number

When the cable is inclined to the flow by an acute angle, Ω , between the free stream and the cable, then the Strouhal relation is:

$$f_s \approx (S V_o \sin \Omega) / d \quad (4-55)$$

When the Strouhal frequency is found to be nearly the same as the natural frequency of the cable, the maximum vibration amplitude (for example, the worst strumming) occurs. The first step in investigating a cable segment for its propensity to strumming is to assign preliminary design values to the parameters in the string and Strouhal equations and then to determine if the resulting frequencies are nearly the same. If the frequencies are close, large-amplitude cable strumming may occur; if the frequencies are not close for several mode numbers, vibrations, if present, will probably be of small amplitude.

*A short cable is one that does not exhibit large variations in normal velocity component due to either streaming (bending) of the cable or non-uniform current profiles.

4.5.2.1.1. Increased Drag Due to Strumming

The following equation has been developed to predict the maximum drag coefficient (values for C_D when $f_s \cong f_n$) that can be expected in short sections of a strumming, smooth, circular cable,

$$C_{D_s} = C_D [1 + 10(d^2/m_c)^2] \quad (4-56)$$

where

C_{D_s} = drag coefficient for strumming cable

C_D = drag coefficient for stationary cable

d = cable diameter, in

m_c = virtual mass of cable, slug/in.

Equation 4-56 has been verified for small-diameter ($0.057 \text{ in} < d < 0.140 \text{ in}$) smooth cables of mass per unit length from 1.16×10^{-2} to 9.3×10^{-4} slug/ft over a range of Reynolds numbers from 300 to 1,300. No verification of the equation has been made for stranded cables.

4.5.2.1.2. Strumming Suppression.

If strumming must be reduced or eliminated in a cable, changes can be made to the cable system so that the natural frequency and Strouhal frequency are much different or a cable fairing can be added to disrupt the vortex-shedding process. Figure 4-18 (Ref. 4-27) shows how four cable fairings compare in terms of strumming drag coefficient and strumming force over a range of Reynolds numbers. In Table 4-3 (Ref. 4-20), several additional fairings are described and performance characteristics listed. It should be noted that for some fairings the drag coefficient is increased over that of a bare cable even though strumming force or vibration amplitude is reduced.

To summarize, analysis and design procedures to predict, describe, and suppress strumming in long cables under oceanic conditions are not possible. Today's procedures consist of comparing the natural frequency of a cable (Equation 4-53) with the Strouhal frequency for the cable in flow (Equations 4-54 and 4-55) to determine if strumming is likely. If strumming is predicted on this basis, changes are made to the system or some fairing is added to the cable.

4.5.2.3. Aircraft Arresting-Gear Cable.

The dynamic effects in aircraft arresting-gear cable used on carriers are probably the most violent of those normally induced in any common wire-rope system. An extensive body of literature exists on the subject covering both analytical and experimental work, but a full discussion of this extremely complex area is clearly beyond the scope of the handbook because of its specialized nature.

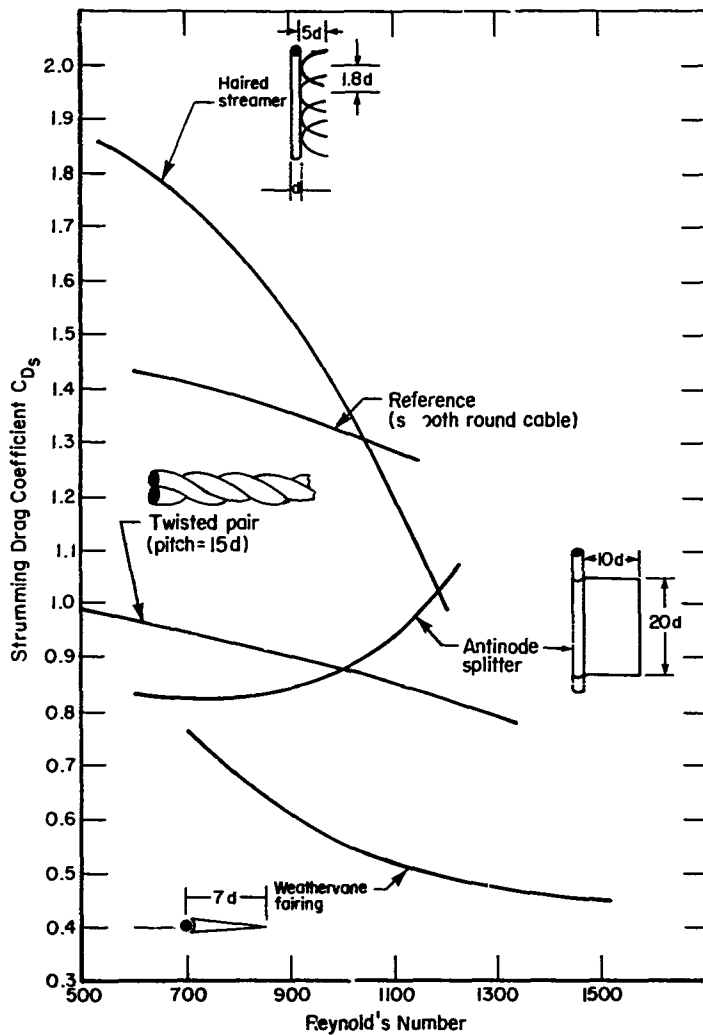


Figure 4-18. Strumming Drag Characteristics

Table 4-3. STRIPPING CHARACTERISTICS AND DRAG COEFFICIENTS FOR SOME BARE AND FAIRED CABLES

(All data in this table are based on results obtained from ocean or water-channel tow tests.)

Slope or Fairing Type	Slope Description	Performance	Reynolds Number	Normal Drag Coefficient	Tangential Drag Coefficient
Bare wire rope	1/2-inch, 7 x 19.	This cable was observed to be vibrating at all tow speeds from 5 to 15 knots.	1.2×10^6	1.4	Approximately 2%
Hair cloth	Five hairs approximately 1/8-inch long resulting from spirally wrapping frayed cloth around the cable.	Vibration amplitudes the same as bare rope at tow speeds from 5 to 15 knots.	1.2×10^6	2.2	Probably quite high.
Flanged fairing I	1/16-inch nylon flange 8 inches long spaced at 2 per inch on 1/2-inch diameter, 7 x 19.	Vibration amplitudes negligible as compared to bare rope for tow speeds from 5 to 10 knots, and reduced for tow speeds from 10 to 15 knots.	1.2×10^6	2.6	Probably quite high.
Flanged fairing II	Same as above except spaced at 4 per inch, 1/2-inch, 7 x 19.	Same as above.	1.2×10^6	1.5	Probably quite high.
Flanged fairing III	1/16-inch nylon flange 8 inches long spaced at 2 per inch, 1/2-inch, 7 x 19.	Same as above.	1.2×10^6	1.3	Probably quite high.
Mesh fairing	Flexible canvas weather-vane fairing approximately 6 inches wide, 1/2-inch, 7 x 19.	Vibration amplitudes negligible for tow speeds of 5 to 10 knots, same as bare cable for speeds from 10 to 15 knots.	1.2×10^6	2.5	Probably quite high.
Bare wire rope	1/2-inch, 1 x 19.	Magnitude of vibration amplitude unknown.	6.3×10^6	1.33	Approximately 2% of normal drag.
Bare wire rope	5/16-inch, 7 x 19.	Same as above.	6.3×10^6	1.37	Same as above.
Bare wire rope	3/16-inch, 3 x 19.	Same as above.	6.3×10^6	1.22	Same as above.
Compacted bare wire rope	9/12-inch, 7 x 19.	Same as above.	6.3×10^6	1.45	Same as above.
Fluorocarbonated wire rope	1/2-inch (9).	Same as above.	6.3×10^6	1.22	Unknown.
Washed covering	rough braid over stranded cable, OD = 11/12-inch.	Same as above.	6.3×10^6	1.46	Unknown.
Braided covering with haired fairing	Same as above but with 1/8-inch by 3-inch hairs spaced at approximately 6 per inch.	Same as above.	6.3×10^6	1.32	Probably quite high.
Double haired fairing	Same as above except two sets of hairs spaced at approximately 6 per inch.	Same as above.	6.3×10^6	1.76	Same as above.
Ribbon fairing	0.015-inch-thick polyurethane film, 2 cable diameters wide, 6 diameters long, spaced at 1 to 3 diameters apart.	Optimal vibration suppression for lead ribbon.	2.28×10^6	Unknown	Unknown.
Helical strak	1/2-inch cable wrapped a around 1-inch tow cable with a pitch of approximately 10 inches. Direction of wrap reversed every 10 feet.	Vibration amplitude reduced by more than 50%.	High.	Unknown	Unknown.

The most extensive and thorough analysis of the problem is contained in a series of reports and articles by Ringleb (Refs. 4-25, 4-27, and 4-30). Though no details of the tests are given, it is stated that the analysis has been confirmed by experiments. Other references on the subject include References 4-2, 4-10, 4-31, and 4-32. For further and more up-to-date information, the serious investigator should contact the Naval Air Engineering Center directly.

5. APPENDIX

5.1. ROTATION AND TRANSLATION OF COORDINATES
WITH MATRICES

A convenient method of obtaining the new coordinates of a vector in an orthogonal system whose axes are not parallel with the present system is that of pre-multiplying the vector's column matrix by 3 x 3 direction cosine matrices and adding translational column matrices where appropriate (Ref. 5-1). This technique is illustrated here for the purpose of obtaining the coordinates of Point P in the Z system for the straight-rope analysis, and is not intended to be a presentation of vector matrix theory.

The general form of the direction cosine matrix is

$$\begin{bmatrix} X_1' \\ X_2' \\ X_3' \end{bmatrix} = \begin{bmatrix} X_1'X_1 & X_1'X_2 & X_1'X_3 \\ X_2'X_1 & X_2'X_2 & X_2'X_3 \\ X_3'X_1 & X_3'X_2 & X_3'X_3 \end{bmatrix} \begin{bmatrix} X_1 \\ X_2 \\ X_3 \end{bmatrix} \quad (5-1)$$

where $X_1'X_1$ is the cosine of the angle between the new X_1' -axis and the old X_1 axis, etc., as shown in Figure A-1.

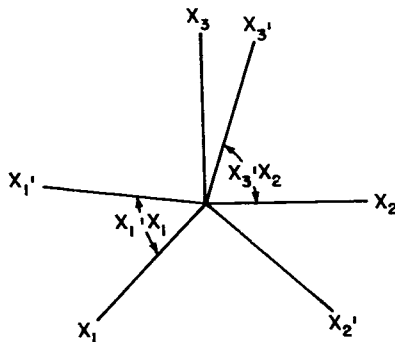


Figure 5-1. Cartesian Coordinates - Common Origin; Arbitrary Orientation.

$$[Y] = \begin{bmatrix} r \cos \phi \\ r \sin \phi \\ 0 \end{bmatrix} \quad (5-2)$$

Before any translation from the Y to the Z system can occur, the respective axes of the two systems must be parallel, which can be accomplished by two rotations of the Y system. The first rotation is through angle θ about the Y_1 axis, resulting in the rotation matrix

$$[\theta] = \begin{bmatrix} 1 & 0 & 0 \\ 0 & \cos \theta & \sin \theta \\ 0 & -\sin \theta & \cos \theta \end{bmatrix} \quad (5-3)$$

Another rotation through angle θ about the new Y_3 axis formed by the θ rotation gives

$$[\theta] = \begin{bmatrix} \cos \theta & -\sin \theta & 0 \\ \sin \theta & \cos \theta & 0 \\ 0 & 0 & 1 \end{bmatrix} \quad (5-4)$$

Point P, now in a system parallel with the Z system, can be translated through the coordinates of Point A to give

$$[Z] = [\theta] [\theta] [Y] + [A] \quad (5-5)$$

where

$$[A] = \begin{bmatrix} R \cos \theta \\ R \sin \theta \\ R \theta \cot \theta \end{bmatrix} \quad (5-6)$$

Expansion of Equation 5-5 produces the Z coordinates of P

$$[Z] = \begin{bmatrix} ((R + r \cos \phi) \cos \theta - r \sin \phi \cos \theta \sin \theta) \\ ((R + r \cos \phi) \sin \theta + r \sin \phi \cos \theta \cos \theta) \\ (R \theta \cot \theta - r \sin \phi \sin \theta) \end{bmatrix} \quad (5-7)$$

5.2. DERIVATION OF REFERENCE ANGLE RELATIONSHIP IN STRAIGHT ROPE

The choice of coordinates for the straight-rope analysis requires that a reference-angle relationship be derived. The derivation presented here results in (ϕ, θ) relationships for both the constant-angle and uniform-motion assumptions.

In the body of the report it was stated that the angle relationship can be determined by noting that the tangents to the helix curve, formed by the strand, and the double-helix curve, formed by the wire, have the angle, α , between them.

The tangent to the helix curve is, by Equation 5-6,

$$[A'] = \begin{bmatrix} -R \sin \theta \\ R \cos \theta \\ R \cot \theta \end{bmatrix} \quad (5-8)$$

and has magnitude

$$|\bar{A}'| = R \csc \theta \quad (5-9)$$

The tangent to the double-helix curve is found by differentiating Equation 5-5

$$[Z'] = \begin{bmatrix} -R \sin \theta - r \cos \phi \sin \theta (1 + \phi' \cos \theta) \\ -r \sin \theta \cos \theta (\phi' + \cos \theta) \\ R \cos \theta + r \cos \phi \cos \theta (1 + \phi' \cos \theta) - \\ -r \sin \theta \sin \theta (\phi' + \cos \theta) \\ R \cot \theta - r \phi' \cos \phi \sin \theta \end{bmatrix} \quad (5-10)$$

and has magnitude

$$|\bar{Z}'| = ((R \csc \theta + r \cos \phi \sin \theta)^2 + r^2 (\cos \theta + \phi')^2)^{\frac{1}{2}} \quad (5-11)$$

The scalar dot product of the two tangents is expressed as

$$\bar{Z}' \cdot \bar{A}' = |\bar{Z}'| |\bar{A}'| \cos \alpha \quad (5-12)$$

Substituting Equation 5-1 through 5-4 into Equation 5-5 and rearranging gives

$$\begin{aligned} ((R \csc \theta + r \sin \theta \cos \phi)^2 + r^2 (\cos \theta + \phi')^2)^{\frac{1}{2}} \cos \alpha = \\ (R \csc \theta + r \sin \theta \cos \phi) \end{aligned} \quad (5-13)$$

Squaring Equation 5-6 and rearranging yields the differential equation,

$$\phi' + \cos \theta = \pm \left(\frac{R \tan \alpha}{r \sin \theta} + \tan \alpha \sin \theta \cos \phi \right) \quad (5-14)$$

For a real Lang-lay wire rope, only the positive sign on the right side of Equation 5-7 has meaning. In all cases, ϕ and θ increase in magnitude simultaneously.

5.3. RADIUS OF CURVATURE EQUATIONS--STRAIGHT ROPE ANALYSIS

The radius of curvature, ρ , may be expressed as (Ref. 4-5)

$$\rho = \frac{(\bar{Z}' \cdot \bar{Z}'')^{1.5}}{|\bar{Z}' \times \bar{Z}''|} = \frac{|\bar{Z}'|^3}{|\bar{Z}''|} \quad (5-15)$$

In the analysis of the reference angle relationship (See Section 5.2.), Z' was derived and expressed in Equation 5-3. It is a simple, though tedious, task to obtain Z'' by differentiating again with respect to θ

$$[Z''] = \begin{bmatrix} -Z_2' + r\phi' \sin \phi \sin \theta (1 + \phi' \cos \beta) - r\phi'' \cos \phi \sin \theta \cos \beta \\ -r\phi' \cos \phi \cos \theta (\phi' + \cos \beta) - r\phi'' \sin \phi \cos \theta \\ Z_1' - r\phi' \sin \phi \cos \theta (1 + \phi' \cos \beta) + r\phi'' \cos \phi \cos \theta \cos \beta \\ -r\phi' \cos \phi \sin \theta (\phi' + \cos \beta) - r\phi'' \sin \phi \sin \theta \\ r\phi^2 \sin \phi \sin \beta - r\phi'' \cos \phi \sin \beta \end{bmatrix} \quad (5-16)$$

Equation 5-15) may be expressed rather simply on a computer program due to the number of repetitive terms.

5.4. COMPUTER PROGRAMS

The numerical results of the analysis were obtained through the use of digital computer programs in Fortran IV. The programs for the constant-angle solution as well as the numerical integration for average alpha, the wire lay angle, are included so that the results may be easily duplicated.

The programs are compatible with the computation services of Tymshare, Inc.* and may have to be altered for individual systems.

For the constant-angle-solution program, Fortran variable names used, and their corresponding quantities, are as follows:

<u>Variable Name</u>	<u>Quantity</u>
RL	R
RS	r
BT	β , measured in degrees
AL	α , measured in degrees
DPH	$d\phi$, incremental ϕ measured in degrees
COE	Conversion from degrees to radians
TH	θ , measured in radians
PH	ϕ , measured in radians
PH1	ϕ'
PH2	ϕ''
Z1, Z2, Z3	\bar{Z}
Z11, Z21, Z31	\bar{Z}'
Z12, Z22, Z32	\bar{Z}''
R	ρ

The program varies ϕ through 180 degrees and outputs ϕ , θ , ρ , and \bar{Z} . The constant-angle-solution program is as follows:

*Tymshare, Inc.; 525 University Avenue; Suite 220; Palo Alto, California 94301.

```

1.      C:DOUBLE HELIX-CONSTANT ANGLE SOLUTION
2.      ACCEPT RL,RS,BT,AL,DPH
3.      COE=.01745329
4.      BTA=BT*COE
5.      ALF=AL*COE
6.      DPHI=DPH*COE
7.      SB=SIN[BTA]
8.      CB=COS[BTA]
9.      Z311=RL*CB/SB
10.     A1=RL*SIN[ALF]/(RS*SB*COS[ALF])
11.     B1=SIN[ALF]*SB/COS[ALF]
12.     IF ((A1-CB)↑2)-GT-(B1↑2)) GO TO 13
13.     JK=1
14.     FG2=SQRT[(B1↑2)-(A1-CB)↑2]
15.     D=(B1-A1+CB)/FG2
16.     PH=0.
17. 14  SP=SIN[PH]
18.     CP=COS[PH]
19.     SP2=SIN[PH/2]
20.     CP2=COS[PH/2]
21.     TP2=SP2/CP2
22.     E=D*TP2
23.     IF ((ABS[E])·GT·) GO TO 99
24.     TH=ALOG[(1+E)/(1-E)]
25.     GO TO 37
26. 99  TH=ALOG[(E+1)/(E-1)]
27.     GO TO 37
28. 13  FG2=SQRT[(A1-CB)↑2-(B1↑2)]
29.     D=(A1-CB-B1)/FG2
30.     JK=0
31.     PH=0.
32. 11  SP=SIN[PH]
33.     CP=COS[PH]
34.     SP2=SIN+PH/2]
35.     CP2=COS[PH/2]
36.     IF (SP2) 30,31,31
37. 31  IF (CP2) 32,33,34
38. 30  IF (CP2) 32,35,36
39. 36  TH=2*(ATAN[D*SP2/CP2]+6·283186)
40.     GO TO 37
41. 34  TH=2*ATAN[D*SP2/CP2]+3·141593]
42.     GO TO 37
43. 33  TH=3·141593
44.     GO TO 37
45. 35  TH=3*3·141593
46.     GO TO 37
47. 37  TH=TH/FG2
48.     ST=SIN[TH]
49.     CT=COS[TH]
50.     PH1=A1-CB+B1*CP
51.     PH2=-B1*SP*PH1
52.     Z11=-RL*ST-RS*CP*ST*(1+PH1*CB)-RS*SP*CT*(PH1+CB)
53.

```

```

54.   Z21=RL*CT+RS*CP*CT*(1+PH1*CB)-RS*SP*ST*(PH1+CB)
55.   Z31=Z311-PH1*RS*CP*SB
56.   Z12=-Z21+RS*SP*ST*(1+PH*CB)*PH1-RS*CP*ST*CB*PH2
      -RS*CP*CT*(PH1+CB)*PH1-RS*SP*CT*PH2
57.   Z22=Z11-RS*SP*CT*(1+PH1*CB)*PH1+RS*CP*CT*CB*PH2
      -RS*CP*ST*(PH1+CB)*PH1-RS*SP*ST*PH2
58.   Z32=RS*SP*SB*PH1 2-PH1-RS*SP*ST*PH2
59.   DENOM=((Z21*Z32-Z31*Z22)+2+(Z31*Z12-Z11*Z32)+2
      +(Z11*Z22-Z21*Z12)+2)+0.5
60.   ZUMER=(Z11+2+Z21+2+Z31+2)+1.5
61.   R=ZUMER/DENOM
62.   Z1=RL*CT+RS*CP*CT-RS*SP*CB*ST
63.   Z2=RL*ST+RS*CP*ST+RS*SP*CB*CT
64.   Z3=Z311*TH-RS*SB*SP
65.   PH1=PH/COE
66.   THT=TH/COE
67.   DISPLAY PH1,THT,R,Z1Z2,Z3
68.   PH=PH+DPHI
69.   IF (180*COE-PH) 12,18,18
70.   18 IF (JK*EQ*1) GO TO 14
71.   GO TO 11
72.   12 STOP
73.   END

```

The program for the uniform-motion solution is not included, as it is merely a simplified version of the constant-angle-solution program. Since well over half of the constant-angle-solution program is devoted to the (ϕ, θ) reference-angle relationship, statements numbers 5, 70, 71, and 10 through 48 may be deleted and the following statements added in their place for the uniform-motion program

```

10.   PH=0
11.   18 SP=SIN[PH]
12.   CP=COS[PH]
13.   TH=PH/PH1
14.   PH2=0

```

In addition, modify statement number 2 to read,

```

2.   ACCEPT RL,RS,BT,PH1,DPH

```

Additional terms in the average-alpha numerical integration program are,

<u>Variable Name</u>	<u>Quantity</u>
T	k
S	Number of intervals of integration
ALPHA	α

Because of the smooth shape of the curve, Figure 4-4, it was found that as few as eight integration intervals, S, produced an accurate answer. The computer program for this integration is as follows:

```

1.  C:AVERAGE ALPHA-UNIFORM MOTION SOLUTION
2.  DIMENSION (750)
3.  ACCEPT RL,RS,BT,T,S
4.  COE=.01745329
5.  BTA=BT*COE
6.  SB=SIN(BTA)
7.  CB=COS(BTA)
8.  B=RL/(RS*SB)
9.  D=T+CB
10. DPH=180/S
11. PH=-DPH
12. M=S+1
13. DO 10 I=1,M
14. PH=PH+DPH
15. CP=COS(PH*COE)
16. 10 A(I)=ATAN[D/(B+SB*CP)]
17. SUMEV=0
18. SUMOD=0
19. N=M-1
20. K=N-1
21. DO 4 I=2,N,2
22. 4 SUMEV=SUMEV+A(I)
23. DO 5 I=3,K,2
24. 5 SUMOD=SUMOD+A(I)
25. AREA=DPH*(A(1)+4*SUMEV+2*SUMOD+A(M))/3
26. ALPHA=AREA/3.141593
27. DISPLAY T,ALPHA
28. END

```

5.5. DERIVATION OF GEOMETRICAL DERIVATIVES FOR THE ROPE BENT ON A SHEAVE

The X system coordinates of Point P were derived for the bent rope by utilization of matrices with the result that

$$[X] = [\psi'] [T] [\theta] [\beta] [Y] + [\psi] [T] [A^*] + [C] \quad (5-17)$$

As mentioned in the text of the analysis, differentiation can be conveniently performed without matrix expansion for reasons of error checking and translation to computer statements.

In the succeeding analysis, all primes denote differentiation with respect to ψ , the sheave reference angle. Then, using the differentiation product rule,

$$\begin{aligned}
 [X'] &= [\psi] [T] [\theta] [\beta] [Y] + [\psi] [T] [\theta'] [\beta] [Y] \\
 &+ [\psi] [T] [\theta] [\beta'] [Y] + [\psi] [T] [\theta] [\beta] [Y'] \\
 &+ [\psi'] [T] [A^*] + [\psi] [T] [A^{*'}] + [C']
 \end{aligned} \quad (5-18)$$

where

$$[\psi'] = \begin{bmatrix} -\sin \psi & -\cos \psi & 0 \\ \cos \psi & -\sin \psi & 0 \\ 0 & 0 & 0 \end{bmatrix}$$

$$[\theta] = \theta' \begin{bmatrix} -\sin \theta & -\cos \theta & 0 \\ \cos \theta & -\sin \theta & 0 \\ 0 & 0 & 0 \end{bmatrix}, \text{ where } \theta' = K_2$$

$$[\beta'] = \beta' \begin{bmatrix} 0 & 0 & 0 \\ 0 & -\sin \beta & \cos \beta \\ 0 & -\cos \beta & -\sin \beta \end{bmatrix},$$

where

$$\beta' = \frac{K_2^2 \sin \theta}{\left(\frac{R_P}{R} + \cos \theta\right)^2 + K_2^2}$$

$$[Y'] = r\phi \begin{bmatrix} -\sin \phi \\ \cos \phi \\ 0 \end{bmatrix}, \text{ where } \phi' = K_1 K_2$$

$$[A^{*'}] = R\theta' \begin{bmatrix} -\sin \theta \\ \cos \theta \\ 0 \end{bmatrix}$$

$$[C'] = R_P \begin{bmatrix} -\sin \psi \\ \cos \psi \\ 0 \end{bmatrix}$$

The definition of the other matrices may be found either in Section 5.1 or in the body of the report. Expansion of individual terms in Equation 5-18 gives the first geometrical derivative of \bar{X} .

The second geometrical derivative may be found by again applying the product rule,

$$\begin{aligned} [X''] &= [\psi''] [\tau] [\theta] [\beta] [Y] + 2[\psi'] [\tau] [\theta'] [\beta] [Y] \\ &+ 2[\psi'] [\tau] [\theta] [\beta'] [Y] + 2[\psi'] [\tau] [\theta] [\beta] [Y'] \\ &+ [\psi] [\tau] [\theta''] [\beta] [Y] + [\psi] [\tau] [\theta'] [\beta'] [Y] \\ &+ 2[\psi] [\tau] [\theta'] [\beta] [Y'] + [\psi] [\tau] [\theta] [\beta''] [Y] \\ &+ 2[\psi] [\tau] [\theta] [\beta'] [Y'] + [\psi] [\tau] [\theta] [\beta] [Y''] \\ &+ [\psi''] [\tau] [A^*] + 2[\psi'] [\tau] [A^{*'}] \\ &+ [\psi] [\tau] [A^{*''}] + [C''] \end{aligned} \quad (5-19)$$

where

$$[\psi''] = \begin{bmatrix} -\cos \psi & \sin \psi & 0 \\ -\sin \psi & -\cos \psi & 0 \\ 0 & 0 & 0 \end{bmatrix}$$

$$[\theta''] = \theta'^2 \begin{bmatrix} -\cos \theta & \sin \theta & 0 \\ -\sin \theta & -\cos \theta & 0 \\ 0 & 0 & 0 \end{bmatrix}$$

$$[\beta''] = \beta'' \begin{bmatrix} 0 & 0 & 0 \\ 0 & -\sin \beta & \cos \beta \\ 0 & -\cos \beta & -\sin \beta \end{bmatrix} + \beta'^2 \begin{bmatrix} 0 & 0 & 0 \\ 0 & -\cos \beta & -\sin \beta \\ 0 & \sin \beta & -\cos \beta \end{bmatrix}$$

and

$$\beta'' = \frac{K_2^3 \cos \theta \left[\left(\frac{R}{R} + \cos \theta \right)^2 + K_2^2 \right] + 2K_2^2 \sin^2 \theta \left(\frac{R}{R} + \cos \theta \right)}{\left[\left(\frac{R}{R} + \cos \theta \right)^2 + K_2^2 \right]}$$

$$[Y''] = r \phi'^2 \begin{bmatrix} -\cos \phi \\ -\sin \phi \\ 0 \end{bmatrix}$$

$$[A^{*''}] = R \theta'^2 \begin{bmatrix} -\cos \theta \\ -\sin \theta \\ 0 \end{bmatrix}$$

$$[C''] = R_p \begin{bmatrix} -\cos \psi \\ -\sin \psi \\ 0 \end{bmatrix}$$

5.6.

BENDING-STRESS ANALYSIS COMPUTER PROGRAM

The results of the straight-rope and the rope-wrapped-on-a-sheave radii-of-curvature analyses were combined with the derived bending-stress equations in a digital Fortran program in order to compute changes in bending stress as the rope is bent. As in previous programs, the statements are compatible with the services of Tymshare, Inc., and should be altered for individual computer systems.

Fortran variable names and the corresponding quantities they represent are:

<u>Variable Name</u>	<u>Quantity</u>
RR, RL, RS, Y	R _p , R, r, r _w
BT, AL	β, α in degrees
DPH, DTH	Δφ, Δθ in degrees

Variable Name	Quantity
E	Young's Modulus
COE	$\pi/180^\circ$
PH1, PH2	K_1, K_2
PH, 14	ϕ, θ in radians
TOP1	$ Z' ^d$
Z12, Z22, Z32	Z''
BOT1	$ Z'' $
R(J)	ρ_1
BT1, BT2	β, β'
X11, X21, X31	\bar{X}'
X12, X22, X32	\bar{X}''
TOP2	$ \bar{X}' ^2$
BOT2	$ \bar{X}'' $
RAD	ρ_2
COANG	$\cos \xi$
STR	σ_b

The program varies ϕ by $\Delta\phi$ at various values of θ . During each iteration, $\rho_1, \rho_2, \cos \xi$ and σ are calculated and ϕ, θ , and σ are outputted. After ϕ has varied through 2π , θ is incremented by $\Delta\theta$ and then ϕ is again varied through 2π . This process continues until all desired values of ϕ and θ have been investigated.

COMPUTER PROGRAM

```

1.      C:WIRE ROPE BENDING STRESS ANALYSIS
2.      ACCEPT RR,RL,RS,BT,AL,DPH,DTH,E,Y
3.      COE=.01745329
4.      BTA=BT*COE
5.      ALF=AL*COE
6.      SBT=SIN[BTA]
7.      CBT=COS[BTA]
8.      SA=SIN[ALF]
9.      CA=COS[ALF]
10.     TH1=SQRT[(RR/RL)+2-1]*SBT/CBT
11.     PH1=SQRT[((RL*SA)/(RS*CA*SBT)-CBT)+2-(SA*SBT/CA)+2]
12.     PH=0
13.     TH=0
14. 10  SP=SIN[PH]
15.     CP=COS[PH]
16.     ST=SIN[TH]
17.     CT=COS[TH]
18.     TOP1=(RL/GBT+RS*CP*SBT)+2+RS+2*(CBT+PH1)+2
19.     Z12=-RL*CT-RS*CP*CT*(1+PH1*CBT)+RS*SP*ST*(PH1+CBT)+RS*PH1*
        SP*ST*(1+PH1*CBT)-RS*PH1*CP*CT*(PH1+CBT)
20.     Z22=-RL*ST-RS*CP*ST*(1+PH1*CBT)-RS*SP*CT*(PH1+CBT)-RS*PH1*
        SP*CT*(1+PH1*CBT)-RS*PH1*CP*ST*(PH1+CBT)
21.     Z32=RS*PH1+2*SP*SBT
22.     BOT1=SQRT[Z12+Z22+Z32+2]
23.     R=TOP1/BOT1
24.     BTA=ATAN[TH1/(RR/RL+CT)]
    
```

```

25. SB=SIN[BTA]
26. CB=COS[BTA]
27. PH1=PH1*TH1
28. BT1=TH1+2*ST/((RR/RL+CT)+2+TH1+2)
29. BT2=(CT*((R/RL+CT)+2+TH1+2)+7*ST+2*(RR/RL+CT))*TH1+3/((RR/
RL+CT)+2+TH1+2)+2
30. X11=RS*(SB*SP-TH1*(ST*CP+CB*CT*SP)+BT1*SB*ST*SP-PH1*(CT*SP
+CB*ST*CP))-RL*TH1*ST
31. X21=RS*(CT*CP-CB*ST*SP-BT1*CB*SP-PH1*SB*CP)+RL*CT+RR
32. X31=RS*(TH1*(-CT*CP+CB*ST*SP)+BT1*SB*CT*SP+PH1*(ST*SP-CB*
CT*CP))-RL*TH1*CT
33. X12=RS*(-CT*CP+CB*ST*SP+2*BT1*CB*SP+2*PH1*SB*CP+2*TH1*BT1*
SB*CT*SP+2*TH1*PH1*(ST*SP-CB*CT*CP)+BT2*SB*ST*SP+BT1+2*CB*
ST*SP+2*PH1*BT1*SB*ST*CP)
34. X12=X12+RS*(PH1+2*(-CT*CP+CB*ST*SP)+TH1+2*(-CT*CP+ST*SP))+
RL*(-CT-TH1+2*CT)-RR
35. X22=RS*(SB*SP-2*TH1*(ST*CP+CB*CT*SP)+2*BT1*SB*ST*SP-2*PH1*
(CT*SP+CB*ST*CP))-BT2*CB*SP+BT1+2*SB*SP-2*PH1*BT1*CB*CP+PH1
2*SB*SP)
36. X22=X22+RS*TH1+2*(SB*ST*CP+SB*CT*SP)-2*RL*TH1*ST
37. X32=RS*(-2*TH1*BT1*SB*ST*SP+2*TH1*PH1*(CT*SP+CB*ST*CP)+B12
*SB*CT*SP+BT1+2*CB*CT*SP+2*PH1*BT1*SB*CT*CP+PH1+2*(ST*CP+
CB*CT*SP))
38. X32=X32+RS*TH1+2*(CB*ST*CP+CB*CT*SP)+RL*TH1+2*ST
39. TOP2=X11+2*X21+2*X31+2
40. BOT2=SQR(X12+2*X22+2*X32+2)
41. RAD=TOP2/BOT2
42. DOT=Z12*X12+Z32*X22-Z22*X32
43. COANG=DOT/(BOT1*BOT2)
44. STR=E*Y*(1/RAD-COANG/R)
45. DISPLAY TH/COE,FX/COE,STR
46. PH=PH+DPH*COE
47. PH1=PH1/TH1
48. IF (PH.LE.(360*COE)) GO TO 10
49. PH=0
50. TH=TH+DTH*COE
51. IF (TH.LE.(180*COE)) GO TO 10
52. END

```

-- END --

6. REFERENCES

- 2-1 Jones, R. D., Gibson, P. T., and Cress, H. A., "Continued Experimental Investigation of Aircraft Arresting Gear Purchase Cable", Final Phase Report from Battelle's Columbus Laboratories to Naval Air Engineering Center under Contract No. N00015-71-S-1225, August 14, 1973.
- 3-1 Bulletin 10, International Organization for the Study of the Endurance of Wire Rope (O.I.P.E.E.C.), 20 Rue D'Athenes, Paris 9E, France, July 30, 1967.
- 3-2 Bulletin 19, International Organization for the Study of the Endurance of Wire Rope (O.I.P.E.E.C.), 20 Rue D'Athenes, Paris 9E, France, 1971.
- 3-3 Gibson, P. T., Fries, R. H., Winegardner, R. D., Pettit, D. E., Hoepfner, D. W., Hyler, W. S., and Cress, H. A., "Analytical and Experimental Investigation of Aircraft Arresting Gear Purchase Cable", Final Report from Battelle's Columbus Laboratories to Naval Air Engineering Center under Contract No. N156-47939, July 3, 1967. Distribution limited. AD-852 074L, if qualified*.
- 3-4 Gibson, P. T., White, F.G., Schalit, L. A., Thomas, R. E., Cole, R. W., and Cress, H. A., "A Study of Parameters That Influence Wire Rope Life", Final Report prepared by Battelle's Columbus Laboratories for the Naval Ship Systems Command Under Contract No. N00024-72-C-5427, October 31, 1974.
- 3-5 Muller, Hugo, "The Properties of Wire Rope Under Alternating Stresses", Wire World International, p. 249, October, 1961.
- 3-6 Gibson, P. T., and Cress, H. A., "Analytical and Experimental Investigation of Aircraft Arresting Gear Purchase Cable", Final Report from Battelle's Columbus Laboratories to Naval Air Engineering Center, November 14, 1968. AD-852 075*.
- 3-7 Gibson, P. T., Larsen, C. H., and Cress, H. A., "Determination of the Effect of Various Parameters on Wear and Fatigue of Wire Rope Used in Navy Rigging Systems", Final Report prepared by Battelle's Columbus Laboratories for the Naval Ship Research and Development Center under Contract No. N00600-70-C-1045, March 15, 1972. AD-776 993*.
- 3-8 Calderale, P. M., "Programming and Statistical Analysis of Fatigue Tests on Wire Rope With the Aid of Least Squares", Wire (Coburg, Germany), Issue 66, pp. 131-138, August, 1965.

*May be ordered using this number from National Technical Information Service, Springfield, Virginia 22151.

- 3-9 Drucker, D. C., and Tachau, H., "A New Design Criterion for Wire Rope", Journal of Applied Mechanics, pp. A33-A58, March, 1945.
- 3-10 Scoble, Walter A., "Wire Ropes Research", Proceedings, Institution of Mechanical Engineers (London), January - April, 1920.
- 3-11 Scoble, Walter A., "Second Report of the Wire Ropes Research Committee", Proceedings, Institution of Mechanical Engineers (London), December, 1924 [probably for April - July]
- 3-12 Scoble, Walter A., "Third Report of the Wire Ropes Research Committee", Proceedings, Institution of Mechanical Engineers (London), January - May, 1928.
- 3-13 Scoble, Walter A., "Fourth Report of the Wire Ropes Research Committee", Proceedings, Institution of Mechanical Engineers (London), January - May, 1939.
- 3-14 Hurt, F., and Walker, R. E., "Design Considerations and Applications of Modern Wire Rope Haulages", Proceedings, AMEME (Association of Mining, Electrical, and Mechanical Engineers), pp. 216-224, April 14, 1967.
- 3-15* VDI Guidelines for Lifting and Hauling, VDI 2358, Published in Germany, English translation is NAVSHIPS Translation 1417, October, 1968.
- 3-16 Anderson, W., "Factors Affecting the Efficiency and Safety of Steel Wire Ropes", Lift, pp. 109-113, May - June, 1972.
- 3-17 Cordiano, H. V., and Wolfe, R. J., "Report of Investigation of Uncoated Wire Rope, Preformed and Nonpreformed", Lab Project 4750-18, Material Laboratory, New York Naval Shipyard, May 24, 1951.
- 3-18 Cordiano, H. V., and Wolfe, R. J., "The Resistance to Fatigue of Uncoated Hot Dip Galvanized and Nongalvanized Wire Rope, Preformed and Nonpreformed", Lab Project 4750, Material Laboratory, New York Naval Ship Yard, June 11, 1953.
- 3-19 Gibson, P. T., Karleen, R. E., and Cress, H. A., "The Continuation of Analytical and Experimental Investigation of Aircraft Arresting Gear Purchase Cable", Final Report prepared by Battelle's Columbus Laboratories for the Naval Air Engineering Center, June 22, 1971. AD-905 835**.
- 3-20 Gambrell, S. C., "Study of Low-Cycle Fatigue of Wire Rope", Wire and Wire Products, pp. 127-130, October, 1969.

*Also appears as bibliography entry No. 62 in Volume I.

**May be ordered using this number from National Technical Information Service, Springfield, Virginia 22151.

- 3-21 Hagarman, P., and Kressley, L., "Evaluate, Test, and Manufacture an Improved Wire Rope and Cable", Final Report on Contract No. N065-92232 from Texas Instruments Corporation to U. S. Bureau of Ships, July 31, 1957. AD 819 202*
- 3-22 Macco, J., and Weiss, J., "Investigation of the Resistance to Fatigue and Wear of Aluminum-Coated and Galvanized Improved Plow Steel Wire Rope", Lab Project 930-44, Naval Applied Science Laboratory, Brooklyn, New York, January 16, 1968.
- 3-23 van de Moortel, D., "The Modern Development of Wire Rope", Wire, English Edition No. 48, August, 1960, and No. 49, October, 1960.
- 3-24 van de Moortel, "Two-Year Study Yields Data for Evaluating Coated Cable", reprinted from Product Engineering, October 10, 1966.
- 3-25** Selection of Wire Rope for Engineering Applications, British Ropes Group, Wire Rope Technical Department, Carr Hill, Doncaster, England, 1967.
- 3-26 Matanzo, Frank, "Axial Fatigue of Wire Rope in Seawater", Offshore Technology Conference Preprints, Volume II, Paper No. 1579, pp. 649-656, Offshore Technology Conference, Dallas, Texas, 1972.
- 3-27 Matanzo, Frank, and Heller, S. R., "Axial Fatigue of Wire Rope", Final Report from The Catholic University of America to NAVSHIPS, Contract No. N00024-70-C-5439, June 25, 1971. AD 726 457*.
- 3-28 Fleming, J. F., "Fatigue of Cables", Report on Project 1201-3N, to American Iron and Steel Institute from the School of Engineering of the University of Pittsburgh, June, 1974.
- 3-29 Reemsnyder, H. R., "The Mechanical Behavior of Steel Wire, Strand, and Rope", presentation to the Ad Hoc Committee on Mechanical Rope and Cable, National Materials Advisory Board, National Research Council, June 6, 1972.
- 3-30 Berteaux, H. O., and Walden, R. G., "An Engineering Program to Improve the Reliability of Deep Sea Moorings", Vol. 1, Marine Technology Society Preprints, Marine Technology Society, Washington, D. C., June 29 - July 1, 1970.
- 3-31 Heller, S. R., Jr., and Metcalf, John T., Jr., "Axial Fatigue Tests of Corroded Wire Rope Specimens", Final Report from Catholic University of America to Naval Ships Engineering Center under Contract No. N00024-72-C-5394, April 25, 1974. AD 779 309*.

*May be ordered using this number from National Technical Information Service, Springfield, Virginia 22151.

**Also appears as bibliography entry No. 8 in Volume I.

- 3-32 Vachon, W. A., "Kink Formation Properties and Other Mechanical Characteristics of Oceanographic Strands and Wire Rope", Final Report from Massachusetts Institute of Technology to Woods Hole Oceanographic Institute, under Purchase Order 17052 of Office of Naval Research, Contract No. N00014-66-C-0242, NRO 83-004, April, 1970.
- 3-33 _____, "Dynamic Testing of Wire Rope and Synthetic Rope", Final Report from Preformed Line Products Company to Naval Civil Engineering Laboratory (Port Hueneme, CA), under Contract N62399-69-C-0013, January, 1970.
- 3-34 Gibson, P. T., Cress, H. A., Kaufman, W. J., and Gallant, W. E., "Analysis of Wire Rope Torque", Wire and Wire Products, pp. 50, 52-58, 60, November, 1970.
- 3-35 Hruska, F. H., "Calculation of Stresses in Wire Ropes", Wire and Wire Products, pp. 766-767, 799-801, September, 1951.
- 4-1* Roebling Wire Rope Handbook, The Colorado Fuel and Iron Corporation, Roebling Wire Rope, Trenton, New Jersey, 1966 (out of print).
- 4-2 Gibson, P. T., and Cress, H. A., "Analytical Study of Aircraft Arresting Gear Cable Design", Final Report from Battelle's Columbus Laboratories to U. S. Navy Bureau of Weapons, May, 1965. AD 617 788**.
- 4-3 Gibson, P. T., Karleen, R. E., Clark, G. A., Dodson, M., Fries, R. H., Beuhring, V. F., Jackson, C. M., and Cress, H. A., "The Continuation of Analytical and Experimental Investigation of Aircraft Arresting Gear Purchase Cable", Final Phase Report from Battelle's Columbus Laboratories to Naval Air Engineering Center under Contract No. N156-69-C-1501, April 7, 1970. AD 869 092**.
- 4-4 Stein, R. A., and Bert, C. W., "Radius of Curvature of a Double Helix", Journal of Engineering for Industry, American Society of Mechanical Engineers, August, 1962.
- 4-5 Taylor, A. E., Advanced Calculus, Ginn and Company, Boston, 1955, pp. 369.
- 4-6 Dwight, H. B., Tables of Integrals and Other Mathematical Data, 4th Edition, The Macmillan Company, New York, 1961, Chapter 2, p. 105.

*Also appears as bibliography entry No. 1 in Volume I.

**May be ordered using this number from National Technical Information Service, Springfield, Virginia 22151.

- 4-7 Starkey, W. L., and Cress, H. A., "An Analysis of Critical Stresses and Mode of Failure of a Wire Rope", Journal of Engineering for Industry, Transactions of the American Society of Mechanical Engineers, Series B, pp. 307-316, 1959.
- 4-8 Kreyszig, E., Advanced Engineering Mathematics, 1st Edition, John Wiley and Sons, Inc., New York, 1962, Chapter 5, pp. 292-296.
- 4-9 Heller, S. R., "The Contact Pressure Between Rope and Sheave", Naval Engineers Journal, pp. 49-57, February, 1970.
- 4-10 Dodson, M., Gibson, P. T., Clark, G. A., and Cress, H. A., "Investigation of the Influence of Hook Abrasion and Wire Materials on the Useful Service Life of Deck Pendants", Final Report from Battelle's Columbus Laboratories to Naval Air Systems Command under Contract No. N00019-69-C-0287, August 5, 1970. Distribution limited. AD 844 423L, if qualified*.
- 4-11 Bruska, F. H., "Radial Forces in Wire Ropes", Wire and Wire Products, pp. 459-463, May, 1952.
- 4-12 Leissa, A. W., "Contact Stresses in Wire Ropes", Wire and Wire Products, Vol. 34, No. 3, pp. 307-317, 372-373, March, 1959.
- 4-13 Seely, F. B., and Smith, J. O., Advanced Mechanics of Materials, 2nd Edition, John Wiley and Sons, Inc., New York, 1957.
- 4-14 Chou, Pei Chi, "Theoretical Analysis of Deck Pendant During Arresting Gear Hook Impact and Runout", Progress Report NAEF-ENG-6682 from Kellett Aviation Corporation to Naval Air Engineering Facility, June 14, 1960.
- 4-15 Chou, Pei Chi, "Plastic Contact Stress in Circular Cylinders", Report NAEF-ENG-6740, from Kellett Aviation Corporation to Naval Air Engineering Facility, January 11, 1961.
- 4-16 Chi, Michael, "Analysis of Multiwire Strands in Tension and Combined Tension and Torsion", Report 71-9 under Navy Contract No. N00014-68-A-0506-0001, Prepared by The Catholic University of America, September, 1971. AD 732 006*.
- 4-17 Chi, Michael, "Analysis of Operating Characteristics of Strands in Tension Allowing End-Rotation", Report 71-10, under Navy Contract No. N00014-68-A-0506-0001, Prepared by The Catholic University of America, September, 1971. AD 732 007*.
- 4-18 Liu, C. L., "Dynamic Stress Response of Lifting Lines for Oceanic Operations", Naval Civil Engineering Laboratory (Port Hueneme, CA), Report E703, November, 1970.

*May be ordered using this number from National Technical Information Service, Springfield, Virginia 22151.

- 4-19 Choo, Young-il, and Casarella, M. J., "A Survey of Analytical Methods for Dynamic Simulation of Cable-Body Systems", Journal of Hydraulics, Vol. 7, No. 4, pp. 137-144, October, 1973.
- 4-20 Albertson, N. D., "A Survey of Techniques for the Analysis and Design of Submerged Mooring Systems", Report R815, Civil Engineering Laboratory, Naval Construction Battalion Center, Naval Facilities Engineering Command, August, 1974. AD 786 487-9W0*.
- 4-21 Choo, Y. I., and Casarella, M. J., "A Survey of Analytical Methods for Dynamic Simulation of Cable-Body Systems", The Catholic University of America Report 73-1, Prepared for Office of Naval Research under Contract No. N00014-68-A-0506-0001, March, 1973.
- 4-22 Dillon, D. B., "An Inventory of Current Mathematical Models of Scientific Data-Gathering Moors", report by Hydrospace-Challenger, Inc., Rockville, Maryland, to Office of Naval Research under Contract No. N00014-72-C-0361, February, 1973. AD 756 225*.
- 4-23 Goeller, J. E., and Laura, P. A., "A Theoretical and Experimental Investigation of Impact Loads in Stranded Steel Cables During Longitudinal Excitation", The Catholic University of America Report 70-2, Prepared for the Office of Naval Research under Contract No. N00014-68-A-0506-0001, April, 1970.
- 4-24 Schneider, L., Mahon, T., and Barton, L. G., "Tow Cable Snap Loads", American Society of Mechanical Engineers, Paper 64-WA/UNT 8, presented at the Annual Meeting of ASME, November 29 - December 4, 1964.
- 4-25 Ringleb, F. O., "Cable Dynamics", Report NAEF-ENG-6169, Naval Air Engineering Facility (Ship Installations, December, 1956.)
- 4-26 Mukherjee, S. N., "Vertical Vibrations of Rope Excited by Sudden Increase in Tension", International Ropeway Review (now Lift), pp. 12-14, 28, October/December, 1970.
- 4-27 Dale, J. R., and McChandlees, J. M., "Water Drag Effects of Flow-Induced Cable Vibrations", Report No. NADC-AE-6731, U. S. Naval Air Development Center, Warminster, Pennsylvania, June, 1967. AD 654 906*.
- 4-28 Dale, J. R., "Determination of Normal Drag Coefficients for Flexible Cables", Report No. NADC-AE-6719, U. S. Naval Air Development Center, Warminster, Pennsylvania, June, 1967. AD 654 906*.

*May be ordered using this number from National Technical Information Service, Springfield, Virginia 22151.

- 4-29 Ringleb, F. O., "Motion and Stress of an Elastic Cable due to Impact", Journal of Applied Mechanics, Transactions of ASME, American Society of Mechanical Engineers, pp. 417-425, September, 1957.
- 4-30 Ringleb, F. O., "Cable Dynamics", Mechanical Design and Systems Handbook, Section 31, McGraw-Hill Book Company, New York, 1964.
- 4-31 Neuhardt, G. L., Eslinger, N. E., and Sasaki, F. S., "An Analytical Approach to the Alleviation of Dynamic Tensions in Aircraft Arresting Gear Cables", Wright Air Development Report 58-217, Prepared by American Machine and Foundry Company for Wright Air Development Center, Air Research and Development Command, U. S. Air Force, Wright-Patterson Air Force Base, Ohio, under Contract No. AF33(616)-5282, Project 1351-60716, May, 1958.
- 4-32 Gibson, P. T., Alexander, G. H., and Cress, H. A., "Validation of Design Theory for Aircraft Arresting Gear Cable", Final Report from Battelle's Columbus Laboratories to Naval Air Systems Command, under Contract No. N0w 65-0503-c, January, 1968. AD 665 328*.
- 5-1 Greenwood, D. T., Principles of Dynamics, First Edition, Prentice Hall, Inc., Englewood Cliffs, New Jersey, 1965, Chapter 7, pp. 297-300.

<u>7.</u>	<u>ALPHABETICAL INDEX</u>	<u>Page</u>
A		
Aircraft Arresting-Gear Cable		4-38
Alignment, Sheave		3-13
Aluminized Wire		3-28
Aluminum Sheaves		3-19
Analysis, Stress, of Wire Rope		
Bending		4-1
Contact		4-29
Shear		4-34
Tensile		4-1
Torsion		4-34
Angles, Fleet, Effect of		3-13
Angles, Wrap, Effect of		3-10
Attachments, Effects of		
on Axial Fatigue Life		3-36
on Bending Fatigue Life		3-15
Axial Fatigue Data		
Wire Rope		3-33
Wire Strand		3-33
Axial Load Characteristics		3-33
Axial Stresses, Calculation of		4-1
B		
Bearing Pressure Ratio		3-8
Bending Fatigue Data, Wire Rope		
Reverse Bend	3-16,	3-32
Single Bend	3-2 to 3-17, 3-19 to	3-31
Bending Stresses, Calculation of		4-24
Breakage, Wire, as a Function of Wrap Angle		3-12
Breaking Strengths, Wire, Effects of		
on Axial Fatigue Life		3-39
on Bending Fatigue Life		3-14
Breaks, Wire, Identification of		2-1
Bright Wire		3-28
C		
Cable, Aircraft Arresting-Gear		4-38
Carbon Steel Wire		3-13
Cast Iron Sheaves		3-19
Coatings, Wire, Effects of		
on Axial Fatigue Life		3-40
on Bending Fatigue Life		3-28
Coefficients, Drag, Cable		4-39
Complex Bending of Wire Segments		4-26
Computer Programs		5-4
Confidence Bands on Bending Fatigue Data		3-8

	<u>Page</u>
Constant Angle Assumption (in Bending Stress Analysis)	4-7
Construction, Rope, Effects of	
on Axial Fatigue Life	3-37
on Bending Fatigue Life	3-15
Contact Stresses, Calculation of Elastic	
at Core-Strand Interface	4-34
at Internal Wire Contact Points	4-30
at Interstrand Locations	4-33
at Wire-Sheave Interface	4-29
Copper-Alloyed Steel Rope, Corrosion Resistance of	3-26
Core Material, Effects of	
on Axial Fatigue Life	3-36
on Bending Fatigue Life	3-19
Corrosion, Wire Rope, Effects of	
on Axial Fatigue Life	3-39
on Bending Fatigue Life	3-26
Cracks, Fatigue, Formation of	2-1
Cycle, Fatigue, Definition of	
in Axial Tension	3-33
in Bending	3-4
Cyclic Impact, Effect of	4-35

D

Data, Wire Rope System Design	
Axial Fatigue	3-33
Bending Fatigue	3-1
Derivation of Geometrical Derivatives for a Rope on a Sheave	5-7
Derivation of Reference Angle Relationships in a Straight Rope	5-2
Design Factor	1-1
Diameter Ratio, Sheave-to-Rope, Effects of	3-3
Diameter, Wire, Effects of	
on Axial Fatigue Life	3-39
on Bending Fatigue Life	3-19
Drag Coefficients, Cable	4-39
Drawn Galvanized Wire	3-28
Dynamics, Wire Rope	4-34

E

Elastic-Plastic Stress Analysis	4-34
Electrogalvanized Wire	3-28
End Fittings, Effect of	
on Axial Fatigue Life	3-36
on Bending Fatigue Life	3-15
Extra-Improved Plow Steel	3-13

	<u>Page</u>
F	
Factor of Safety (Design Factor)	1-1
Failure Modes, Rope Wire	
Fatigue	2-1
Tensile	2-3
Faired Cables, Strumming Characteristics of	4-39
Fatigue, Wire Rope	
Axial	3-33
Bending	3-1
Fiber Core Rope	3-19
Finally Galvanized Wire	3-28
Filler-Wire Construction	3-19
Fleet Angle, Effects of	3-13
Formulas, Bending Stress, Comparison of	4-4
Frequency, Effects of (on Axial Fatigue Life)	3-37
Friction, Internal Wire	3-61
G	
Galvanizing, Effects of	3-28
Geometry, Wire Rope	
in Bending	4-16
in Tension	4-2
Grades, Wire	3-13
Groove Shape, Effects of	3-24
H	
Hardness, Sheave, Effect of	3-19
I	
Improved Plow Steel Wire	3-13
Independent Wire Rope Cores	3-19
Initiation of Fatigue Cracks in Rope Wire	2-1
Interstrand Contact Stresses	4-33
Iron, Cast, Sheaves	3-19
J	
K	
Kink Formation	3-40
L	
Laboratory Test Facilities, Effects of	3-2
Lang-Lay Rope	3-15

	<u>Page</u>
Lay Angle and Direction, Effects of	
on Axial Fatigue Life	3-36
on Bending Fatigue Life	3-15
Lay Length, Measurement of Rope and Strand	3-54
Life Factor	3-11
Load Cycle Characteristics, Axial	3-33
Load Level, Effect of	
on Axial Fatigue Life	3-33
on Bending Fatigue Life	3-5
Load Range, Effects of (on Axial Fatigue Life)	3-35
Longitudinal Forces Due to Rope Dynamics	4-35
Lubrication, Effects of	
on Axial Fatigue Life	3-40
on Bending Fatigue Life	3-28

M

Material, Core, Effects of	
on Axial Fatigue Life	3-36
on Bending Fatigue Life	3-19
Material, Wire, Effects of	
on Axial Fatigue Life	3-37
on Bending Fatigue Life	3-13
Matrix Analysis (in Bending Stress Analysis)	5-1
Maximum Load, Effect of (on Axial Fatigue Life)	3-35
Mean Load, Effect of (on Axial Fatigue Life)	3-35
Metallic Cores	3-19
Mechanical Properties of Rope Wire	3-13
Mild Plow Steel Wire	3-13
Modes of Wire Failure	2-1
Multiple Operation Strands	3-19

N

Nickel-Alloyed Steel, Corrosion Resistance of	3-26
Nodal Angles, Sheave	3-58
Nonrotating (Low Rotation) Ropes,	
Torsional Characteristics	3-43
Ultimate Strength Under Rotation	3-42
Nylon-Jacketed Cable	3-31
Nylon-Lined Sheaves	3-25

O

P

Plastic Coatings	3-31
Plasticity, Cross-Wire, Analysis of	4-34
Plow Steel	3-13
Polypropylene Cores	3-25

	<u>Page</u>
Preforming, Effects of	3-19
Pressure, Rope-to-Sheave Bearing	3-8

Q

R

Radius of Curvature, Change in Rope Wire	
Computer Program for Determination of	5-9
Due to Bending Over a Sheave	4-23
Due to Tensile Loading	4-10
Range of Load, Effects of (on Axial Fatigue Life)	3-35
Ratio, Sheave-to-Rope Diameter, Effect of	3-3
Regular-Lay Rope	3-19
Relative Motion of Strands in a Rope	3-55
Reversed Bends, Effect of	3-30
Rotation, Rope. Effects of	3-40

S

Shear Failures in Rope Wire	2-2
Shear Stresses, Calculation of	4-34
Sheave Hardness, Effects of	3-19
Sheave Throat Shape, Effects of	3-24
Single Operation Strands	3-15
Socketing Technique, Effects of (on Axial Fatigue Life)	3-36
Statistical Variation in Bending Fatigue Data	3-8
Strands, Axial Fatigue of Steel	3-33
Strands, Number of (as it Affects Bending Fatigue Life)	3-15
Strength, Wire, Effects of	
on Axial Fatigue Life	3-37
on Bending Fatigue Life	3-13
Stress Analysis, Wire Rope	
Bending	4-2
Contact	4-29
Shear	4-34
Tensile	4-1
Torsion	4-34
Strumming, Effects of	4-36
Suppression of Strumming	4-38
Swaged Sockets, Effects of (on Axial Fatigue Life)	3-37

T

Tensile Failures in Rope Wire	2-3
Tensile Stresses, Calculation of	4-1
Throat Shape, Sheave, Effect of	3-24
Torsional Characteristics of Various Rope Constructions	3-41
Torsional Stresses, Calculation of	4-34
Torque, Wire Rope	3-40

	<u>Page</u>
Translation of Coordinates (in Bending Stress Analysis)	5-1
Transverse Forces Due to Rope Dynamics	4-36
U	
Uniform-Motion Assumption (in Bending Stress Analysis)	4-8
V	
W	
Wire Coatings	3-28
Wire Failure Modes	2-1
Wire Sizes	3-19
Wire Strengths	3-13
Wire, Types of Rope	3-13
Wires, Arrangement of (in a Rope)	3-19
Wrap Angle, Effects of	3-10
X	
Y	
Z	
Zinc Coatings	3-28
Zinc Sockets, Effect of (on Axial Fatigue Life)	3-36